Decay rates and electromagnetic transitions of heavy quarkonia *

J. N. Pandya[1;1)] N. R. Soni[1] N. Devlani[2] A. K. Rai[3]

[1] Applied Physics Department, Faculty of Technology & Engineering, The M S University of Baroda, Vadodara 390001, Gujarat, INDIA
[2] Applied Physics Department, Polytechnic, The M S University of Baroda, Vadodara 390002, Gujarat, INDIA
[3] Department of Applied Physics, Sardar Vallabhbhai National Institute of Technology, Surat 395007, Gujarat, INDIA

Abstract: The electromagnetic radiative transition widths for heavy quarkonia, as well as digamma and digluon decay widths, are computed in the framework of the extended harmonic confinement model (ERHM) and Coulomb plus power potential (CPP$_\nu$) with varying potential index ν. The outcome is compared with the values obtained from other theoretical models and experimental results. While the mass spectra, digamma and digluon widths from ERHM as well as CPP$_{\nu=1}$ are in good agreement with experimental data, the electromagnetic transition widths span over a wide range for the potential models considered here making it difficult to prefer a particular model over the others because of the lack of experimental data for most transition widths.

Key words: heavy quarkonia, radiative decays, electromagnetic transitions

PACS: 12.39.Jh, 12.39.Pn, 13.20.Gd **DOI:** 10.1088/1674-1137/39/12/123101

1 Introduction

Decay properties of mesons are of special experimental and theoretical interest because they provide us with further insights into the dynamics of these systems in addition to the knowledge we have gained from the spectra of these families. A large number of experimental facilities worldwide have provided and continue to provide enormous amounts of data which need to be interpreted using the available theoretical approaches [1]. Many phenomenological studies on numerous observables of the $c\bar{c}$ and $b\bar{b}$ bound states have established that the non-relativistic nature appears to be an essential ingredient to understand the dynamics of heavy quarkonia [2]. Thus, the heavy quarkonium spectroscopy is mostly dependent on the quark mass m, the momentum mv and the binding energy mv^2 in the non-relativistic limit. Two effective field theories, non-relativistic QCD (NRQCD) [3, 4] and potential NRQCD (pNRQCD) [5, 6], have been developed leading to a large number of new results for several observables in quarkonium physics [7].

Radiative transitions in heavy quarkonia have been a subject of interest as the CLEO-c experiment has measured the magnetic dipole (M1) transitions $J/\psi(1S)\to\gamma\eta_c(1S)$ and $J/\psi(2S)\to\gamma\eta_c(1S)$ using a combination of inclusive and exclusive techniques and reconciling with theoretical calculations of lattice QCD and effective field theory techniques [8, 9]. M1 transition rates are normally weaker than E1 rates, but they are of more interest because they may allow access to spin-singlet states that are very difficult to produce otherwise. It is also interesting that the known M1 rates show serious disagreement between theory and experiment when it comes to potential models. This is in part due to the fact that M1 transitions between different spatial multiplets, such as $J/\psi(1S)\to\gamma\eta_c(2S\to1S)$ are nonzero only due to small relativistic corrections to a vanishing lowest-order M1 matrix element [10].

We use the spectroscopic parameters of the extended harmonic confinement model (ERHM), which has been successful in predictions of masses of open flavour mesons from light to heavy flavour sectors [11–13]. The mass spectra of charmonia and bottomonia predicted by this model, and a Coulomb plus power potential (CPP$_\nu$) with varying potential index ν (from 0.5 to 2.0), employing a non-relativistic treatment for heavy quarks [14–17], have been utilized for the present computations along with other theoretical and experimental results.

2 Theoretical framework

One of the tests for the success of any theoretical

Received 23 December 2014, Revised 26 June 2015

∗ Supported by University Grants Commission, India for Major Research Project F. No.42-775/2013(SR) (J N Pandya) and Dept. of Science and Technology, India under SERC fast track scheme SR/FTP/PS-152/2012 (A K Rai)

1) E-mail: jnpandya-apphy@msubaroda.ac.in

model for mesons is the correct prediction of their decay rates. Many phenomenological models predict the masses correctly but overestimate the decay rates [14, 15, 18]. We have successfully employed a phenomenological harmonic potential scheme and CPP$_\nu$ potential with varying potential index for different confinement strengths to compute masses of bound states of heavy quarkonia, and the resulting parameters and wave functions have been used to study various decay properties [13].

The choice of scalar plus vector potential for quark confinement has been successful in predictions of the low lying hadronic properties in the relativistic schemes for quark confinement [19–21], which have been extended to accommodate multiquark states from lighter to heavier flavour sectors with unequal quark masses [11, 12]. The coloured quarks are assumed to be confined through a Lorentz scalar plus a vector potential of the form

$$V(r)=\frac{1}{2}(1+\gamma_0)A^2r^2+B, \tag{1}$$

where A and B are the model parameters and γ_0 is the Dirac matrix.

The wave functions for quarkonia are constructed here by retaining the nature of the single particle wave function but with a two particle size parameter $\Omega_N(q_iq_j)$,

$$R_{n\ell}(r) = \left[\frac{\Omega_{\rm N}^{3/2}}{2\pi}\frac{n!}{\Gamma\left(n+\ell+\frac{3}{2}\right)}\right]^{\frac{1}{2}}(\Omega_{\rm N}^{1/2}r)^{\ell} \times\exp\left(\frac{-\Omega_{\rm N}\ r^2}{2}\right)L_n^{\ell+\frac{1}{2}}(\Omega_{\rm N}r^2). \tag{2}$$

The Coulombic part of the energy is computed using the residual Coulomb potential using the colour dielectric "coefficient", which is found to be state dependent [11], so as to get a consistent Coulombic contribution to the excited states of the hadrons. This is a measure of the confinement strength through the non-perturbative contributions to the confinement scale at the respective threshold energies of the quark-antiquark excitations.

The spin average (center of weight) masses of the $c\bar{c}$ and $b\bar{b}$ ground states are obtained by choosing the model parameters m_c=1.428 GeV, m_b=4.637 GeV, k= 0.1925 and the confinement parameter A=0.0685 GeV$^{3/2}$ [11, 12].

In the other approach using the CPP$_\nu$ scheme for the heavy-heavy bound state systems such as $c\bar{c}$ and $b\bar{b}$, we treat the motion of both the quarks and antiquarks nonrelativistically [13]. The CPP$_\nu$ potential is given by

$$V(r)=\frac{-\alpha_c}{r}+Ar^\nu, \tag{3}$$

Here, for the study of heavy flavoured mesons, $\alpha_c = 4\alpha_s/3$, α_s being the strong running coupling constant, A is the potential parameter and ν is a general power, such that the choice $\nu=1$ corresponds to the Coulomb plus linear potential.

We have employed the hydrogenic trial wave function here for the present calculations. For excited states we consider the wave function multiplied by an appropriate orthogonal polynomial function such that the generalized variational wave function gets orthonormalized. Thus, the trial wave function for the (n,l) state is assumed to be the form given by

$$R_{nl}(r)=\left(\frac{\mu^3(n-l-1)!}{2n(n+l)!}\right)^{\frac{1}{2}}(\mu\ r)^l{\rm e}^{-\mu r/2}L_{n-l-1}^{2l+1}(\mu r). \tag{4}$$

Here, μ is the variational parameter and $L_{n-l-1}^{2l+1}(\mu r)$ is a Laguerre polynomial.

For a chosen value of ν, the variational parameter μ is determined for each state using the virial theorem

$$\langle KE\rangle=\frac{1}{2}\left\langle\frac{r{\rm d}V}{{\rm d}r}\right\rangle. \tag{5}$$

The potential index ν is chosen to vary from 0.5 to 2.

Table 1. Digamma decay width of charmonia (keV).

	1^1S_0	2^1S_0	3^1S_0	4^1S_0	1^3P_0	1^3P_2	2^3P_0	2^3P_2
ERHM	8.76	5.94	3.05	1.43	69.97	73.93	6.93	6.98
ERHM(corr)	6.21	4.21	2.17	1.01	71.04	75.06	5.87	5.91
CPP$_{\nu=0.5}$	12.85	3.47	1.83	1.24	5.74	1.54	21.11	5.69
CPP$_{\nu=0.5}$(corr)	7.32	1.98	1.04	0.71	5.84	1.19	21.59	4.40
CPP$_{\nu=1.0}$	22.79	9.88	6.73	5.28	27.29	7.45	143.30	39.41
CPP$_{\nu=1.0}$(corr)	12.99	5.63	3.84	3.01	27.91	5.76	146.57	30.49
CPP$_{\nu=1.5}$	30.84	17.55	14.16	12.65	63.35	17.52	511.88	144.33
CPP$_{\nu=1.5}$(corr)	17.58	10.00	8.07	7.21	64.79	13.56	523.53	111.66
CPP$_{\nu=2.0}$	37.43	25.11	22.88	22.43	108.06	30.26	1058.7	305.98
CPP$_{\nu=2.0}$(corr)	21.34	14.31	13.04	12.79	110.52	23.41	1082.8	236.72
[29]	10.38	3.378	1.9	1.288	–	–	–	–
[30]	8.5	2.4	0.88	–	2.5	0.31	1.7	0.23
[31]	7.8	3.5	–	–	–	–	–	–
[32]	11.8	–	–	–	–	–	–	–

Table 2. Digluon decay width of charmonia (MeV).

	1^1S_0	2^1S_0	3^1S_0	4^1S_0	1^3P_0	1^3P_2	2^3P_0	2^3P_2
ERHM	13.48	9.14	4.7	2.19	0.11	0.11	9.07	9.13
ERHM(corr)	19.04	12.91	6.64	3.1	0.19	0.2	5.31	5.43
$\mathrm{CPP}_{\nu=0.5}$	43.41	11.73	6.17	4.19	0.019	3.71	0.07	13.74
$\mathrm{CPP}_{\nu=0.5}$(corr)	69.94	18.89	9.94	6.76	0.040	1.43	0.15	5.29
$\mathrm{CPP}_{\nu=1.0}$	77.01	33.37	22.74	17.84	0.092	17.99	0.48	95.21
$\mathrm{CPP}_{\nu=1.0}$(corr)	124.08	53.77	36.64	28.74	0.195	6.93	1.02	36.69
$\mathrm{CPP}_{\nu=1.5}$	104.18	59.28	47.85	42.73	0.214	42.33	1.73	348.66
$\mathrm{CPP}_{\nu=1.5}$(corr)	167.85	95.51	77.09	68.85	0.453	16.31	3.66	134.38
$\mathrm{CPP}_{\nu=2}$	126.46	84.83	77.29	75.79	0.365	73.11	3.58	739.15
$\mathrm{CPP}_{\nu=2.0}$(corr)	203.75	136.67	124.53	122.12	0.773	28.18	7.57	284.88
[22]	26.7±3.0	–	–	–	10.2±0.7	2.034±0.12	–	–
[23]	48.927	–	–	–	38.574	4.396	–	–
[33]pert.	15.70	–	–	–	4.68	1.72	–	–
[33]nonpert.	10.57	–	–	–	4.88	0.69	–	–

Table 3. Digamma decay width of bottomonia (keV).

	1^1S_0	2^1S_0	3^1S_0	4^1S_0	1^3P_0	1^3P_2	2^3P_0	2^3P_2
ERHM	0.47	0.26	0.12	0.01	1.37	1.39	0.12	0.12
ERHM(corr)	0.35	0.20	0.09	0.07	1.39	1.40	0.10	0.10
$\mathrm{CPP}_{\nu=0.5}$	0.36	0.06	0.03	0.038	0.02	0.005	0.057	0.015
$\mathrm{CPP}_{\nu=0.5}$(corr)	0.24	0.04	0.02	0.026	0.02	0.004	0.058	0.013
$\mathrm{CPP}_{\nu=1.0}$	0.55	0.15	0.09	0.080	0.08	0.022	0.42	0.11
$\mathrm{CPP}_{\nu=1.0}$(corr)	0.37	0.10	0.06	0.054	0.08	0.018	0.43	0.09
$\mathrm{CPP}_{\nu=1.5}$	0.71	0.27	0.18	0.123	0.20	0.055	1.34	0.36
$\mathrm{CPP}_{\nu=1.5}$(corr)	0.48	0.18	0.12	0.084	0.21	0.045	1.36	0.30
$\mathrm{CPP}_{\nu=2.0}$	0.84	0.38	0.29	0.165	0.35	0.095	2.83	0.76
$\mathrm{CPP}_{\nu=2.0}$(corr)	0.57	0.26	0.20	0.112	0.36	0.078	2.88	0.63
[29]	0.496	0.212	0.135	0.099	–	–	–	–
[30]	0.527	0.263	0.172	–	0.037	0.0066	0.037	0.0067
[31]	0.460	0.20	–	–	–	–	–	–
[32]	0.580	–	–	–	–	–	–	–

Table 4. Digluon decay width of bottomonia (MeV).

	1^1S_0	2^1S_0	3^1S_0	4^1S_0	1^3P_0	1^3P_2	2^3P_0	2^3P_2
ERHM	7.61	4.31	1.99	1.58	22.45	22.68	1.93	1.94
ERHM(corr)	9.95	5.64	2.61	2.07	38.17	38.57	1.92	1.92
$\mathrm{CPP}_{\nu=0.5}$	10.92	1.77	0.78	1.17	0.61	0.16	1.74	0.46
$\mathrm{CPP}_{\nu=0.5}$(corr)	15.51	2.51	1.11	1.66	1.20	0.16	3.40	0.46
$\mathrm{CPP}_{\nu=1.0}$	16.71	4.65	2.72	2.43	2.51	0.67	12.81	3.42
$\mathrm{CPP}_{\nu=1.0}$(corr)	23.72	6.61	3.86	3.45	4.90	0.66	25.04	3.39
$\mathrm{CPP}_{\nu=1.5}$	21.53	8.14	5.60	3.76	6.22	1.67	40.70	10.91
$\mathrm{CPP}_{\nu=1.5}$(corr)	30.58	11.55	7.95	5.34	12.16	1.65	79.57	10.81
$\mathrm{CPP}_{\nu=2.0}$	25.55	11.66	8.95	5.03	10.74	2.88	86.12	23.15
$\mathrm{CPP}_{\nu=2.0}$(corr)	36.29	16.56	12.72	7.14	21.00	2.85	168.36	22.93
[23]	14.64	–	–	–	2.745	0.429	–	–
[33]pert.	11.49	–	–	–	0.96	0.33	–	–
[33]nonpert.	12.39	–	–	–	2.74	0.25	–	–
[39]	12.46	–	–	–	2.15	0.22	–	–

Quark mass parameters are fitted to get the experimental ground state masses of m_c=1.31 GeV, m_b=4.66 GeV, α_c=0.4 (for $c\bar{c}$) and α_c=0.3 (for $b\bar{b}$). The potential parameter A also varies with ν [16].

We have done a completely parameter-free computation of digamma and digluon decay widths and radiative electric and magnetic dipole transition widths using the parameters of these phenomenological models that were fixed to obtain the ground state masses of the quarkonia systems.

Table 5. E1 transition partial widths of $c\bar{c}$ (keV).

transitions	ERHM	CPP$_\nu$				[34]	[35]	[23]	[36]	[30]	[22]
		ν=0.5	ν=1.0	ν=1.5	ν=2.0						
$2^3S_1\to1^3P_0$	9.2	6.7	38.2	89.2	145.8	51.7	45	–	47	74	29.8±1.29
$2^3S_1\to1^3P_1$	18.6	13.8	73.6	164.6	259.7	44.9	40.9	–	42.8	62	28.2±1.47
$2^3S_1\to1^3P_2$	11.3	8.4	37.2	72.4	100.3	30.9	26.5	–	30.1	43	26.5±1.3
$3^3S_1\to2^3P_0$	16.4	5.9	51.4	164.3	349.2	–	87.3	–	–	–	
$3^3S_1\to2^3P_1$	43.3	8.4	65.2	192.7	382.9	65.7	–	–	–	–	
$3^3S_1\to2^3P_2$	54.2	1.6	4	4.1	3.1	–	31.6	–	–	–	
$3^3S_1\to1^3P_0$	129.4	105.1	583.9	1389	2274	–	1.2	–	–	–	
$3^3S_1\to1^3P_1$	336.4	281.5	1531	3607	5863	–	2.5	–	–	–	
$3^3S_1\to1^3P_2$	410.1	1897	4379	6998	–	–	3.3	–	–	–	
$1^3P_2\to1^3S_1$	680.7	168	421	652	828	448	390.6	250	315	424	390±26
$1^3P_1\to1^3S_1$	426.2	127	269	363	409	333	287	229	41	314	299±22
$1^3P_0\to1^3S_1$	325.9	110	209	256	264	161	142	173	120	152	133±9
$1^1P_1\to1^1S_0$	1076.2	401	1015	1569	2000	723	610	451	482	498	
$2^3P_2\to2^3S_1$	325.3	151	701	1707	2883	–	358.6	83	–	225	
$2^3P_1\to2^3S_1$	258.9	92	316	596	824	–	208.3	73.8	–	103	
$2^3P_0\to2^3S_1$	231.0	68	190	291	322	–	53.6	49.4	–	61	
$2^1P_1\to2^1S_0$	611.7	184	843	1961	3219	–	–	146.9	–	309	
$2^3P_2\to1^3S_1$	700.1	187	1279	3510	5896	–	33	140	–	101	
$2^3P_1\to1^3S_1$	661.3	160	962	2352	3590	–	28	133	–	83	
$2^3P_0\to1^3S_1$	643.5	146	822	1880	2683	–	21	114	–	74	
$2^3P_1\to1^1S_0$	951.6	93	549	1321	2013	–	–	227	–	134	

Table 6. E1 transition partial widths of $b\bar{b}$ (keV).

transitions	ERHM	CPP$_\nu$				[34]	[35]	[23]	[36]	[30]	[22]
		ν=0.5	ν=1.0	ν=1.5	ν=2.0						
$2^3S_1\to1^3P_0$	0.24	0.06	0.4	1.08	1.63	1.65	1.15	–	1.29	1.67	1.21±0.16
$2^3S_1\to1^3P_1$	0.40	0.12	0.74	1.75	2.71	2.57	1.87	–	2.0	2054	2.21±0.22
$2^3S_1\to1^3P_2$	0.12	0.04	0.38	1.39	3.03	2.53	1.88	–	2.04	2.62	2.29±0.22
$3^3S_1\to2^3P_0$	0.35	0.04	0.32	1.03	2.16	1.65	1.67	–	1.35	1.83	1.2±0.16
$3^3S_1\to2^3P_1$	0.82	0.08	0.62	1.78	3.60	2.65	2.74	–	2.20	2.96	2.56±0.34
$3^3S_1\to2^3P_2$	0.80	0.06	0.30	0.62	0.98	2.89	2.80	–	2.40	3.23	2.66±0.41
$3^3S_1\to1^3P_0$	3.91	2.38	15.4	40.4	72.0	0.124	0.03	–	0.001	0.07	0.055±0.08
$3^3S_1\to1^3P_1$	9.50	6.38	41.1	106.8	188.8	0.307	0.09	–	0.008	0.17	<0.018±0.001
$3^3S_1\to1^3P_2$	9.86	8.22	54.7	153.7	290.8	0.445	0.13	–	0.015	0.25	<0.2±0.32
$1^3P_2\to1^3S_1$	61.96	11.3	26.7	40.1	48.8	42.7	31	44.0	31.6	38	
$1^3P_1\to1^3S_1$	39.58	09.4	21.3	33.3	43.5	37.1	27	42.0	27.8	34	
$1^3P_0\to1^3S_1$	30.72	08.6	18.7	27.8	35.0	29.5	22	37.0	22.0	27	
$1^1P_1\to1^3S_0$	62.70	15.7	37.7	60.4	81.6	–	38	60.0	–	56.8	
$2^3P_2\to2^3S_1$	14.57	04.9	23.4	55.5	96.1	18.8	17	20.4	14.5	18.8	
$2^3P_1\to2^3S_1$	10.65	04.3	18.2	39.5	63.7	15.9	14	12.5	12.4	15.9	
$2^3P_0\to2^3S_1$	8.98	03.9	15.9	32.8	51.1	11.7	10	4.4	9.2	11.7	
$2^1P_1\to2^1S_0$	15.67	05.4	25.4	60.0	102.1	23.6	–	25.8	–	24.7	
$2^3P_2\to1^3S_1$	45.03	09.0	33.0	67.2	104.0	8.41	7.74	20.8	12.7	13	
$2^3P_1\to1^3S_1$	41.71	08.6	30.2	58.9	88.0	8.01	7.31	19.9	12.7	12.4	
$2^3P_0\to1^3S_1$	40.12	08.4	28.8	55.0	80.8	7.36	6.69	14.1	10.9	11.4	
$2^1P_1\to1^1S_1$	49.57	0.3	01.7	04.5	08.2	9.9	–	14.1	10.9	15.9	

3 Digamma and digluon decay widths

Using the model parameters and the radial wave functions, we compute the digamma ($\Gamma_{\gamma\gamma}(\eta_Q)$) and digluon ($\Gamma_{gg}(\chi_Q)$) decay widths. The digamma decay width of the P-wave $Q\bar{Q}$ state χ_{Q1} is forbidden according to the Landau-Yang theorem. Most of the quark model predictions for the S-wave $\eta_Q\to\gamma\gamma$ width are comparable with the experimental result, while the theoretical predictions for the P-wave ($\chi_{Q0,2}\to\gamma\gamma$) widths differ significantly

Table 7. Radiative M1 transition widths of $c\bar{c}$ in (keV).

transition	$1^3S_1\to1^1S_0$	$2^3S_1\to2^1S_0$	$3^3S_1\to3^1S_0$	$2^3S_1\to1^1S_0$
ERHM	0.703 (110)	0.151 (62)	0.023 (17)	20.521 (654)
$CPP_{\nu=0.5}$	1.86	0.03	0.004	16.52
$CPP_{\nu=1.0}$	9.68	0.55	0.135	58.13
$CPP_{\nu=1.5}$	20.45	2.60	0.942	108.44
$CPP_{\nu=2.0}$	38.35	6.92	3.241	157.23
[9]	1.5±1.0	–	–	–
[10]NR	2.90 (116)	0.21 (48)	0.046 (29)	–
[23]	1.29	0.12	0.04	–
[35]	2.7	1.2	–	–
[22]	1.21±0.37	< 0.67	–	3000±500

Table 8. Radiative M1 transition widths of $b\bar{b}$ in (eV).

transition	$1^3S_1\to1^1S_0$	$2^3S_1\to2^1S_0$	$3^3S_1\to3^1S_0$	$2^3S_1\to1^1S_0$
ERHM	2.33 (36)	0.169 (15)	0.050 (10)	1395.9 (580)
$CPP_{\nu=0.5}$	2.51	0.01	0.001	223.23
$CPP_{\nu=1.0}$	9.13	0.17	0.036	799.45
$CPP_{\nu=1.5}$	19.12	0.98	0.244	1629.06
$CPP_{\nu=2.0}$	31.20	2.51	1.088	2514.04
[23]	7.28	0.67	0.19	–
[34]	5.8 (60)	1.40 (33)	0.80 (27)	–
[35]	4.0	0.5	–	–
[36]	8.95	1.51	0.826	–
[37]	9.2	0.6	0.6	–
[38]	7.7 (59)	0.53 (25)	0.13 (16)	–

from the experimental observations [22]. The contribution from QCD corrections takes care of this discrepancy. The one-loop QCD radiative corrections in the digamma decay widths of $^1S_0(\eta_Q)$, $^3P_0(\chi_{Q0})$ and $^3P_2(\chi_{Q2})$ are computed using the non relativistic expressions given by [23, 24]:

$$\Gamma_{\gamma\gamma}(\eta_Q) = \frac{3e_Q^4\alpha_{em}^2 M_{\eta_Q}|R_0(0)|^2}{2m_Q^3}\left[1-\frac{\alpha_s}{\pi}\frac{(20-\pi^2)}{3}\right], \quad (6)$$

$$\Gamma_{\gamma\gamma}(\chi_{Q0}) = \frac{27e_Q^4\alpha_{em}^2 M_{\chi_{Q0}}|R_1^{'}(0)|^2}{2m_Q^5}\left[1+B_0\frac{\alpha_s}{\pi}\right], \quad (7)$$

$$\Gamma_{\gamma\gamma}(\chi_{Q2}) = \frac{4}{15}\frac{27e_Q^4\alpha_{em}^2 M_{\chi_{Q2}}|R_1^{'}(0)|^2}{2m_Q^5}\left[1+B_2\frac{\alpha_s}{\pi}\right], \quad (8)$$

where $B_0=\pi^2/3-28/9$ and $B_2=-16/3$ are the next-to-leading-order (NLO) QCD radiative corrections [25–27].

Similarly, the digluon decay widths of the η_Q, χ_{Q0} and χ_{Q2} states are given by [28]:

$$\Gamma_{gg}(\eta_Q)=\frac{\alpha_s^2 M_{\eta_Q}|R_0(0)|^2}{3m_Q^3}[1+C_Q(\alpha_s/\pi)], \quad (9)$$

$$\Gamma_{gg}(\chi_{Q0})=\frac{3\alpha_s^2 M_{\chi_{Q0}}|R_1^{'}(0)|^2}{m_Q^5}[1+C_{0Q}(\alpha_s/\pi)]. \quad (10)$$

$$\Gamma_{gg}(\chi_{Q2})=\left(\frac{4}{15}\right)\frac{3\alpha_s^2 M_{\chi_{Q2}}|R_1^{'}(0)|^2}{m_Q^5}[1+C_{2Q}(\alpha_s/\pi)]. \quad (11)$$

Here, the quantities in the brackets are the NLO QCD radiative corrections [27] and the coefficients have values of $C_Q=4.4$, $C_{0Q}=10.0$ and $C_{2Q}=-0.1$ for the bottom quark.

4 Radiative E1 and M1 transitions

In the non-relativistic limit, the M1 transition width between two S-wave states is given by [9]

$$\Gamma_{n^3S_1\to n'^1S_0\gamma} = \frac{4}{3}\alpha e_Q^2\frac{k_\gamma^3}{m^2}\left|\int_0^\infty r^2 dr R_{n'0}(r)R_{n0}(r)j_0\left(\frac{k_\gamma r}{2}\right)\right|^2, \quad (12)$$

where e_Q is the fraction of electrical charge of the heavy quark ($e_b=-1/3$, $e_c=2/3$), α is the fine structure constant and $R_{nl}(r)$ are the radial Schrödinger wave functions. The photon energy k_γ is nearly equal to the mass difference of the two quarkonia, so it is of order mv^2 or smaller. This is unlike radiative transitions from a heavy quarkonium to a light meson, such as $J/\psi\to\eta\gamma$, where a hard photon is emitted. Since $r\sim 1/(mv)$, the spherical Bessel function is expanded as $j_0(k_\gamma r/2)=1-(k_\gamma r)^2/24+\cdots$ [9]. While the overlap integral in (12) is unity at leading order for $n=n'$ (allowed transitions), it vanishes for $n\neq n'$ (hindered transitions). The widths of hindered transitions are determined by higher-order and relativistic corrections only.

In the non-relativistic limit, radiative E1 and M1 transition partial widths are given by [9]

$$\Gamma_{n^{2S+1}L_{iJ_i}\to n'^{2S+1}L_{fJ_f}\gamma} = \frac{4\alpha e_Q^2 k_\gamma^3}{3}(2J'+1)\max(L_i,L_f) \times\begin{Bmatrix} J_i & 1 & J_f \\ L_f & S & L_i\end{Bmatrix}\times|\langle f|r|i\rangle|^2, \quad (13)$$

$$\Gamma_{n^3S_1\to n'^1S_0\gamma} = \frac{4}{3}\frac{2J'+1}{2L+1}\delta_{LL'}\delta_{S,S'\pm1}\alpha e_Q^2\frac{k_\gamma^3}{m^2} \times\left|\int_0^\infty r^2 dr R_{n'0}(r)R_{n0}(r)j_0\left(\frac{k_\gamma r}{2}\right)\right|^2. \quad (14)$$

The CLEO-c experiment has measured the magnetic dipole (M1) transitions $J/\psi(1S)\to\gamma\eta_c(1S)$ and $\psi(2S)\to\gamma\eta_c(1S)$ using a combination of inclusive and exclusive techniques reconciling with the theoretical calculations of lattice QCD and effective field theory techniques [8, 9]. M1 transition rates are normally weaker than E1 rates, but they are of more interest because they may allow access to spin-singlet states that are very difficult to produce otherwise. The spectroscopic parameters of ERHM and CPP_ν are utilized for the present computations.

5 Results and conclusions

In this paper, we have employed the masses of the pseudoscalar and vector mesons, their wave functions, and other input parameters from our earlier work [13] for the calculations of the digamma, digluon decay widths as well as E1 & M1 transitions. E1 and M1 radiative transitions of the $c\bar{c}$ and $b\bar{b}$ mesons in the ERHM and Coulomb plus power potential CPP_ν models and computed numerical results are tabulated in Tables 1–8. The digamma and digluon decay widths of the $c\bar{c}$ and $b\bar{b}$ mesons are computed with and without QCD corrections. The ERHM predictions of digamma decay widths of charmonia for the ground state are found to be comparable to the other theoretical results. In case of the CPP_ν model these values are fairly close around $\nu<1$. A similar trend is found in the case of digluon decay rates of charmonia. The digamma and digluon decay widths predicted by the ERHM and CPP_ν models are very close to the other theoretical predictions.

The computations of E1 transition widths are done without any relativistic correction terms. This indicates the possible inclusion of the same in the wave function with a single center size parameter. The E1 and M1 transitions of the $c\bar{c}$ and $b\bar{b}$ mesons have been calculated by several groups (See Tables 5–8) but their predictions are not in mutual agreement. The predictions from References [34, 35] and the CPP_ν model (at $\nu \simeq 1$ for $c\bar{c}$ and at $\nu \simeq 1.5$ for $b\bar{b}$ mesons) are in fair agreement with experimental values. One of the limitations of the CPP_ν model is the inability to obtain the mass spectra of the $c\bar{c}$ and $b\bar{b}$ mesons at the same potential index ν. The computed magnetic radiative transition rates are tabulated along with other theoretical predictions and available experimental values in Tables 7 and 8. The values in the parentheses are the energy of the photon in MeV. The transition widths obtained by the potential models show a large deviation from the experimental data; however, the values computed using effective mean field theories ($\Gamma_{J/\psi\to\eta_c\gamma} = 1.5\pm1.0$ keV and $\Gamma_{\Upsilon(1S)\to\eta_b\gamma} = 3.6\pm2.9$ eV [9]), are found to be nearly the same as the potential model results. The photon energies in all the models are found to be nearly the same as the mass splitting. The wide variation in predicted hyperfine splitting leads to considerable uncertainty in the predicted rates for these transitions. Differences in the theoretical assumptions of the potential models make it difficult to draw sharp conclusion about the validity of a particular model because of the lack of experimental data.

References

1 Wiedner U. Progress in Particle and Nucl. Phys. 2011, **66**: 477
2 Brambilla N et al. hep-ph/0412158
3 Caswell W E, Lepage G P. Phys. Lett. B, 1986, **167**: 437
4 Bodwin G T, Braaten E, Lepage G P. Phys. Rev. D, 1995, **51**: 1125; 1997, **55**: 5853
5 Pineda A, Soto J. Nucl. Phys. Proc. Suppl., 1998, **64**: 428 [arXiv:hep-ph/9707481]
6 Brambilla N, Pineda A, Soto J, Vairo A. Nucl. Phys. B, 2000, **566**: 275 [arXiv:hep-ph/9907240]
7 Brambilla N et al. Eur. Phys. J. C, 2011, **71**: 1534
8 Mitchell R E et al. (CLEO collaboration). Phys. Rev. Lett., 2009, **102**: 011801; Erratum-ibid., 2011, **106**: 159903
9 Brambilla N, JIA Y, Vairo A. Phys. Rev. D, 2006, **73**: 054005
10 Barnes T, Godfrey S, Swanon E S. Phys. Rev. D, 2005, **72**: 054026
11 Vinodkumar P C, Pandya J N, Bannur V M, Khadkikar S B. Eur. Phys. J., A, 1999, **4**: 83
12 Pandya J N, Vinodkumar P C. Pramana J. Phys., 2001 **57**: 821
13 Rai A K, Pandya J N, Vinodkumar P C. Eur. Phys. Jnl. A, 2008, **38**: 77; Jnl. Phys. G, 2005 **31**: 1453
14 Rai A K, Parmar R H, Vinodkumar P C. Jnl. Phys. G, 2002, **28**: 2275
15 Rai A K, Vinodkumar P C. Pramana J. Phys., 2006. **66**: 953
16 Rai A K, Patel B, Vinodkumar P C. Phys. Rev. C, 2008 **78**: 055202
17 Rai A K, Pandya J N, Vinodkumar P C. Nucl. Phys. A, 2007, **782**: 406; Indian J.Phys. A, 2006, **80**: 387
18 Buchmüller W, Tye S H H. Phys. Rev. D, 1981, **24**: 132
19 Khadkikar S B, Gupta S K. Phys. Lett. B, 1983, **124**: 523
20 Gupta S K, Khadkikar S B. Phys. Rev. D, 1987, **36**: 307
21 Jena S N, Behera M R, Panda S. Phys. Rev. D, 1996, **54**: 11
22 Olive K A et al. (Particle Data Group). Chin. Phys. C, 2014 **38**: 090001
23 Parmar A et al. Nucl. Phys. A, 2010, **848**: 299
24 Patel B, Vinodkumar P C. J. Phys. G: Nucl. Part. Phys. 2009 **36**: 035003
25 Kwong Waikwok et al. Phys. Rev. D, 1988 **37**: 3210
26 Barbieri R, Caffo M, Gatto R, Remiddi E. Nucl. Phys. B 1981 **192**: 61
27 Mangano M, Petrelli A. Phys. Lett. B, 1945, **352**: 445
28 Lansberg J P, Pham T N. Phys. Rev. D, 2009, **79**: 094016
29 Shah M, Parmar A, Vinodkumar P C. Phys. Rev. D, 2012, **86**: 034015
30 B. Quing Li, K. Ta Chao. Phys. Rev. D, 2009, **79**: 094004; Bai Quing Li, Kung- Ta Chao. Commun. Theor. Phys. 2009, **52**: 653
31 Schuler G A, Berends F A, van Gulik R. Nucl. Phys. B, 1998, **523**: 423
32 Ahmady M R, Mendel R R. Phys. Rev. D, 1995, **51**: 141
33 Laverty J T, Radford S F, Repko W W. arXiv:0901.3917 [hep-ph]
34 Ebert D, Faustov N, Galkin V O. Phys. Rev. D, 2003, **67**: 014027
35 Radford S F, Repko W W. Phys. Rev. D, 2007 **75**: 074031
36 Brambilla N et al. CERN Yellow Report 2005-005; arxiv://hep-ph/0412158
37 Anisovich V V, Dakhno L G, Matveev M A, Nikonov V A, Sarantsev A V. Phys. Atom. Nucl., 2007, **70**: 63
38 Lähde T A. Nucl.Phys. A, 2003, **714**: 183
39 Gupta Suraj N, Johnson James M, Repko Wayne W. Phys. Rev. D, 1996, **54**: 2075. arXiv:hep-ph/9606349

PHYSICAL REVIEW D **96,** 016017 (2017)

Decay $D \to K^{(*)}\ell^+\nu_\ell$ in covariant quark model

N. R. Soni* and J. N. Pandya†

Applied Physics Department, Faculty of Technology and Engineering,
The Maharaja Sayajirao University of Baroda, Vadodara 390001 Gujarat, India

(Received 6 June 2017; published 24 July 2017)

We study the leptonic and semileptonic D-meson decays ($D \to \ell^+\nu_\ell$ and $D \to K^{(*)}\ell^+\nu_\ell$) in the framework of covariant quark model with built-in infrared confinement. We compute the required form factors in the entire kinematical momentum transfer region. The calculated form factors are used to evaluate the branching fractions of these transitions. We determine the following ratios of the partial widths: $\Gamma(D^0 \to K^- e^+\nu_e)/\Gamma(D^+ \to \bar{K}^0 e^+\nu_e) = 1.02$, $\Gamma(D^0 \to K^-\mu^+\nu_\mu)/\Gamma(D^+ \to \bar{K}^0\mu^+\nu_\mu) = 0.99$ and $\Gamma(D^+ \to \bar{K}^0\mu^+\nu_\mu)/\Gamma(D^+ \to \bar{K}^0 e^+\nu_e) = 0.97$ which are in close resemblance with the isospin invariance and experimental results.

DOI: 10.1103/PhysRevD.96.016017

I. INTRODUCTION

The semileptonic decays involve strong as well as weak interactions. The extraction of Cabibbo-Kobayashi-Maskawa (CKM) matrix elements from these exclusive decays can be parametrized by form factor calculations. As $|V_{cd}|$ and $|V_{cs}|$ are constrained by CKM unitarity, the calculation of semileptonic decays of D-mesons can also be an important test to look for new physics. The decay $D \to K^{(*)}\ell^+\nu_\ell$ provides accurate determination of $|V_{cs}|$. Thus, the theoretical prediction for the form factors and their q^2-dependence need to be tested. A comprehensive review of experimental and theoretical challenges in study of hadronic decays of D and D_s mesons along with required experimental and theoretical tools [1] provide motivation to look into semileptonic decays in this paper.

Recently, BESIII [2–5] and *BABAR* [6] collaborations have reported precise and improved measurements on semileptonic form factors and branching fractions on decays of $D \to K\ell^+\nu_\ell$ and $D \to \pi\ell^+\nu_\ell$. A brief review of the earlier work and present experimental status of D-meson decays are given in [7]. Also there are variety of theoretical models available in the literature for the computation of hadronic form factors. One of the oldest models is based on the quark model known as ISGW model for CP violation in semileptonic B meson decays based on the nonrelativistic constituent quark picture [8]. The advanced version (ISGW2 model [9]) includes the heavy quark symmetry and has been used for semileptonic decays of $B_{(s)}$, $D_{(s)}$ and B_c mesons. The form factors are also calculated in lattice quantum chromodynamics (LQCD) [10–15], light-cone sum rules (LCSR) [16–18] and LCSR with heavy quark effective theory [19]. The form factor calculations from LCSR provide good results at low ($q^2 \simeq 0$) and high ($q^2 \simeq q^2_{\rm max}$) momentum transfers. The form factors have also been calculated for the process $D \to K\ell\nu_\ell$ in the entire momentum transfer range [15] using the LQCD. Also recently the Flavour Lattice Averaging Group (FLAG) have reported the latest lattice results for determination of CKM matrices within the standard model [20].

The form factors of $D, B \to P, V, S$ transitions with P, V and S corresponding to pseudoscalar, vector and scalar meson respectively have been evaluated in the light front quark model (LFQM) [21]. The form factors for $D \to P, V$ are also computed in the framework of chiral quark model (χQM) [22] as well in the phenomenological model based on heavy meson chiral theory (HMχT) [23,24]. The form factors of $B_{(s)}, D_{(s)} \to \pi, K, \eta$ have been evaluated in three flavor hard pion chiral perturbation theory [25]. The form factors for $D \to \pi e^+\nu_e$ have been computed in the framework of "charm-changing current" [26]. The authors of [27,28] have determined the form factors $f_+^{K(\pi)}$ by globally analyzing the available measurements of branching fractions for $D \to K(\pi)e^+\nu_e$. The vector form factors for $D \to K\ell\nu_\ell$ were also parameterized in [29]. The evaluation of transition form factors and decays of $B_{(s)}, D_{(s)} \to f_0(980), K_0^*(1430)\ell\nu_\ell$ has been done in [30,31] from QCD sum rules. The computation of differential branching fractions for $D_{(s)} \to (P, V, S)\ell\nu_\ell$ was also performed using chiral unitary approach [32,33], generalized linear sigma model [34,35] and sum rules [36]. Various decay properties of $D_{(s)}$ and $B_{(s)}$ are also studied in the formalism of semirelativistic [37–40] and relativistic [41–43] potential models.

In this paper, we employ the covariant constituent quark model (CQM) with built-in infrared confinement [44–49] to compute the leptonic and semileptonic decays. The form factors of these transitions are expressed through only few universal functions. One of the key features of CQM is access to the entire physical range of momentum transfer. Our aim is to perform independent calculations of these

*nrsoni-apphy@msubaroda.ac.in
†jnpandya-apphy@msubaroda.ac.in

decays including q^2 behavior of the transition form factors, leptonic decay constants of D and K mesons and ratios of branching fractions for the decay $D \to K^{(*)}\ell^+\nu_\ell$ and $D \to \pi\ell^+\nu_\ell$.

This paper is organized as follows. After a brief introduction of the semileptonic D-meson decays in Sec. I, in Sec. II we introduce the theoretical framework of CQM and also discuss the method of extracting the model parameters. In Sec. III, we give the definition of the form factors for the decays $D \to K^{(*)}\ell^+\nu_\ell$. In Sec. IV for numerical results, we first compute the leptonic branching fractions of D^+-meson. Next we give numerical results of the form factors. We also parametrize the form factors using double pole approximation. From the form factors, we compute the differential branching fraction for the $D \to K^{(*)}\ell^+\nu_\ell$, with $\ell = e$ and μ and the branching fractions. We also calculate the forward-backward asymmetry and convexity parameters. We compare our results with available experimental, lattice and other theoretical results. Finally, we summarize the present work in Sec. V.

II. MODEL

The CQM is an effective quantum field approach [44–49] for hadronic interactions based on an effective Lagrangian of hadrons interacting with their constituent quarks. In this paper, we restrict ourselves to weak decays of D-mesons only. The interaction Lagrangian describing the coupling of meson $M(q_1\bar{q}_2)$ to the constituent quarks q_1 and $\bar{q}_2$ in the framework of CQM is given by

$$\mathcal{L}_{\rm int} = g_M M(x) \int dx_1 dx_2 F_M(x; x_1, x_2)\bar{q}_2(x_2)\Gamma_M q_1(x_1) + \text{H.c.} \quad (1)$$

where Γ_M is the Dirac matrix and projects onto the spin quantum number of relevant mesonic field $M(x)$. g_M is the coupling constant and F_M is the vertex function that is related to the scalar part of the Bethe-Salpeter amplitude. F_M also characterizes the finite size of the mesons. We choose the vertex function that satisfies the Lorentz invariance of the Lagrangian Eq. (1),

$$F_M(x, x_1, x_2) = \delta\left(x - \sum_{i=1}^{2} w_i x_i\right)\Phi_M((x_1 - x_2)^2) \quad (2)$$

with Φ_M is the correlation function of two constituent quarks with masses m_{q_1} and m_{q_2} and $w_{q_i} = m_{q_i}/(m_{q_1} + m_{q_2})$ such that $w_1 + w_2 = 1$. We choose Gaussian function for vertex function as

$$\tilde{\Phi}_M(-p^2) = \exp(p^2/\Lambda_M^2) \quad (3)$$

with the parameter Λ_M characterized by the finite size of the meson. In the Euclidian space, we can write $p^2 = -p_E^2$, so that the vertex function has the appropriate falloff behavior so as to remove the ultraviolet divergence in the loop integral.

We use the compositeness conditions [50,51] to determine the coupling strength g_M in Eq. (5) that requires the renormalization constant Z_M for the bare state to composite mesonic state $M(x)$ set to zero, i.e.,

$$Z_M = 1 - \tilde{\Pi}'_M(m_M^2) = 0, \quad (4)$$

where $\tilde{\Pi}'_M$ is the derivative of meson mass operator and Z_M is the wave function renormalization constant of the meson M. Here, $Z_M^{1/2}$ is the matrix element between the physical state and the corresponding bare state. The above condition guarantees that the physical state does not contain any bare quark state i.e. bound state. The constituents are virtual and are introduced to realize the interaction and as a result the physical state turns dressed and its mass and wave function are renormalized.

The meson mass operator Fig. 1 for any meson is defined as

$$\tilde{\Pi}_M(p^2) = N_c g_M^2 \int \frac{d^4k}{(2\pi)^4 i}\tilde{\Phi}_M^2(-k^2) \times \text{tr}(\Gamma_1 S_1(k + w_1 p)\Gamma_2 S_2(k - w_2 p)) \quad (5)$$

where $N_c = 3$ is the number of colors. Γ_1, Γ_2 are the Dirac matrices and for scalar, vector and pseudoscalar mesons, we choose the gamma matrices accordingly. $S's$ are the quark propagator and we use the free fermion propagator for the constituent quark. For the computation of loop integral in Eq. (5), we write the quark propagator in terms of Fock-Schwinger representation as

$$S_q(k+p) = \frac{1}{m_q - \not{k} - \not{p}} = \frac{m_q + \not{k} + \not{p}}{m_q^2 - (k+p)^2} = (m_q + \not{k} + \not{p})\int_0^\infty d\alpha e^{-\alpha[m_q^2 - (k+p)^2]}, \quad (6)$$

where k is the loop momentum and p is the external momentum. The use of Fock-Schwinger representation allows to do the tensor integral in an efficient way since

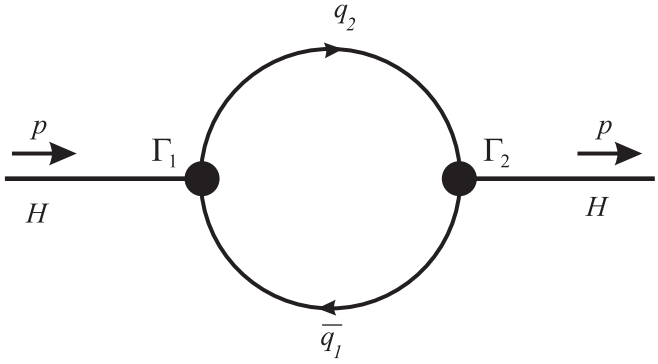

FIG. 1. Diagram describing meson mass operator.

the loop momenta can be converted into the derivative of exponential function [49]. All the necessary trace evaluation and loop integrals are done in FORM [52]. For the remaining integral over the Fock-Schwinger parameters $0 \le \alpha_i \le \infty$, we use an additional integration converting the Fock-Schwinger parameters into a simplex. The transformation reads [53]

$$\prod_{i=1}^{n}\int_0^\infty d\alpha_i f(\alpha_1,\ldots,\alpha_n) = \int_0^\infty dt t^{n-1}\prod_{i=1}^{n}\int d\alpha_i \delta\left(1-\sum_{i=1}^{n}\alpha_i\right) f(t\alpha_1,\ldots,t\alpha_n) \tag{7}$$

For meson case $n = 2$.

While the integral over t in Eq. (7) is convergent below the threshold $p^2 < (m_{q_1} + m_{q_2})^2$, its convergence above threshold $p^2 \ge (m_{q_1} + m_{q_2})^2$ is guaranteed by augmenting the quark mass by an imaginary part, i.e. $m_q \to m_q - i\epsilon, \epsilon > 0$, in the quark propagator Eq. (6). This makes it possible to rotate the integration variable t to the imaginary axis $t \to it$. The integral Eq. (7) in turn becomes convergent but obtains an imaginary part corresponding to quark pair production. However, by reducing the scale of integration at the upper limit corresponding to the introduction of an infrared cutoff

$$\int_0^\infty dt(\ldots) \to \int_0^{1/\lambda^2} dt(\ldots), \tag{8}$$

one can remove all possible thresholds present in the initial quark diagram [49]. Thus the infrared cutoff parameter λ effectively guarantees the confinement of quarks within hadrons.

Before going for the semileptonic decays, we need to specify the independent model parameters namely size parameter of meson Λ and constituent quark masses m_{q_i}. These model parameters are determined by fitting calculated decay constants of basic processes such as leptonic (Fig. 2) and radiative decays to available experimental data

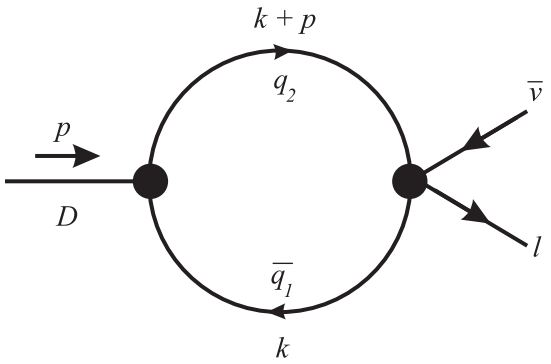

FIG. 2. Quark model diagrams for the D-meson leptonic decay.

TABLE I. Leptonic decay constants f_H (in MeV).

f_H	Present	Data	Reference
f_D	206.1	204.6 ± 5.0	PDG [57]
		207.4 (3.8)	LQCD [58]
		210 ± 11	QCDSR [59]
f_{D^*}	244.3	263 ± 21	QCDSR [59]
		$278 \pm 13 \pm 10$	LQCD [60]
f_{D_s}	257.5	257.5 ± 4.6	PDG [57]
		254 (2) (4)	LQCD [61]
		250.2 ± 3.6	LQCD [12]
		247.2 (4.1)	LQCD [58]
		259 ± 10	QCDSR [59]
$f_{D_s^*}$	272.0	308 ± 21	QCDSR [59]
		311 ± 9	LQCD [60]
f_{D_s}/f_D	1.249	1.258 ± 0.038	PDG [57]
		1.192 (0.22)	LQCD [58]
		1.23 ± 0.07	QCDSR [59]
f_K	156.0	155.0 (1.9)	LQCD [58]
		155.37 (34)	LQCD [62]
		157.9 ± 1.5	LQCD [12]
f_{K^*}	226.8	217 ± 7	PDG [57]
f_π	130.3	132.3 ± 1.6	LQCD [12]
		130.39 (20)	LQCD [62]

or LQCD for vector and pseudoscalar mesons. We use the updated least square fit performed in the recent papers of the model parameters [54–56] (all in GeV). We take the infrared cutoff parameter λ to be the same throughout this study.

$m_{u/d}$	m_s	m_c	m_b	λ	
0.241	0.428	1.67	5.05	0.181	GeV

and the size parameters

Λ_D	Λ_{D^*}	Λ_K	Λ_{K^*}	Λ_π	
1.6	1.53	1.01	0.80	0.87	GeV

We have listed our results for the leptonic decay constants of $D_{(s)}^{(*)}$, $K^{(*)}$ and π mesons in the Table I. The decay constants we use in our calculations match quite well with Particle Data Group (PDG), LQCD and QCD sum rules (QCDSR) results.

III. FORM FACTORS

In the standard model of particle physics, semileptonic decays of any meson is caused by weak force in which one lepton and corresponding neutrino is produced in addition to one or more hadrons (Fig. 3).

The invariant matrix element for the semileptonic $D \to K^{(*)}\ell^+\nu_\ell$ decay can be written as

$$M(D \to K^{(*)}\ell^+\nu_\ell) = \frac{G_F}{\sqrt{2}} V_{cs} \langle K^{(*)}|\bar{s}O^\mu c|D\rangle \ell^+ O^\mu \nu_\ell \tag{9}$$

where $O^\mu = \gamma^\mu(1-\gamma_5)$ is the weak Dirac matrix with left chirality. The matrix elements for the above semileptonic transitions in the covariant quark model are written as

$$\begin{aligned}\langle K_{[\bar{d}s]}(p_2)|\bar{s}O^\mu c|D_{[\bar{d}c]}(p_1)\rangle &= N_c g_D g_K \int \frac{d^4k}{(2\pi)^4 i}\tilde{\phi}_D(-(k+w_{13}p_1)^2)\tilde{\phi}_K(-(k+w_{23}p_2)^2) \\ &\times \mathrm{tr}[O^\mu S_1(k+p_1)\gamma^5 S_3(k)\gamma^5 S_2(k+p_2)] \\ &= F_+(q^2)P^\mu + F_-(q^2)q^\mu \end{aligned} \tag{10}$$

$$\begin{aligned}\langle K^*_{[\bar{d}s]}(p_2,\epsilon_\nu)|\bar{s}O^\mu c|D_{[\bar{d}c]}(p_1)\rangle &= N_c g_D g_{K^*} \int \frac{d^4k}{(2\pi)^4 i}\tilde{\phi}_D(-(k+w_{13}p_1)^2)\tilde{\phi}_{K^*}(-(k+w_{23}p_2)^2) \\ &\times \mathrm{tr}[O^\mu S_1(k+p_1)\gamma^5 S_3(k)\epsilon_\nu^\dagger S_2(k+p_2)] \\ &= \frac{\epsilon_\nu^\dagger}{m_1+m_2}[-g^{\mu\nu}P\cdot qA_0(q^2) + P^\mu P^\nu A_+(q^2) + q^\mu P^\nu A_-(q^2) + i\varepsilon^{\mu\nu\alpha\beta}P_\alpha q_\beta V(q^2)] \end{aligned} \tag{11}$$

with $P = p_1 + p_2$, $q = p_1 - p_2$ and ϵ_ν to be the polarization vector such that $\epsilon_\nu^\dagger \cdot p_2 = 0$ and on-shell conditions of particles require $p_1^2 = m_1^2 = m_D^2$ and $p_2^2 = m_2^2 = m_{K^{(*)}}^2$. Since there are three quarks involved in this transition, we use the notation $w_{ij} = m_{q_j}/(m_{q_i} + m_{q_j})$ $(i,\ j = 1,\ 2,\ 3)$ such that $w_{ij} + w_{ji} = 1$.

IV. NUMERICAL RESULTS

Having determined the necessary model parameters and form factors, we are now in position to present our numerical results. We first compute pure leptonic decays of D^+-meson and then using the form factors obtained in Sec. III, we compute branching fractions for semileptonic D-meson decays.

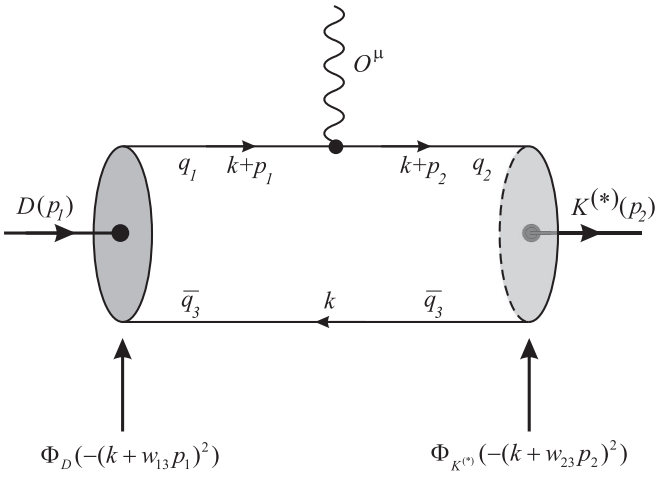

FIG. 3. Quark model diagrams for the D-meson semileptonic decay.

We compute the pure leptonic decays of $D^+ \to \ell^+\nu_\ell$ within the standard model. The branching fraction for leptonic decay is given by

$$\mathcal{B}(D^+ \to \ell^+\nu_\ell) = \frac{G_F^2}{8\pi} m_D m_\ell^2 \left(1 - \frac{m_\ell^2}{m_D^2}\right)^2 f_D^2 |V_{cd}|^2 \tau_D \tag{12}$$

where G_F is the fermi coupling constant, m_D and m_ℓ are the D-meson and lepton masses respectively and τ_D is the D-meson lifetime. f_D is the leptonic decay constant of D-meson from Table I. The resultant branching fractions for $\ell = \tau$, μ and e are given in Table II. It is important to note that the helicity flip factor $(1 - m_\ell^2/m_D^2)$ affects the leptonic branching fractions because of the different lepton masses. We also compare our results with the experimental data. The branching fraction for $D^+ \to \mu^+\nu_\mu$ shows very good agreement with BESIII [63] and CLEO-c [64] data. The branching fractions for $D^+ \to e^+\nu_e$ and $D^+ \to \tau^+\nu_\tau$ also fulfill the experimental constraints.

In Figs. 4 and 5, we plot our calculated form factors as a function of momentum transfer squared in the entire range $0 \le q^2 \le q^2_{\max} = (m_D - m_{K^{(*)}})^2$. The multidimensional integral (three-fold for semileptonic case) appearing in Eqs. (10) and (11) are computed numerically using

TABLE II. Leptonic D^+-decay branching fraction ($\tau_{D^+} = 1.040 \times 10^{-12}$ s [57]).

Channel	Present	Data	Reference
$D^+ \to e^+\nu_e$	8.953×10^{-9}	$<8.8 \times 10^{-6}$	PDG [57]
$D^+ \to \mu^+\nu_\mu$	3.803×10^{-4}	$(3.71 \pm 0.19) \times 10^{-4}$	BESIII [63]
		$(3.82 \pm 0.32) \times 10^{-4}$	CLEO-c [64]
$D^+ \to \tau^+\nu_\tau$	1.013×10^{-3}	$<1.2 \times 10^{-3}$	PDG [57]

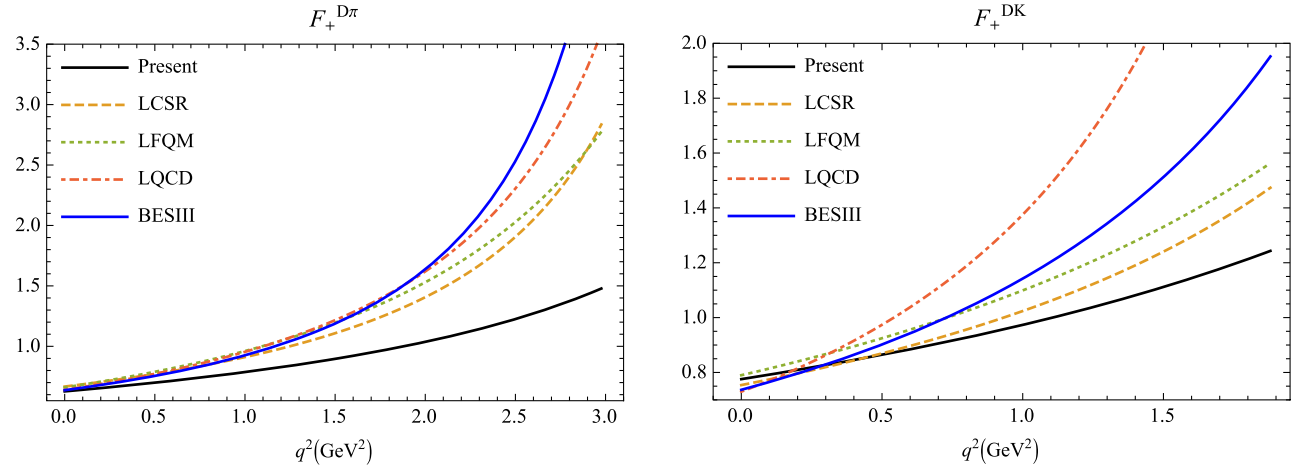

FIG. 4. The results for the form factors appearing in Eq. (10) for semileptonic $D \to \pi$ and $D \to K$ transitions. We compare our plot with the results from LCSR Ref. [18], LFQM Ref. [21], LQCD Ref. [10] as well with the BESIII data Ref. [4].

Mathematica. Our form factor results are also well represented by the double-pole parametrization

$$F(q^2) = \frac{F(0)}{1 - as + bs^2}, \qquad s = \frac{q^2}{m_1^2}. \tag{13}$$

The numerical results of form factors and associated double-pole parameters are listed in Table III. In Fig. 4, we plot the form factor F_+ for $D \to K(\pi)\ell^+\nu_\ell$ decays in the entire kinematical range of momentum transfer. We compare our plot with the results from LCSR Ref. [18], LFQM

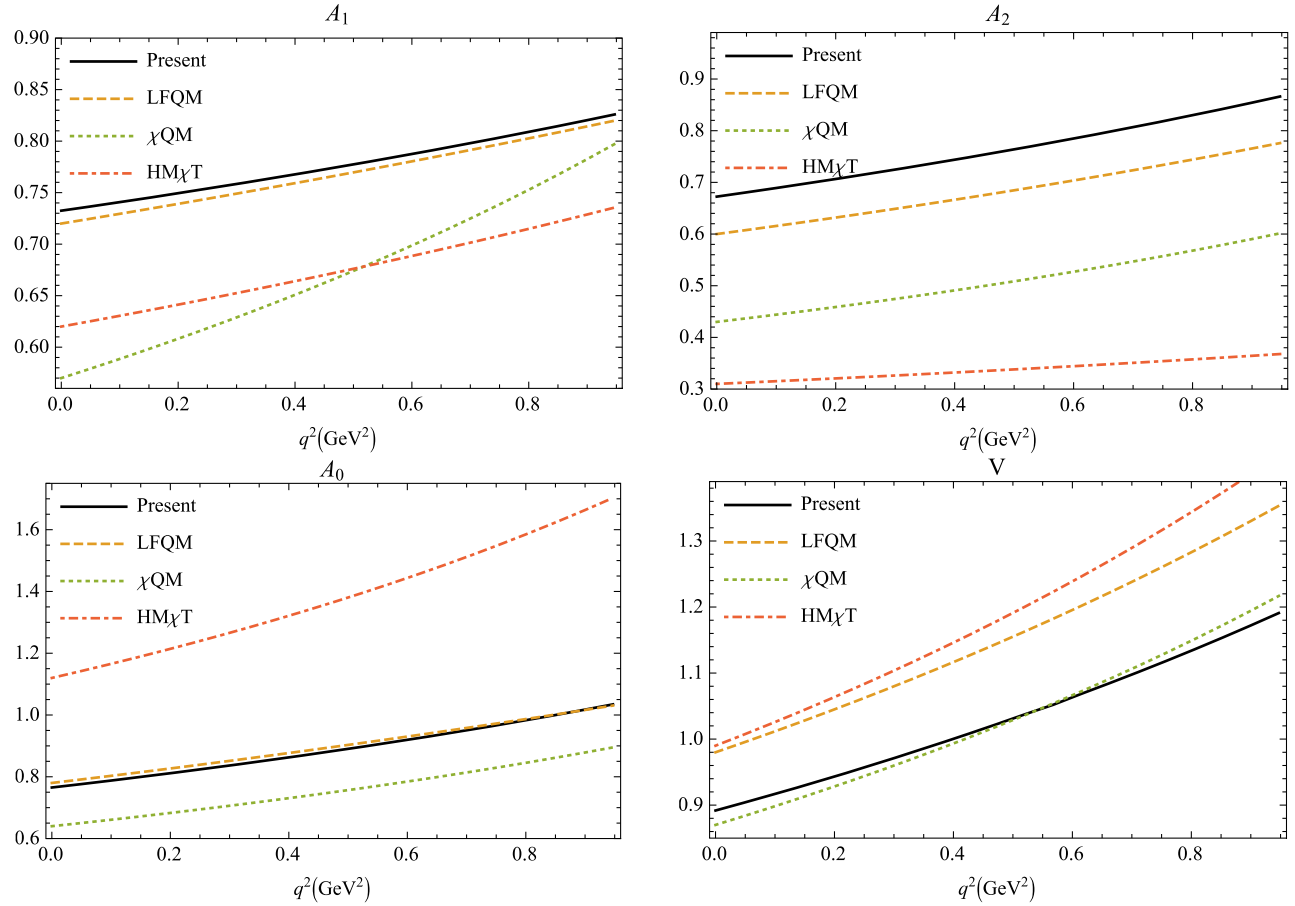

FIG. 5. The form factors appearing in Eq. (11) for semileptonic $D \to K^*$ transitions. We compare our results with LFQM Ref. [21], chiral quark model (χQM) Ref. [22] and heavy meson chiral theory (HMχT) [24].

TABLE III. Double pole parameters for the computation of form factors in Eq. (13).

	F_+	F_-	A_0	A_+	A_-	V
$F(0)$	0.76	−0.39	2.07	0.67	−0.90	0.89
a	0.72	0.75	0.39	0.84	0.95	0.96
b	0.046	0.032	−0.10	0.087	0.13	0.13

Ref. [21], LQCD Ref. [10] as well with the BESIII data Ref. [4]. Our results at maximum recoil point $q^2 \to 0$ are in very good agreement with the other approaches as well as with the experimental result. A similar plot can be obtained for form factor F_-. We also plot the vector form factors and for the comparison of the form factors for $D \to K^* \ell^+ \nu_\ell$ transition with other approaches, we need to write our form factors Eq. (11) in terms of those used in Ref. [17]. The relations read

$$A_0 = \frac{m_1 + m_2}{m_1 - m_2} A_1, \qquad A_+ = A_2,$$
$$A_- = \frac{2m_2(m_1 + m_2)}{q^2}(A_3 - A_0), \qquad V = V. \quad (14)$$

The form factors in Eq. (14) also satisfy the constraints

$$A_0(0) = A_3(0)$$
$$2m_2 A_3(q^2) = (m_1 + m_2)A_1(q^2) - (m_1 - m_2)A_2(q^2). \quad (15)$$

Figure 5 shows form factors from the present calculation along with the results from LFQM [21], chiral quark model (χQM) [22] and with heavy meson chiral theory (HMχT) [24]. The plot shows that our results of the form factors A_0, A_1 and A_2 match with LFQM [21] and the vector form factors match with the χQM [22] where the authors have used energy scaling parameters extracted from modified low energy effective theory in $H \to V$ transitions. Our results show little deviation from those obtained using HMχT [24]. In computation of form factors for $q^2 = 0$ using LCSR, the authors of [18] have used the $\overline{\text{MS}}$ scheme for c-quark mass and the computation of form factors for $q \geq 0$ is performed in the form of conformal mapping and series parametrization. In the LFQM [21], the authors have used the method of double pole approximation, where as in BESIII [4] and *BABAR* [6] experiment, the form factors are parametrized in terms of two and three parameters series expansion respectively.

The differential branching fractions for semileptonic $D \to K \ell^+ \nu_\ell$ decay are computed using [65,66]

$$\frac{d\Gamma(D \to K \ell^+ \nu_\ell)}{dq^2} = \frac{G_F^2 |V_{cs}|^2 |p_2| q^2 v^2}{12(2\pi)^3 m_1^2} \times ((1 + \delta_\ell)\mathcal{H}_L + 3\delta_\ell \mathcal{H}_{SL}) \quad (16)$$

where the helicity flip factor $\delta_\ell = m_\ell^2/2q^2$, $|p_2| = \lambda^2(m_1^2, m_2^2, q^2)/2m_1$ is momentum of K meson in the rest frame of D-meson and velocity-type parameter $v = 1 - m_\ell^2/q^2$.

The bilinear combinations of the helicity amplitudes $\mathcal{H}$ are defined as [48],

$$\mathcal{H}_L = |H_0|^2, \qquad \mathcal{H}_S = |H_t|^2, \qquad \mathcal{H}_{SL} = \text{Re}(H_0 H_t^\dagger) \quad (17)$$

and the helicity amplitudes are expressed via the form factor in the matrix element as,

$$H_t = \frac{1}{\sqrt{q^2}}(PqF_+ + q^2 F_-) \quad (18)$$

$$H_0 = \frac{2m_1|p_2|}{\sqrt{q^2}} F_+. \quad (19)$$

Similarly the differential branching fractions for semileptonic $D \to K^* \ell^+ \nu_\ell$ decay is computed by [65,66]

$$\frac{d\Gamma(D \to K^* \ell^+ \nu_\ell)}{dq^2} = \frac{G_F^2 |V_{cs}|^2 |p_2| q^2 v^2}{12(2\pi)^3 m_1^2} \times ((1 + \delta_\ell)(\mathcal{H}_U + \mathcal{H}_L) + 3\delta_\ell \mathcal{H}_S). \quad (20)$$

The bilinear combinations of the helicity amplitudes $\mathcal{H}$ are defined as [48]

$$\mathcal{H}_U = |H_{+1+1}|^2 + |H_{-1-1}|^2,$$
$$\mathcal{H}_P = |H_{+1+1}|^2 - |H_{-1-1}|^2,$$
$$\mathcal{H}_L = |H_{00}|^2, \qquad \mathcal{H}_S = |H_{t0}|^2,$$
$$\mathcal{H}_{SL} = \text{Re}(H_{00} H_{t0}^\dagger) \quad (21)$$

here also the helicity amplitudes are expressed via the form factor in the matrix element as

$$H_{t0} = \frac{1}{m_1 + m_2} \frac{m_1|p_2|}{m_2\sqrt{q^2}}(Pq(-A_0 + A_+) + q^2 A_-) \quad (22)$$

$$H_{\pm 1 \pm 1} = \frac{1}{m_1 + m_2}(-PqA_0 \pm 2m_1|p_2|V) \quad (23)$$

$$H_{00} = \frac{1}{m_1 + m_2} \frac{1}{2m_2\sqrt{q^2}} \times (-Pq(m_1^2 - m_2^2 - q^2)A_0 + 4m_1^2|p_2|^2 A_+). \quad (24)$$

In Fig. 6, we present our results for differential branching fractions of $D \to K^{(*)} \ell^+ \nu_\ell$ in the entire kinematical range of momentum transfer. The semileptonic branching

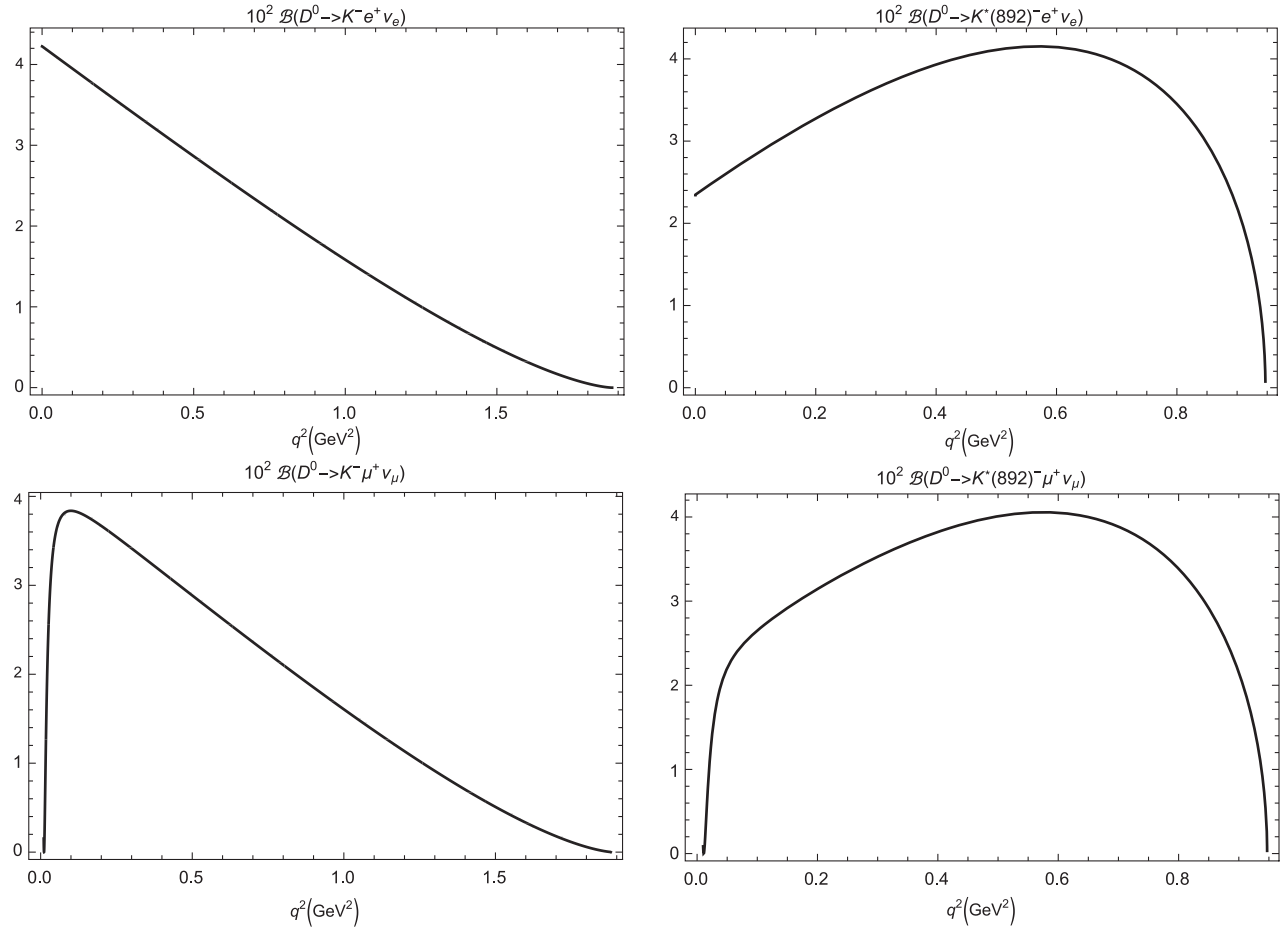

FIG. 6. Differential branching fractions of the decays $D \to K^{(*)}\ell^+\nu_\ell$.

TABLE IV. Branching fractions of $D \to K^{(*)}\ell^+\nu_\ell$ and $D \to \pi\ell^+\nu_\ell$ (in %).

Channel	Present	Data	Reference
$D^+ \to \bar{K}^0 e^+\nu_e$	8.84	$8.60 \pm 0.06 \pm 0.15$	BESIII [2]
		$8.83 \pm 0.10 \pm 0.20$	CLEO-c [72]
$D^+ \to \bar{K}^0\mu^+\nu_\mu$	8.60	$8.72 \pm 0.07 \pm 0.18$	BESIII [3]
$D^+ \to \pi^0 e^+\nu_e$	0.619	$0.363 \pm 0.08 \pm 0.05$	BESIII [2]
		$0.405 \pm 0.016 \pm 0.009$	CLEO-c [72]
$D^+ \to \pi^0\mu^+\nu_\mu$	0.607	–	–
$D^+ \to \bar{K}^*(892)^0 e^+\nu_e$	8.35	–	–
$D^+ \to \bar{K}^*(892)^0\mu^+\nu_\mu$	7.94	–	–
$D^0 \to K^- e^+\nu_e$	3.46	3.538 ± 0.033	PDG [57]
		$3.505 \pm 0.014 \pm 0.033$	BESIII [4]
		$3.50 \pm 0.03 \pm 0.04$	CLEO-c [72]
		$3.45 \pm 0.07 \pm 0.20$	Belle [73]
$D^0 \to K^-\mu^+\nu_\mu$	3.36	3.33 ± 0.13	PDG [57]
		$3.505 \pm 0.014 \pm 0.033$	BESIII
$D^0 \to \pi^- e^+\nu_e$	0.239	$0.2770 \pm 0.0068 \pm 0.0092$	*BABAR* [6]
		$0.295 \pm 0.004 \pm 0.003$	BESIII [4]
		$0.288 \pm 0.008 \pm 0.003$	CLEO-c [72]
		$0.255 \pm 0.019 \pm 0.016$	Belle [73]
$D^0 \to \pi^-\mu^+\nu_\mu$	0.235	0.238 ± 0.024	PDG [57]
$D^0 \to K^*(892)^- e^+\nu_e$	3.25	2.16 ± 0.16	PDG [57]
$D^0 \to K^*(892)^-\mu^+\nu_\mu$	3.09	1.92 ± 0.25	PDG [57]

TABLE V. Ratios of the semileptonic decays of D mesons.

Ratio	Value
$\Gamma(D^0 \to K^- e^+ \nu_e)/\Gamma(D^+ \to \bar{K}^0 e^+ \nu_e)$	1.02
$\Gamma(D^0 \to K^- \mu^+ \nu_\mu)/\Gamma(D^+ \to \bar{K}^0 \mu^+ \nu_\mu)$	0.99
$\Gamma(D^+ \to \bar{K}^0 \mu^+ \nu_\mu)/\Gamma(D^+ \to \bar{K}^0 e^+ \nu_e)$	0.97

fractions in Eqs. (16) and (20) are computed by numerically integrating the differential branching fractions shown in Fig. 6. The branching fractions for $D \to K^{(*)} \ell^+ \nu_\ell$ and $D \to \pi \ell^+ \nu_\ell$ are presented in Table IV. We also compare our results with experimental results. The results for $\mathcal{B}(D^+ \to \bar{K}^0 \ell^+ \nu_\ell)$ and $\mathcal{B}(D^0 \to K^- \ell^+ \nu_\ell)$, ($\ell = e$ and μ) show excellent agreement with the recent BESIII data [2–4] as well with the other experimental collaborations. Also the ratios of the different semileptonic decay widths for the channels $D \to K \ell^+ \nu_\ell$ are presented in Table V and our results are well within the isospin conservation rules given in Ref. [67]. We also present our results for $\mathcal{B}(D^0 \to K^*(892)^- \ell^+ \nu_e)$ but our results overestimate the data given in PDG [57]. This deviation of the present study within the standard model might be explained through hadronic uncertainty or ratios of differential distributions for longitudinal and transverse polarizations of these K^* mesons [68]. The FOCUS [69] and CLEO-c [70] experiments have also reported mixing of scalar amplitudes with dominant vector decays. These observations open up new possibilities of investigations in charm semileptonic decays. There have also been attempts to explain these exclusive decays using R-parity violating supersymmetric effects [71] and their direct correlation with possible supersymmetric signals expected from LHC and BESIII data. We predict the branching fractions for $D^+ \to \bar{K}^*(892)^0 \ell^+ \nu_e$ but we do not compare our results since no experimental results are available for this channel.

We also present our results for branching fractions of $D^+ \to \pi^0 \ell^+ \nu_\ell$ and $D^0 \to \pi^- \ell^+ \nu_\ell$ transitions. Our prediction for $\mathcal{B}(D^+ \to \pi^0 e^+ \nu_e)$ is higher than BESIII [2] and CLEO-c data [72] while the trend is opposite in the case of $\mathcal{B}(D^0 \to \pi^- e^+ \nu_e)$. The deviation of the $\mathcal{B}(D^+ \to \pi^0 e^+ \nu_e)$ from experimental and LQCD data might be attributed to the computed form factors. However, our $\mathcal{B}(D^0 \to \pi^- e^+ \nu_e)$ is in close proximity to that by Belle [73] and $\mathcal{B}(D^0 \to \pi^- \mu^+ \nu_\mu)$ is in excellent agreement with PDG data [57].

We also list some more physical observables in terms of helicity amplitudes. We have already shown the computed differential branching fractions in Fig. 6. Next, the helicity amplitudes defined above are used to plot the

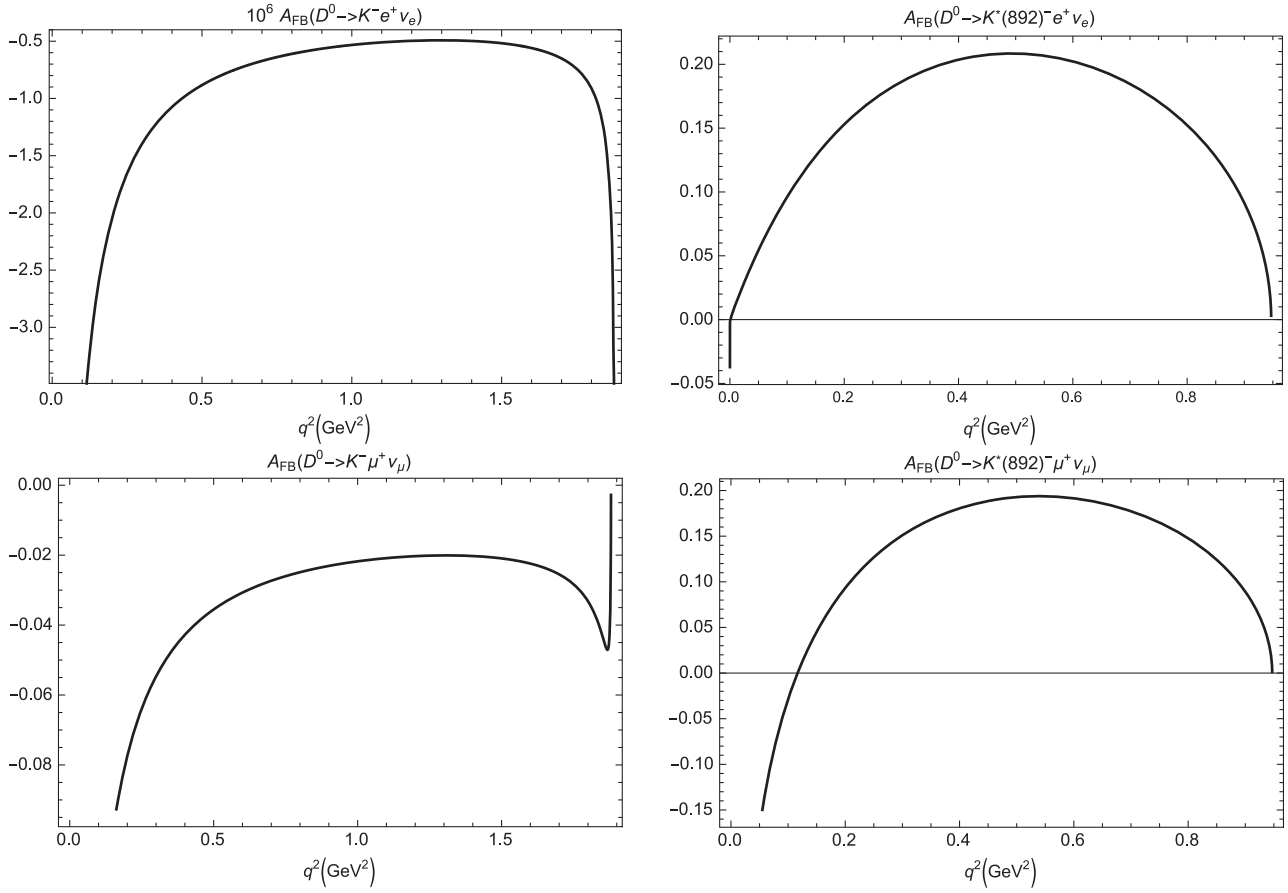

FIG. 7. Forward-backward asymmetries of the decays $D \to K^{(*)} \ell^+ \nu_\ell$.

TABLE VI. Averages of forward-backward asymmetry and convexity parameters.

Channel	ℓ	$\langle A_{FB}^{\ell}\rangle$	$\langle C_F^{\ell}\rangle$	$\langle C_F^{h}\rangle$
$D \to K$	e	-4.27×10^{-6}	-1.5	3
	μ	-0.058	-1.32	3
$D \to K^*$	e	0.17	-0.45	0.91
	μ	0.13	-0.37	0.89

forward-backward asymmetry in Fig. 7 for $D \to K^{(*)}\ell^+\nu_\ell$ in the entire kinematical range of momentum transfer. We use the following relation for plotting the forward-backward asymmetry (A_{FB}) [55,65]

$$\mathcal{A}_{FB}(q^2) = -\frac{3}{4}\frac{\mathcal{H}_P + 4\delta_\ell \mathcal{H}_{SL}}{(1+\delta_\ell)(\mathcal{H}_U + \mathcal{H}_L) + 3\delta_\ell \mathcal{H}_S}. \quad (25)$$

It is evident from Fig. 7 that the $A_{FB}(q^2)$ for $D \to K\ell^+\nu_\ell$ and $D \to K^*\ell^+\nu_\ell$ are similar for both e and μ modes. $A_{FB}(q^2) \to 0$ for in the both zero recoil and larger recoil limits because of the zero recoil relations of the helicity functions $\mathcal{H}_P = \mathcal{H}_{SL} = 0$ and longitudinal dominance in the partial rates at the maximum recoil.

Also the lepton and hadron side convexity parameter are defined as [55,65]

$$C_F^{\ell} = \frac{3}{4}\frac{(1-2\delta_\ell)(\mathcal{H}_U - 2\mathcal{H}_L)}{(1+\delta_\ell)(\mathcal{H}_U + \mathcal{H}_L) + 3\delta_\ell \mathcal{H}_S} \quad (26)$$

and

$$C_F^{h} = -\frac{3}{2}\frac{(1+\delta_\ell)(\mathcal{H}_U - 2\mathcal{H}_L) - 6\delta_\ell \mathcal{H}_S}{(1+\delta_\ell)(\mathcal{H}_U + \mathcal{H}_L) + 3\delta_\ell \mathcal{H}_S}. \quad (27)$$

The plot for the convexity parameters Eqs. (26) and (27) as a function of entire momentum transfer range can easily be obtained. In Table VI, we give the q^2 averages of the above observables. Note that in order to obtain the averages of these observables, we need to multiply the numerator and denominator by phase space factor $|p_2|q^2v^2$. Also in computation of leptonic and semileptonic branching fractions, forward-backward asymmetry and convexity parameters, the values of CKM matrices namely $|V_{cs}|$ and $|V_{cd}|$, meson masses, lepton masses and their lifetimes are taken from PDG [57].

V. CONCLUSION

In this article, we have analyzed the leptonic ($D^+ \to e^+\nu_e$) and semileptonic ($D \to K^{(*)}\ell^+\nu_\ell$, $D \to \pi\ell^+\nu_\ell$) decays using covariant quark model with infrared confinement within the standard model framework. The ratios of the partial widths are found to be consistent with the isospin conservation holding within uncertainties in experimental data. It is interesting to note here that the $\mathcal{B}(D^+ \to \pi^0\ell^+\nu_\ell)$ deviate from existing data while $\mathcal{B}(D^0 \to \pi^-\ell^+\nu_\ell)$ match well. Further exploration to this observation may lead to interesting outcome.

The deviation of branching fractions in case of $D \to K^*\ell\nu_\ell$ might be understood by underlying hadronic uncertainty or ratios of differential distributions for longitudinal and transverse polarizations of the K^* mesons. We are looking forward to analyzing $D \to K^*\ell^+\nu_\ell$ decay and expect the experimental facilities to throw more light on their form factor shapes in forthcoming attempts that will help in understanding the charm decays and possibly the dynamics of these systems beyond the standard model.

ACKNOWLEDGMENTS

We thank Prof. Mikhail A. Ivanov for the continuous support through out this work and providing critical remarks for improvement of the manuscript. N. R. S. would like to thank Bogoliubov Laboratory of Theoretial Physics, Joint Institute for Nuclear Research for warm hospitality during Helmholtz-DIAS International Summer School "Quantum Field Theory at the Limits: from Strong Field to Heavy Quarks" where this work was initiated. This work is done under Major Research Project F.No. 42-775/2013 (SR) with financial support from the University Grants Commission of India.

[1] A. Ryd and A. A. Petrov, Rev. Mod. Phys. **84**, 65 (2012).
[2] M. Ablikim *et al.* (BESIII Collaboration), arXiv:1703.09084.
[3] M. Ablikim *et al.* (BESIII Collaboration), Eur. Phys. J. C **76**, 369 (2016).
[4] M. Ablikim *et al.* (BESIII Collaboration), Phys. Rev. D **92**, 072012 (2015).
[5] M. Ablikim *et al.* (BESIII Collaboration), Phys. Rev. D **92**, 112008 (2015).
[6] J. P. Lees *et al.* (*BABAR* Collaboration), Phys. Rev. D **91**, 052022 (2015).
[7] Y. Amhis *et al.*, arXiv:1612.07233.
[8] N. Isgur, D. Scora, B. Grinstein, and M. B. Wise, Phys. Rev. D **39**, 799 (1989).
[9] D. Scora and N. Isgur, Phys. Rev. D **52**, 2783 (1995).
[10] C. Aubin *et al.* (Fermilab Lattice, HPQCD, MILC Collaboration), Phys. Rev. Lett. **94**, 011601 (2005).

[11] C. Bernard *et al.* (Fermilab Lattice and MILC Collaborations), Phys. Rev. D **80**, 034026 (2009).
[12] H. Na, C. T. H. Davies, E. Follana, G. P. Lepage, and J. Shigemitsu (HPQCD Collaboration), Phys. Rev. D **82**, 114506 (2010).
[13] A. Al-Haydari, A. Ali Khan, V. M. Braun, S. Collins, M. Göckeler, G. N. Lacagnina, M. Panero, A. Schäfer, and G. Schierholz (QCDSF Collaboration), Eur. Phys. J. A **43**, 107 (2010).
[14] H. Na, C. T. H. Davies, E. Follana, J. Koponen, G. P. Lepage, and J. Shigemitsu (HPQCD Collaboration), Phys. Rev. D **84**, 114505 (2011).
[15] J. Koponen, C. T. H. Davies, G. C. Donald, E. Follana, G. P. Lepage, H. Na, and J. Shigemitsu, arXiv:1305.1462.
[16] A. Khodjamirian, R. Ruckl, S. Weinzierl, C. W. Winhart, and O. I. Yakovlev, Phys. Rev. D **62**, 114002 (2000).
[17] A. Khodjamirian, T. Mannel, and N. Offen, Phys. Rev. D **75**, 054013 (2007).
[18] A. Khodjamirian, C. Klein, T. Mannel, and N. Offen, Phys. Rev. D **80**, 114005 (2009).
[19] W. Y. Wang, Y. L. Wu, and M. Zhong, Phys. Rev. D **67**, 014024 (2003).
[20] S. Aoki *et al.*, Eur. Phys. J. C **77**, 112 (2017).
[21] R. C. Verma, J. Phys. G **39**, 025005 (2012).
[22] T. Palmer and J. O. Eeg, Phys. Rev. D **89**, 034013 (2014).
[23] S. Fajfer and J. F. Kamenik, Phys. Rev. D **71**, 014020 (2005).
[24] S. Fajfer and J. F. Kamenik, Phys. Rev. D **72**, 034029 (2005).
[25] J. Bijnens and I. Jemos, Nucl. Phys. **B846**, 145 (2011).
[26] B. Ananthanarayan, I. Caprini, and I. Sentitemsu Imsong, Eur. Phys. J. A **47**, 147 (2011).
[27] G. Rong, Y. Fang, H. L. Ma, and J. Y. Zhao, Phys. Lett. B **743**, 315 (2015).
[28] Y. Fang, G. Rong, H. L. Ma, and J. Y. Zhao, Eur. Phys. J. C **75**, 10 (2015).
[29] S. Descotes-Genon and A. Le Yaouanc, J. Phys. G **35**, 115005 (2008).
[30] M.-Z. Yang, Phys. Rev. D **73**, 034027 (2006); **73**, 079901 (E) (2006).
[31] I. Bediaga, F. S. Navarra, and M. Nielsen, Phys. Lett. B **579**, 59 (2004).
[32] T. Sekihara and E. Oset, Phys. Rev. D **92**, 054038 (2015).
[33] J.-J. Xie, L.-R. Dai, and E. Oset, Phys. Lett. B **742**, 363 (2015).
[34] A. H. Fariborz, R. Jora, J. Schechter, and M. N. Shahid, Int. J. Mod. Phys. A **30**, 1550012 (2015).
[35] A. H. Fariborz, R. Jora, J. Schechter, and M. Naeem Shahid, Phys. Rev. D **84**, 094024 (2011).
[36] W. Wang and C.-D. Lü, Phys. Rev. D **82**, 034016 (2010).
[37] V. Kher, N. Devlani, and A. K. Rai, Chin. Phys. C **41**, 073101 (2017).
[38] N. Devlani and A. K. Rai, Int. J. Theor. Phys. **52**, 2196 (2013).
[39] N. Devlani and A. K. Rai, Eur. Phys. J. A **48**, 104 (2012).
[40] N. Devlani and A. K. Rai, Phys. Rev. D **84**, 074030 (2011).
[41] M. Shah, B. Patel, and P. C. Vinodkumar, Phys. Rev. D **93**, 094028 (2016).
[42] M. Shah, B. Patel, and P. C. Vinodkumar, Eur. Phys. J. C **76**, 36 (2016).
[43] M. Shah, B. Patel, and P. C. Vinodkumar, Phys. Rev. D **90**, 014009 (2014).
[44] G. V. Efimov and M. A. Ivanov, Int. J. Mod. Phys. A **04**, 2031 (1989).
[45] G. V. Efimov and M. A. Ivanov, *The Quark Confinement Model of Hadrons* (IOP, Bristol, 1993).
[46] M. A. Ivanov and P. Santorelli, Phys. Lett. B **456**, 248 (1999).
[47] M. A. Ivanov, P. Santorelli, and N. Tancredi, Eur. Phys. J. A **9**, 109 (2000).
[48] A. Faessler, T. Gutsche, M. A. Ivanov, J. G. Körner, and V. E. Lyubovitskij, Eur. Phys. J. direct C **4**, 1 (2002).
[49] T. Branz, A. Faessler, T. Gutsche, M. A. Ivanov, J. G. Korner, V. E. Lyubovitskij, and B. Oexl, Phys. Rev. D **81**, 114036 (2010).
[50] A. Salam, Nuovo Cimento **25**, 224 (1962).
[51] S. Weinberg, Phys. Rev. **130**, 776 (1963).
[52] J. A. M. Vermaseren, Nucl. Phys. B, Proc. Suppl. **183**, 19 (2008).
[53] R. P. Feynman, Phys. Rev. **76**, 769 (1949).
[54] S. Dubnička, A. Z. Dubničková, A. Issadykov, M. A. Ivanov, A. Liptaj, and S. K. Sakhiyev, Phys. Rev. D **93**, 094022 (2016).
[55] T. Gutsche, M. A. Ivanov, J. G. Körner, V. E. Lyubovitskij, P. Santorelli, and N. Habyl, Phys. Rev. D **91**, 074001 (2015); **91**, 119907(E).
[56] G. Ganbold, T. Gutsche, M. A. Ivanov, and V. E. Lyubovitskij, J. Phys. G **42**, 075002 (2015).
[57] C. Patrignani *et al.* (Particle Data Group), Chin. Phys. C **40**, 100001 (2016).
[58] N. Carrasco *et al.* (ETM Collaboration), Phys. Rev. D **91**, 054507 (2015).
[59] Z.-G. Wang, Eur. Phys. J. C **75**, 427 (2015).
[60] D. Becirevic, V. Lubicz, F. Sanfilippo, S. Simula, and C. Tarantino, J. High Energy Phys. 02 (2012) 042.
[61] Y.-B. Yang *et al.*, Phys. Rev. D **92**, 034517 (2015),
[62] R. J. Dowdall, C. T. H. Davies, G. P. Lepage, and C. McNeile, Phys. Rev. D **88**, 074504 (2013).
[63] M. Ablikim *et al.* (BESIII Collaboration), Phys. Rev. D **89**, 051104 (2014).
[64] B. I. Eisenstein *et al.* (CLEO Collaboration), Phys. Rev. D **78**, 052003 (2008).
[65] M. A. Ivanov, J. G. Körner, and C. T. Tran, Phys. Rev. D **92**, 114022 (2015).
[66] M. A. Ivanov, J. G. Körner, and C. T. Tran, Phys. Rev. D **94**, 094028 (2016).
[67] J. G. Körner and G. A. Schuler, Z. Phys. C **46**, 93 (1990).
[68] S. Fajfer, I. Nišandžić, and U. Rojec, Phys. Rev. D **91**, 094009 (2015).
[69] J. M. Link *et al.* (FOCUS Collaboration), Phys. Lett. B **535**, 43 (2002).
[70] M. R. Shepherd *et al.* (CLEO Collaboration), Phys. Rev. D **74**, 052001 (2006).
[71] R.-M. Wang, J. Zhu, J.-H. Sheng, M.-L. Liu, and Y.-G. Xu, Nucl. Phys. **B901**, 22 (2015).
[72] D. Besson *et al.* (CLEO Collaboration), Phys. Rev. D **80**, 032005 (2009).
[73] L. Widhalm *et al.* (Belle Collaboration), Phys. Rev. Lett. **97**, 061804 (2006).

Erratum: Decay $D \to K^{(*)}\ell^+\nu_\ell$ in covariant quark model [Phys. Rev. D 96, 016017 (2017)]

N. R. Soni and J. N. Pandya

(Received 15 February 2019; published 4 March 2019)

DOI: 10.1103/PhysRevD.99.059901

For computing the branching fraction for $D^+ \to \pi^0\ell^+\nu_\ell$ using Eq. (20), there was a factor of $1/2$ missing. The updated correct results of the branching fraction (Table IV) should read $\mathcal{B}(D^+ \to \pi^0 e^+\nu_e) = 0.309\%$ and $\mathcal{B}(D^+ \to \pi^0\mu^+\nu_\mu) = 0.303\%$. Accordingly, in the numerical results section, the statement, "Our prediction for $\mathcal{B}(D^+ \to \pi^0 e^+\nu_e)$ is higher than BESIII [2] and CLEO-c data [72] while the trend is opposite in the case of $\mathcal{B}(D^0 \to \pi^- e^+\nu_e)$." (on page 8) should be read as, "Our predictions for $\mathcal{B}(D^+ \to \pi^0 e^+\nu_e)$ and $\mathcal{B}(D^0 \to \pi^- e^+\nu_e)$ are lower than BESIII [2] and CLEO-c data [72] data." The other numerical results of the paper are not affected by this unintended error. The conclusion remains unchanged.

Eur. Phys. J. C (2018) 78:592
https://doi.org/10.1140/epjc/s10052-018-6068-6

THE EUROPEAN PHYSICAL JOURNAL C

Regular Article - Theoretical Physics

$Q\bar{Q}$ ($Q \in \{b, c\}$) spectroscopy using the Cornell potential

N. R. Soni[a], **B. R. Joshi, R. P. Shah, H. R. Chauhan, J. N. Pandya**[b]

Applied Physics Department, Faculty of Technology and Engineering, The Maharaja Sayajirao University of Baroda, Vadodara, Gujarat 390001, India

Received: 17 November 2017 / Accepted: 13 July 2018

Abstract The mass spectra and decay properties of heavy quarkonia are computed in nonrelativistic quark-antiquark Cornell potential model. We have employed the numerical solution of Schrödinger equation to obtain their mass spectra using only four parameters namely quark mass (m_c, m_b) and confinement strength ($A_{c\bar{c}}$, $A_{b\bar{b}}$). The spin hyperfine, spin-orbit and tensor components of the one gluon exchange interaction are computed perturbatively to determine the mass spectra of excited S, P, D and F states. Digamma, digluon and dilepton decays of these mesons are computed using the model parameters and numerical wave functions. The predicted spectroscopy and decay properties for quarkonia are found to be consistent with available data from experiments, lattice QCD and other theoretical approaches. We also compute mass spectra and life time of the B_c meson without additional parameters. The computed electromagnetic transition widths of heavy quarkonia and B_c mesons are in tune with available experimental data and other theoretical approaches.

1 Introduction

Mesonic bound states having both heavy quark and antiquark ($c\bar{c}$, $b\bar{b}$ and $c\bar{b}$) are among the best tools for understanding the quantum chromodynamics. Many experimental groups such as CLEO, LEP, CDF, D0 and NA50 have provided data and *BABAR*, Belle, CLEO-III, ATLAS, CMS and LHCb are producing and expected to produce more precise data in upcoming experiments. Comprehensive reviews on the status of experimental heavy quarkonium physics are found in literature [1–6].

Within open flavor threshold, the heavy quarkonia have very rich spectroscopy with narrow and experimentally characterized states. The potential between the interacting quarks within the hadrons demands the understanding of underlying physics of strong interactions. In PDG [7], large amount of experimental data is available for masses along with different decay modes. There are many theoretical groups viz. the lattice quantum chromodynamics (LQCD) [8–18], QCD [19,20], QCD sum rules [21,22], perturbative QCD [23], lattice NRQCD [24,25] and effective field theories [26] that have attempted to explain the production and decays of these states. Others include phenomenological potential models such as the relativistic quark model based on quasi-potential approach [27–33], where the relativistic quasi-potential including one loop radiative corrections reproduce the mass spectrum of quarkonium states. The quasi-potential has also been employed along with leading order radiative correction to heavy quark potential [34–37], relativistic potential model [38–40] as well as semirelativistic potential model [41]. In nonrelativistic potential models, there exist several forms of quark antiquark potentials in the literature. The most common among them is the coulomb repulsive plus quark confinement interaction potential. In our previous work [42–45], we have employed the confinement scheme based on harmonic approximation along with Lorentz scalar plus vector potential. The authors of [46–52] have considered the confinement of power potential Ar^{ν} with ν varying from 0.1 to 2.0 and the confinement strength A to vary with potential index ν. Confinement of the order $r^{2/3}$ have also been attempted [53]. Linear confinement of quarks has been considered by many groups [54–66] and they have provided good agreement with the experimental data for quarkonium spectroscopy along with decay properties. The Bethe–Salpeter approach was also employed for the mass spectroscopy of charmonia and bottomonia [60,61,67]. The quarkonium mass spectrum was also computed in the nonrelativistic quark model [68], screened potential model [65,66] and constituent quark model [69]. There are also other nonlinear potential models that predict the mass spectra of the heavy quarkonia successfully [70–80].

In 90's, the nonrelativistic potential models predicted not only the ground state mass of the tightly bound state of c

[a] e-mail: nrsoni-apphy@msubaroda.ac.in

[b] e-mail: jnpandya-apphy@msubaroda.ac.in

Published online: 21 July 2018

and $\bar{b}$ in the range of 6.2–6.3 GeV [81,82] but also predicted to have very rich spectroscopy. In 1998, CDF collaboration [83] reported B_c mesons in $p\bar{p}$ collisions at $\sqrt{s} = 1.8$ TeV and was later confirmed by D0 [84] and LHCb [85] collaborations. The LHCb collaboration has also made the most precise measurement of the life time of B_c mesons [86]. The first excited state is also reported by ATLAS Collaborations [87] in $p\bar{p}$ collisions with significance of 5.2σ.

It is important to show that any given potential model should be able to compute mass spectra and decay properties of B_c meson using parameters fitted for heavy quarkonia. Attempts in this direction have been made in relativistic quark model based on quasi-potential along with one loop radiative correction [27], quasistatic and confinement QCD potential with confinement parameters along with quark masses [88] and rainbow-ladder approximation of Dyson–Schwinger and Bethe–Salpeter equations [67].

The interaction potential for mesonic states is difficult to derive for full range of quark antiquark separation from first principles of QCD. So most forms of QCD inspired potential would result in uncertainties in the computation of spectroscopic properties particularly in the intermediate range. Different potential models may produce similar mass spectra matching with experimental observations but they may not be in mutual agreement when it comes to decay properties like decay constants, leptonic decays or radiative transitions. Moreover, the mesonic states are identified with masses along with certain decay channels, therefore the test for any successful theoretical model is to reproduce the mass spectrum along with decay properties. Relativistic as well as nonrelativistic potential models have successfully predicted the spectroscopy but they are found to differ in computation of the decay properties [22,47–51,55,78–80]. In this article, we employ nonrelativistic potential with one gluon exchange (essentially Coulomb like) plus linear confinement (Cornell potential) as this form of the potential is also supported by LQCD [89–91]. We solve the Schrödinger equation numerically for the potential to get the spectroscopy of the quarkonia. We first compute the mass spectra of charmonia and bottomonia states to determine quark masses and confinement strengths after fitting the spin-averaged ground state masses with experimental data of respective mesons. Using the potential parameters and numerical wave function, we compute the decay properties such as leptonic decay constants, digamma, dilepton, digluon decay width using the Van-Royen Weiskopf formula. These parameters are then used to compute the mass spectra and life-time of B_c meson. We also compute the electromagnetic ($E1$ and $M1$) transition widths of heavy quarkonia and B_c mesons.

2 Methodology

Bound state of two body system within relativistic quantum field is described in Bethe–Salpeter formalism. However, the Bethe–Salpeter equation is solved only in the ladder approximations. Also, Bethe–Salpeter approach in harmonic confinement is successful in low flavor sectors [92,93]. Therefore the alternative treatment for the heavy bound state is nonrelativistic. Significantly low momenta of quark and antiquark compared to mass of quark-antiquark system $m_{Q,\bar{Q}} \gg \Lambda_{QCD} \sim |\mathbf{p}|$ also constitutes the basis of the nonrelativistic treatment for the heavy quarkonium spectroscopy. Here, for the study of heavy bound state of mesons such as $c\bar{c}$, $c\bar{b}$ and $b\bar{b}$, the nonrelativistic Hamiltonian is given by

$$H = M + \frac{p^2}{2M_{cm}} + V_{\text{Cornell}}(r) + V_{SD}(r) \tag{1}$$

where

$$M = m_Q + m_{\bar{Q}} \quad \text{and} \quad M_{cm} = \frac{m_Q m_{\bar{Q}}}{m_Q + m_{\bar{Q}}} \tag{2}$$

where m_Q and $m_{\bar{Q}}$ are the masses of quark and antiquark respectively, $\mathbf{p}$ is the relative momentum of the each quark and $V_{\text{Cornell}}(r)$ is the quark-antiquark potential of the type coulomb plus linear confinement (Cornell potential) given by

$$V_{\text{Cornell}}(r) = -\frac{4}{3}\frac{\alpha_s}{r} + Ar. \tag{3}$$

Here, $1/r$ term is analogous to the Coulomb type interaction corresponding to the potential induced between quark and antiquark through one gluon exchange that dominates at small distances. The second term is the confinement part of the potential with the confinement strength A as the model parameter. The confinement term becomes dominant at the large distances. α_s is a strong running coupling constant and can be computed as

$$\alpha_s(\mu^2) = \frac{4\pi}{\left(11 - \frac{2}{3}n_f\right)\ln\left(\mu^2/\Lambda^2\right)} \tag{4}$$

where n_f is the number of flavors, μ is renormalization scale related to the constituent quark masses as $\mu = 2m_Q m_{\bar{Q}}/(m_Q + m_{\bar{Q}})$ and Λ is a QCD scale which is taken as 0.15 GeV by fixing $\alpha_s = 0.1185$ [7] at the Z-boson mass.

The confinement strengths with respective quark masses are fine tuned to reproduce the experimental spin averaged ground state masses of both $c\bar{c}$ and $b\bar{b}$ mesons and they are given in Table 1. We compute the masses of radially and orbitally excited states without any additional parameters. Similar work has been done by [47,51,52] and they have considered different values of confinement strengths for different potential indices. The Cornell potential has been shown to be

Table 1 Parameters for quarkonium spectroscopy

m_c	m_c	A_{cc}	A_{bb}
1.317 GeV	4.584 GeV	0.18 GeV^2	0.25 GeV^2

independently successful in computing the spectroscopy of ψ and Υ families. In this article, we compute the mass spectra of the ψ and Υ families along with B_c meson with minimum number of parameters.

Using the parameters defined in Table 1, we compute the spin averaged masses of quarkonia. In order to compute masses of different $n^m L_J$ states according to different J^{PC} values, we use the spin dependent part of one gluon exchange potential (OGEP) $V_{SD}(r)$ perturbatively. The OGEP includes spin-spin, spin-orbit and tensor terms given by [20,22,59,68]

$$V_{SD}(r) = V_{SS}(r)\left[S(S+1) - \frac{3}{2}\right] + V_{LS}(r)(\mathbf{L}\cdot\mathbf{S}) + V_T(r)\left[S(S+1) - 3(S\cdot\hat{r})(S\cdot\hat{r})\right] \quad (5)$$

The spin-spin interaction term gives the hyper-fine splitting while spin-orbit and tensor terms gives the fine structure of the quarkonium states. The coefficients of spin dependent terms of the Eq. (5) can be written as [20]

$$V_{SS}(r) = \frac{1}{3m_Q m_{\bar{Q}}}\nabla^2 V_V(r) = \frac{16\pi\alpha_s}{9m_Q m_{\bar{Q}}}\delta^3(\mathbf{r}) \quad (6)$$

$$V_{LS}(r) = \frac{1}{2m_Q m_{\bar{Q}} r}\left(3\frac{dV_V(r)}{dr} - \frac{dV_S(r)}{dr}\right) \quad (7)$$

$$V_T(r) = \frac{1}{6m_Q m_{\bar{Q}}}\left(3\frac{dV_V^2(r)}{dr^2} - \frac{1}{r}\frac{dV_V(r)}{dr}\right) \quad (8)$$

Where $V_V(r)$ and $V_S(r)$ correspond to the vector and scalar part of the Cornell potential in Eq. (3) respectively. Using all the parameters defined above, the Schrödinger equation is numerically solved using *Mathematica* notebook utilizing the Runge–Kutta method [94]. It is generally believed that the charmonia need to be treated relativistically due to their lighter masses, but we note here that the computed wave functions of charmonia using relativistic as well as nonrelativistic approaches do not show significant difference [33]. So we choose to compute the charmonium mass spectra nonrelativistically in present study. The computed mass spectra of heavy quarkonia and B_c mesons are listed in Tables 2, 3, 4, 5, 6 and 7.

3 Decay properties

The mass spectra of the hadronic states are experimentally determined through detection of energy and momenta of daughter particles in various decay channels. Generally, most phenomenological approaches obtain their model parameters like quark masses and confinement/Coulomb strength by fitting with the experimental ground states. So it becomes necessary for any phenomenological model to validate their fitted parameters through proper evaluation of various decay rates in general and annihilation rates in particular. In the nonrelativistic limit, the decay properties are dependent on the wave function. In this section, we test our parameters and wave functions to determine various annihilation widths and electromagnetic transitions.

3.1 Leptonic decay constants

The leptonic decay constants of heavy quarkonia play very important role in understanding the weak decays. The matrix elements for leptonic decay constants of pseudoscalar and vector mesons are given by

$$\langle 0|\bar{Q}\gamma^\mu\gamma_5 Q|P_\mu(k)\rangle = if_P k^\mu \quad (9)$$

$$\langle 0|\bar{Q}\gamma^\mu Q|P_\mu(k)\rangle = if_V M_V \epsilon^{*\mu} \quad (10)$$

where k is the momentum of pseudoscalar meson, $\epsilon^{*\mu}$ is the polarization vector of meson. In the nonrelativistic limit, the decay constants of pseudoscalar and vector mesons are given by Van Royen-Weiskopf formula [96]

$$f^2_{P/V} = \frac{3|R_{nsP/V}(0)|^2}{\pi M_{nsP/V}}\bar{C}^2(\alpha_S). \quad (11)$$

Here the QCD correction factor $\bar{C}^2(\alpha_S)$ [97,98]

$$\bar{C}^2(\alpha_S) = 1 - \frac{\alpha_s}{\pi}\left(\delta^{P,V} - \frac{m_Q - m_{\bar{Q}}}{m_Q + m_{\bar{Q}}}\ln\frac{m_Q}{m_{\bar{Q}}}\right). \quad (12)$$

With $\delta^P = 2$ and $\delta^V = 8/3$. Using the above relations, we compute the leptonic decay constants f_p and f_v for charmonia, bottomonia and B_c mesons. The results are listed in Tables 8, 9, 10, 11, 12 and 13 in comparison with other models including LQCD.

3.2 Annihilation widths of heavy quarkonia

Digamma, digluon and dilepton annihilation decay widths of heavy quarkonia are very important in understanding the dynamics of heavy quarks within the mesons. The measurement of digamma decay widths provides the information regarding the internal structure of meson. The decay $\eta_c \to \gamma\gamma$, $\chi_{c0,2} \to \gamma\gamma$ was reported by CLEO-c [103], *BABAR* [104] and then BESIII [105] collaboration have reported high accuracy data. LQCD is found to underestimate the decay widths of $\eta_c \to \gamma\gamma$ and $\chi_{c0} \to \gamma\gamma$ when compared to experimental data [106,107]. Other approaches to attempt computation of annihilation rates of heavy quarkonia include NRQCD [108–112], relativistic quark model [31,32], effective Lagrangian [113,114] and next-to-next-to

Table 2 Mass spectrum of S and P-wave charmonia (in GeV)

State	Present	[27]	[65]	[67]	[76]	[39]	[73]	[59]	[68]	[70]	LQCD [17]	PDG [7]
1^1S_0	2.989	2.981	2.984	2.925	2.979	2.980	2.980	2.982	3.088	2.979	2.884	2.984
1^3S_1	3.094	3.096	3.097	3.113	3.097	3.097	3.097	3.090	3.168	3.096	3.056	3.097
2^1S_0	3.602	3.635	3.637	3.684	3.623	3.597	3.633	3.630	3.669	3.600	3.535	3.639
2^3S_1	3.681	3.685	3.679	3.676	3.673	3.685	3.690	3.672	3.707	3.680	3.662	3.686
3^1S_0	4.058	3.989	4.004	–	3.991	4.014	3.992	4.043	4.067	4.011	–	–
3^3S_1	4.129	4.039	4.030	3.803	4.022	4.095	4.030	4.072	4.094	4.077	–	4.039
4^1S_0	4.448	4.401	4.264	–	4.250	4.433	4.244	4.384	4.398	4.397	–	–
4^3S_1	4.514	4.427	4.281	–	4.273	4.477	4.273	4.406	4.420	4.454	–	4.421
5^1S_0	4.799	4.811	4.459	–	4.446	–	4.440	–	–	–	–	–
5^3S_1	4.863	4.837	4.472	–	4.463	–	4.464	–	–	–	–	–
6^1S_0	5.124	5.155	–	–	4.595	–	4.601	–	–	–	–	–
6^3S_1	5.185	5.167	–	–	4.608	–	4.621	–	–	–	–	–
1^3P_0	3.428	3.413	3.415	3.323	3.433	3.416	3.392	3.424	3.448	3.488	3.412	3.415
1^3P_1	3.468	3.511	3.521	3.489	3.510	3.508	3.491	3.505	3.520	3.514	3.480	3.511
1^1P_1	3.470	3.525	3.526	3.433	3.519	3.527	3.524	3.516	3.536	3.539	3.494	3.525
1^3P_2	3.480	3.555	3.553	3.550	3.556	3.558	3.570	3.556	3.564	3.565	3.536	3.556
2^3P_0	3.897	3.870	3.848	3.833	3.842	3.844	3.845	3.852	3.870	3.947	–	3.918
2^3P_1	3.938	3.906	3.914	3.672	3.901	3.940	3.902	3.925	3.934	3.972	–	–
2^1P_1	3.943	3.926	3.916	3.747	3.908	3.960	3.922	3.934	3.950	3.996	–	–
2^3P_2	3.955	3.949	3.937	–	3.937	3.994	3.949	3.972	3.976	4.021	4.066	3.927
3^3P_0	4.296	4.301	4.146	–	4.131	–	4.192	4.202	4.214	–	–	–
3^3P_1	4.338	4.319	4.192	3.912	4.178	–	4.178	4.271	4.275	–	–	–
3^1P_1	4.344	4.337	4.193	–	4.184	–	4.137	4.279	4.291	–	–	–
3^3P_2	4.358	4.354	4.211	–	4.208	–	4.212	4.317	4.316	–	–	–
4^3P_0	4.653	4.698	–	–	–	–	–	–	–	–	–	–
4^3P_1	4.696	4.728	–	–	–	–	–	–	–	–	–	–
4^1P_1	4.704	4.744	–	–	–	–	–	–	–	–	–	–
4^3P_2	4.718	4.763	–	–	–	–	–	–	–	–	–	–
5^3P_0	4.983	–	–	–	–	–	–	–	–	–	–	–
5^3P_1	5.026	–	–	–	–	–	–	–	–	–	–	–
5^1P_1	5.034	–	–	–	–	–	–	–	–	–	–	–
5^3P_2	5.049	–	–	–	–	–	–	–	–	–	–	–

leading order QCD correction to $\chi_{c0,2} \to \gamma\gamma$ in the framework of nonrelativistic QCD factorization [115].

The meson decaying into digamma suggests that the spin can never be one [116,117]. Corresponding digamma decay width of a pseudoscalar meson in nonrelativistic limit is given by Van Royen-Weiskopf formula [96,118]

$$\Gamma_{n^1S_0\to\gamma\gamma} = \frac{3\alpha_e^2 e_Q^4 |R_{nsP}(0)|^2}{m_Q^2}\left[1+\frac{\alpha_s}{\pi}\left(\frac{\pi^2-20}{3}\right)\right] \tag{13}$$

$$\Gamma_{n^3P_0\to\gamma\gamma} = \frac{27\alpha_e^2 e_Q^4 |R'_{nP}(0)|^2}{M_Q^4}\left[1+\frac{\alpha_s}{\pi}\left(\frac{3\pi^2-28}{9}\right)\right] \tag{14}$$

$$\Gamma_{n^3P_2\to\gamma\gamma} = \frac{36\alpha_e^2 e_Q^4 |R'_{nP}(0)|^2}{5M_Q^4}\left[1-\frac{16}{3}\frac{\alpha_s}{\pi}\right] \tag{15}$$

where the bracketed quantities are QCD next-to-leading order radiative corrections [118,119].

Digluon annihilation of quarkonia is not directly observed in detectors as digluonic state decays into various hadronic states making it a bit complex to compute digluon annihilation widths from nonrelativistic approximations derived from first principles. The digluon decay width of pseudoscalar meson along with the QCD leading order radiative correction is given by [113,118–120]

Table 3 Mass spectrum of D and F-wave charmonia (in GeV)

State	Present	[27]	[65]	[67]	[76]	[39]	[73]	[59]	[68]	[70]
1^3D_3	3.755	3.813	3.808	3.869	3.799	3.831	3.844	3.806	3.809	3.798
1^1D_2	3.765	3.807	3.805	3.739	3.796	3.824	3.802	3.799	3.803	3.796
1^3D_2	3.772	3.795	3.807	3.550	3.798	3.824	3.788	3.800	3.804	3.794
1^3D_1	3.775	3.783	3.792	–	3.787	3.804	3.729	3.785	3.789	3.792
2^3D_3	4.176	4.220	4.112	3.806	4.103	4.202	4.132	4.167	4.167	4.425
2^1D_2	4.182	4.196	4.108	–	4.099	4.191	4.105	4.158	4.158	4.224
2^3D_2	4.188	4.190	4.109	–	4.100	4.189	4.095	4.158	4.159	4.223
2^3D_1	4.188	4.105	4.095	–	4.089	4.164	4.057	4.142	4.143	4.222
3^3D_3	4.549	4.574	4.340	–	4.331	–	4.351	–	–	–
3^1D_2	4.553	3.549	4.336	–	4.326	–	4.330	–	–	–
3^3D_2	4.557	4.544	4.337	–	4.327	–	4.322	–	–	–
3^3D_1	4.555	4.507	4.324	–	4.317	–	4.293	–	–	–
4^3D_3	4.890	4.920	–	–	–	–	4.526	–	–	–
4^1D_2	4.892	4.898	–	–	–	–	4.509	–	–	–
4^3D_2	4.896	4.896	–	–	–	–	4.504	–	–	–
4^3D_1	4.891	4.857	–	–	–	–	4.480	–	–	–
1^3F_2	3.990	4.041	–	–	–	4.068	–	4.029	–	–
1^3F_3	4.012	4.068	–	3.999	–	4.070	–	4.029	–	–
1^1F_3	4.017	4.071	–	4.037	–	4.066	–	4.026	–	–
1^3F_4	4.036	4.093	–	–	–	4.062	–	4.021	–	–
2^3F_2	4.378	4.361	–	–	–	–	–	4.351	–	–
2^3F_3	4.396	4.400	–	–	–	–	–	3.352	–	–
2^1F_3	4.400	4.406	–	–	–	–	–	4.350	–	–
2^3F_4	4.415	4.434	–	–	–	–	–	4.348	–	–
3^3F_2	4.730	–	–	–	–	–	–	–	–	–
3^3F_3	4.746	–	–	–	–	–	–	–	–	–
3^1F_3	4.749	–	–	–	–	–	–	–	–	–
3^3F_4	4.761	–	–	–	–	–	–	–	–	–

$$\Gamma_{n^1S_0\to gg} = \frac{2\alpha_s^2|R_{nsP}(0)|^2}{3m_Q^2}[1+C_Q(\alpha_s/\pi)] \tag{16}$$

$$\Gamma_{n^3P_0\to gg} = \frac{6\alpha_s^2|R'_{nP}(0)|^2}{m_Q^4}[1+C_{0Q}(\alpha_s/\pi)] \tag{17}$$

$$\Gamma_{n^3P_2\to gg} = \frac{4\alpha_s^2|R'_{nP}(0)|^2}{5m_Q^4}[1+C_{2Q}(\alpha_s/\pi)] \tag{18}$$

Here, the coefficients in the bracket have values of $C_Q = 4.8$, $C_{0Q} = 9.5$, $C_{2Q} = -2.2$ for the charm quark and $C_Q = 4.4$, $C_{0Q} = 10.0$, $C_{2Q} = -0.1$ for the bottom quark [118].

The vector mesons have quantum numbers 1^{--} and can annihilate into dilepton. The dileptonic decay of vector meson along with one loop QCD radiative correction is given by [96,118]

$$\Gamma_{n^3S_1\to\ell^+\ell^-} = \frac{4\alpha_e^2e_Q^2|R_{nsV}(0)|^2}{M_{nsV}^2}\left[1-\frac{16\alpha_s}{3\pi}\right] \tag{19}$$

Here, α_e is the electromagnetic coupling constant, α_s is the strong running coupling constant in Eq. (4) and e_Q is the charge of heavy quark in terms of electron charge. In above relations, $|R_{nsP/V}(0)|$ corresponds to the wave function of S-wave at origin for pseudoscalar and vector mesons while $|R'_{nP}(0)|$ is the derivative of P-wave function at origin. The annihilation rates of heavy quarkonia are listed in Tables 14, 15, 16, 17, 18 and 19.

3.3 Electromagnetic transition widths

The electromagnetic transitions can be determined broadly in terms of electric and magnetic multipole expansions and their study can help in understanding the non-perturbative regime of QCD. We consider the leading order terms i.e. electric ($E1$) and magnetic ($M1$) dipoles with selection rules $\Delta L = \pm 1$ and $\Delta S = 0$ for the $E1$ transitions while $\Delta L = 0$ and $\Delta S = \pm 1$ for $M1$ transitions. We now employ the numerical

Table 4 Mass spectrum of S and P-wave bottomonia (in GeV)

State	Present	[64]	[27]	[66]	[67]	[77]	[40]	[73]	[69]	PDG [7]
1^1S_0	9.428	9.402	9.398	9.390	9.414	9.389	9.393	9.392	9.455	9.398
1^3S_1	9.463	9.465	9.460	9.460	9.490	9.460	9.460	9.460	9.502	9.460
2^1S_0	9.955	9.976	9.990	9.990	9.987	9.987	9.987	9.991	9.990	9999
2^3S_1	9.979	10.003	10.023	10.015	10.089	10.016	10.023	10.024	10.015	10.023
3^1S_0	10.338	10.336	10.329	10.326	–	10.330	10.345	10.323	10.330	–
3^3S_1	10.359	10.354	10.355	10.343	10.327	10.351	10.364	10.346	10.349	10.355
4^1S_0	10.663	10.523	10.573	10.584	–	10.595	10.623	10.558	–	–
4^3S_1	10.683	10.635	10.586	10.597	–	10.611	10.643	10.575	10.607	10.579
5^1S_0	10.956	10.869	10.851	10.800	–	10.817	–	10.741	–	–
5^3S_1	10.975	10.878	10.869	10.811	–	10.831	–	10.755	10.818	10.876
6^1S_0	11.226	11.097	11.061	10.997	–	11.011	–	10.892	–	–
6^3S_1	11.243	11.102	11.088	10.988	–	11.023	–	10.904	10.995	11.019
1^3P_0	9.806	9.847	9.859	9.864	9.815	9.865	9.861	9.862	9.855	9.859
1^3P_1	9.819	9.876	9.892	9.903	9.842	9.897	9.891	9.888	9.874	9.893
1^1P_1	9.821	9.882	9.900	9.909	9.806	9.903	9.900	9.896	9.879	9.899
1^3P_2	9.825	9.897	9.912	9.921	9.906	9.918	9.912	9.908	9.886	9.912
2^3P_0	10.205	10.226	10.233	10.220	10.254	10.226	10.230	10.241	10.221	10.232
2^3P_1	10.217	10.246	10.255	10.249	10.120	10.251	10.255	10.256	10.236	10.255
2^1P_1	10.220	10.250	10.260	10.254	10.154	10.256	10.262	10.261	10.240	10.260
2^3P_2	10.224	10.261	10.268	10.264	–	10.269	10.271	10.268	10.246	10.269
3^3P_0	10.540	10.552	10.521	10.490	–	10.502	–	10.511	10.500	–
3^3P_1	10.553	10.538	10.541	10.515	10.303	10.524	–	10.507	10.513	–
3^1P_1	10.556	10.541	10.544	10.519	–	10.529	–	10.497	10.516	–
3^3P_2	10.560	10.550	10.550	10.528	–	10.540	–	10.516	10.521	–
4^3P_0	10.840	10.775	10.781	–	–	10.732	–	–	–	–
4^3P_1	10.853	10.788	10.802	–	–	10.753	–	–	–	–
4^1P_1	10.855	10.790	10.804	–	–	10.757	–	–	–	–
4^3P_2	10.860	10.798	10.812	–	–	10.767	–	–	–	–
5^3P_0	11.115	11.004	–	–	–	10.933	–	–	–	–
5^3P_1	11.127	11.014	–	–	–	10.951	–	–	–	–
5^1P_1	11.130	11.016	–	–	–	10.955	–	–	–	–
5^3P_2	11.135	11.022	–	–	–	10.965	–	–	–	–

wave function for computing the electromagnetic transition widths among quarkonia and B_c meson states in order to test parameters used in present work. For $M1$ transition, we restrict our calculations for transitions among S-waves only. In the nonrelativistic limit, the radiative $E1$ and $M1$ widths are given by [4,54,55,124,125]

$$\Gamma\left(n^{2S+1}L_{iJ_i} \to n'^{2S+1}L_{fJ_f} + \gamma\right) = \frac{4\alpha_e\langle e_Q\rangle^2\omega^3}{3}(2J_f+1)S_{if}^{E1}|M_{if}^{E1}|^2 \tag{20}$$

$$\Gamma\left(n^3S_1 \to n'^1S_0 + \gamma\right) = \frac{\alpha_e\mu^2\omega^3}{3}(2J_f+1)|M_{if}^{M1}|^2 \tag{21}$$

where, mean charge content $\langle e_Q\rangle$ of the $Q\bar{Q}$ system, magnetic dipole moment μ and photon energy ω are given by

$$\langle e_Q\rangle = \left|\frac{m_{\bar{Q}}e_Q - e_{\bar{Q}}m_Q}{m_Q + m_{\bar{Q}}}\right| \tag{22}$$

$$\mu = \frac{e_Q}{m_Q} - \frac{e_{\bar{Q}}}{m_{\bar{Q}}} \tag{23}$$

and

$$\omega = \frac{M_i^2 - M_f^2}{2M_i} \tag{24}$$

Table 5 Mass spectrum of D and F-wave bottomonia (in GeV)

State	Present	[64]	[27]	[66]	[67]	[77]	[40]	[73]	[69]	PDG [7]
1^3D_3	10.073	10.115	10.166	10.157	10.232	10.156	10.163	10.177	10.127	–
1^1D_2	10.074	10.148	10.163	10.153	10.194	10.152	10.158	10.166	10.123	–
1^3D_2	10.075	10.147	10.161	10.153	10.145	10.151	10.157	10.162	10.122	10.163
1^3D_1	10.074	10.138	10.154	10.146	–	10.145	10.149	10.147	10.117	–
2^3D_3	10.423	10.455	10.449	10.436	–	10.442	10.456	10.447	10.422	–
2^1D_2	10.424	10.450	10.445	10.432	–	10.439	10.452	10.440	10.419	–
2^3D_2	10.424	10.449	10.443	10.432	–	10.438	10.450	10.437	10.418	–
2^3D_1	10.423	10.441	10.435	10.425	–	10.432	10.443	10.428	10.414	–
3^3D_3	10.733	10.711	10.717	–	–	10.680	–	10.652	–	–
3^1D_2	10.733	10.706	10.713	–	–	10.677	–	10.646	–	–
3^3D_2	10.733	10.705	10.711	–	–	10.676	–	10.645	–	–
3^3D_1	10.731	10.698	10.704	–	–	10.670	–	10.637	–	–
4^3D_3	11.015	10.939	10.963	–	–	10.886	–	10.817	–	–
4^1D_2	11.015	10.935	10.959	–	–	10.883	–	10.813	–	–
4^3D_2	11.016	10.934	10.957	–	–	10.882	–	10.811	–	–
4^3D_1	11.013	10.928	10.949	–	–	10.877	–	10.805	–	–
1^3F_2	10.283	10.350	10.343	10.338	–	–	10.353	–	10.315	–
1^3F_3	10.287	10.355	10.346	10.340	10.302	–	10.356	–	10.321	–
1^1F_3	10.288	10.355	10.347	10.339	10.319	–	10.356	–	10.322	–
1^3F_4	10.291	10.358	10.349	10.340	–	–	10.357	–	–	–
2^3F_2	10.604	10.615	10.610	–	–	–	10.610	–	–	–
2^3F_3	10.607	10.619	10.614	–	–	–	10.613	–	–	–
2^1F_3	10.607	10.619	10.647	–	–	–	10.613	–	–	–
2^3F_4	10.609	10.622	10.617	–	–	–	10.615	–	–	–
3^3F_2	10.894	10.850	–	–	–	–	–	–	–	–
3^3F_3	10.896	10.853	–	–	–	–	–	–	–	–
3^1F_3	10.897	10.853	–	–	–	–	–	–	–	–
3^3F_4	10.898	10.856	–	–	–	–	–	–	–	–

respectively. Also the symmetric statistical factor is given by

$$S_{if}^{E1} = \max(L_i, L_f) \begin{Bmatrix} J_i & 1 & J_f \\ L_f & S & L_i \end{Bmatrix}^2. \tag{25}$$

The matrix element $|M_{if}|$ for $E1$ and $M1$ transition can be written as

$$\left|M_{if}^{E1}\right| = \frac{3}{\omega}\left\langle f \left| \frac{\omega r}{2} j_0\left(\frac{\omega r}{2}\right) - j_1\left(\frac{\omega r}{2}\right)\right| i\right\rangle \tag{26}$$

and

$$\left|M_{if}^{M1}\right| = \left\langle f \left| j_0\left(\frac{\omega r}{2}\right)\right| i\right\rangle \tag{27}$$

The electromagnetic transition widths are listed in Tables 20, 21, 22, 23, 24 and 25 and also compared with experimental results as well as theoretical predictions.

3.4 Weak decays of B_c mesons

The decay modes of B_c mesons are different from charmonia and bottomonia because of the inclusion of different flavor quarks. Their decay properties are very important probes for the weak interaction as B_c meson decays only through weak decays, therefore have relatively quite long life time. The pseudoscalar state can not decay via strong or electromagnetic decays because of this flavor asymmetry.

In the spectator model [126], the total decay width of B_c meson can be broadly classified into three classes. (i) Decay of b quark considering c quark as a spectator, (ii) Decay of c quark considering b quark as a spectator and (iii) Annihilation channel $B_c \to \ell^+\nu_\ell$. The total width is given by

$$\Gamma(B_c \to X) = \Gamma(b \to X) + \Gamma(c \to X) + \Gamma(Anni) \tag{28}$$

In the calculations of total width we have not considered the interference among them as all these decays lead to different

Table 6 Mass spectrum of S and P-wave B_c meson (in GeV)

State	Present	[46]	[27]	[63]	[95]	PDG [7]
1^1S_0	6.272	6.278	6.272	6.271	6.275	6.275
1^3S_1	6.321	6.331	6.333	6.338	6.314	–
2^1S_0	6.864	6.863	6.842	6.855	6.838	6.842
2^3S_1	6.900	6.873	6.882	6.887	6.850	–
3^1S_0	7.306	7.244	7.226	7.250	–	–
3^3S_1	7.338	7.249	7.258	7.272	–	–
4^1S_0	7.684	7.564	7.585	–	–	–
4^3S_1	7.714	7.568	7.609	–	–	–
5^1S_0	8.025	7.852	7.928	–	–	–
5^3S_1	8.054	7.855	7.947	–	–	–
6^1S_0	8.340	8.120	–	–	–	–
6^3S_1	8.368	8.122	–	–	–	–
1^3P_0	6.686	6.748	6.699	6.706	6.672	–
1^3P_1	6.705	6.767	6.750	6.741	6.766	–
1^1P_1	6.706	6.769	6.743	6.750	6.828	–
1^3P_2	6.712	6.775	6.761	6.768	6.776	–
2^3P_0	7.146	7.139	7.094	7.122	6.914	–
2^3P_1	7.165	7.155	7.134	7.145	7.259	–
2^1P_1	7.168	7.156	7.094	7.150	7.322	–
2^3P_2	7.173	7.162	7.157	7.164	7.232	–
3^3P_0	7.536	7.463	7.474	–	–	–
3^3P_1	7.555	7.479	7.510	–	–	–
3^1P_1	7.559	7.479	7.500	–	–	–
3^3P_2	7.565	7.485	7.524	–	–	–
4^3P_0	7.885	–	7.817	–	–	–
4^3P_1	7.905	–	7.853	–	–	–
4^1P_1	7.908	–	7.844	–	–	–
4^3P_2	7.915	–	7.867	–	–	–
5^3P_0	8.207	–	–	–	–	
5^3P_1	8.226	–	–	–	–	
5^1P_1	8.230	–	–	–	–	
5^3P_2	8.237	–	–	–	–	

Table 7 Mass spectrum of D and F-wave B_c meson (in GeV)

State	Present	[46]	[27]	[63]	[95]
1^3D_3	6.990	7.026	7.029	7.045	6.980
1^1D_2	6.994	7.035	7.026	7.041	7.009
1^3D_2	6.997	7.025	7.025	7.036	7.154
1^3D_1	6.998	7.030	7.021	7.028	7.078
2^3D_3	7.399	7.363	7.405	–	–
2^1D_2	7.401	7.370	7.400	–	–
2^3D_2	7.403	7.361	7,399	–	–
2^3D_1	7.403	7.365	7.392	–	–
3^3D_3	7.761	–	7.750	–	–
3^1D_2	7.762	–	7.743	–	–
3^3D_2	7.764	–	7.741	–	–
3^3D_1	7.762	–	7.732	–	–
4^3D_3	8.092	–	–	–	–
4^1D_2	8.093	–	–	–	–
4^3D_2	8.094	–	–	–	–
4^3D_1	8.091	–	–	–	–
1^3F_2	7.234	–	7.273	7.269	–
1^3F_3	7.242	–	7.269	7.276	–
1^1F_3	7.241	–	7.268	7.266	–
1^3F_4	7.244	–	7.277	7.271	–
2^3F_2	7.607	–	7.618	–	–
2^3F_3	7.615	–	7.616	–	–
2^1F_3	7.614	–	7.615	–	–
2^3F_4	7.617	–	7.617	–	–
3^3F_2	7.946	–	–	–	–
3^3F_3	7.954	–	–	–	–
3^1F_3	7.953	–	–	–	–
3^3F_4	7.956	–	–	–	–

channel. In the spectator approximation, the inclusive decay width of b and c quark is given by

$$\Gamma(b \to X) = \frac{9G_F^2|V_{cb}|^2 m_b^5}{192\pi^3} \tag{29}$$

$$\Gamma(c \to X) = \frac{9G_F^2|V_{cs}|^2 m_c^5}{192\pi^3} \tag{30}$$

$$\Gamma(Anni) = \frac{G_F^2}{8\pi}|V_{bc}|^2 f_{B_c}^2 M_{B_c} m_q^2 \left(1 - \frac{m_q^2}{M_{B_c^2}}\right)^2 C_q \tag{31}$$

where $C_q = 3|V_{cs}|$ for D_s mesons and m_q is the mass of heaviest fermions. V_{cs} and V_{cb} are the CKM matrices and we have taken the value of CKM matrices from the PDG. G_f is the Fermi coupling constant. Here we have used the model quark masses, B_c meson mass and decay constants for the computation of total width. Here we compute the decay width of B_c meson using Eq. (28) and corresponding life time. The computed life time comes out to be 0.539×10^{-12} s which is in very good agreement with the world averaged mean life time $(0.507 \pm 0.009) \times 10^{-12}$ s [7].

4 Numerical results and discussion

Having determined the confinement strengths and quark masses, we are now in position to present our numerical results. We first compute the mass spectra of heavy quarkonia and B_c meson. In most of the potential model computations, the confinement strength is fixed by experimental ground state masses for $c\bar{c}$, $b\bar{b}$ and $c\bar{b}$ independently. We observe here that the confinement strength A for B_c meson is arithmetic mean of those for $c\bar{c}$ and $b\bar{b}$ which discards the

Table 8 Pseudoscalar decay constant of charmonia (in MeV)

State	f_p	[52]	[99]	[68]	LQCD [100]	QCDSR [100]	PDG [7]
$1S$	350.314	363	378	402	387(7)(2)	309 ± 39	335 ± 75
$2S$	278.447	275	82	240	–	–	–
$3S$	249.253	239	206	193	–	–	–
$4S$	231.211	217	87	–	–	–	–
$5S$	218.241	202	–	–	–	–	
$6S$	208.163	197	–	–	–	–	–

Table 9 Vector decay constant of charmonia (in MeV)

State	f_v	[52]	[99]	[68]	LQCD [100]	QCDSR [100]	PDG [7]
$1S$	325.876	338	411	393	418(8)(5)	401 ± 46	416 ± 6
$2S$	257.340	254	155	293	–	–	304 ± 4
$3S$	229.857	220	188	258	–	–	–
$4S$	212.959	200	262	–	–	–	–
$5S$	200.848	186	–	–	–	–	–
$6S$	191.459	175	–	–	–	–	–

Table 10 Pseudoscalar decay constant of bottomonia (in MeV)

State	f_p	[52]	[99]	[43]	[68]
$1S$	646.025	744	756	711	599
$2S$	518.803	577	285	–	411
$3S$	474.954	511	333	–	354
$4S$	449.654	471	40	–	–
$5S$	432.072	443	–	–	–
$6S$	418.645	422	–	–	–

Table 11 Vector decay constant of bottomonia (in MeV)

State	f_v	[52]	[99]	[68]	[101]	LQCD [102]	PDG [7]
$1S$	647.250	706	707	665	$498 \pm (20)$	649(31)	715 ± 5
$2S$	519.436	547	393	475	$366 \pm (27)$	481(39)	498 ± 8
$3S$	475.440	484	9	418	$304 \pm (27)$	–	430 ± 4
$4S$	450.066	446	20	388	$259 \pm (22)$	–	336 ± 18
$5S$	432.437	419	–	367	$228 \pm (16)$	–	–
$6S$	418.977	399	–	351	–	–	–

Table 12 Pseudoscalar decay constant of B_c meson (in MeV)

State	f_p	[52]	[30]	[22]	[82]	[95]
$1S$	432.955	465	503	$460 \pm (60)$	500	554.125
$2S$	355.504	361	–	–	–	
$3S$	325.659	319	–	–	–	
$4S$	307.492	293	–	–	–	
$5S$	294.434	275	–	–	–	
$6S$	284.237	261	–	–	–	

Table 13 Vector decay constant of B_c meson (in MeV)

State	f_v	[52]	[30]	[22]	[82]
$1S$	434.642	435	433	$460 \pm (60)$	500
$2S$	356.435	337	–	–	–
$3S$	326.374	297	–	–	–
$4S$	308.094	273	–	–	–
$5S$	294.962	256	–	–	–
$6S$	284.709	243	–	–	–

Table 14 Digamma decay width of S and P-wave charmonia (in keV)

State	$\Gamma_{\gamma\gamma}$	[76]	[32]	[68]	[121]	PDG [7]
1^1S_0	7.231	8.5	5.5	7.18	7.14 ± 0.95	5.1 ± 0.4
2^1S_0	5.507	2.4	1.8	1.71	4.44 ± 0.48	2.15 ± 1.58
3^1S_0	4.971	0.88	–	1.21	–	–
4^1S_0	4.688	–	–	–	–	–
5^1S_0	4.507	–	–	–	–	–
6^1S_0	4.377	–	–	–	–	–
1^3P_0	8.982	2.5	2.9	3.28	–	2.34 ± 0.19
1^3P_2	1.069	0.31	0.50	–	–	0.53 ± 0.4
2^3P_0	9.111	1.7	1.9	–	–	–
2^3P_2	1.084	0.23	0.52	–	–	–
3^3P_0	9.104	1.2	–	–	–	–
3^3P_2	1.0846	0.17	–	–	–	–
4^3P_0	9.076	–	–	–	–	–
4^3P_2	1.080	–	–	–	–	–
5^3P_0	9.047	–	–	–	–	–
5^3P_2	1.077	–	–	–	–	–

Table 15 Digamma decay width of S and P-wave bottomonia (in keV)

State	$\Gamma_{\gamma\gamma}$	[77]	[62]	[32]	[68]	[121]
1^1S_0	0.387	0.527	0.214	0.35	0.23	0.384 ± 0.047
2^1S_0	0.263	0.263	0.121	0.15	0.07	0.191 ± 0.025
3^1S_0	0.229	0.172	0.906	0.10	0.04	–
4^1S_0	0.212	0.105	0.755	–	–	–
5^1S_0	0.201	0.121	–	–	–	–
6^1S_0	0.193	0.050	–	–	–	–
1^3P_0	0.0196	0.050	0.0208	0.038	–	–
1^3P_2	0.0052	0.0066	0.0051	0.008	–	–
2^3P_0	0.0195	0.037	0.0227	0.029	–	–
2^3P_2	0.0052	0.0067	0.0062	0.006	–	–
3^3P_0	0.0194	0.037	–	–	–	–
3^3P_2	0.0051	0.0064	–	–	–	–
4^3P_0	0.0192	–	–	–	–	–
4^3P_2	0.0051	–	–	–	–	–
5^3P_0	0.0191	–	–	–	–	–
5^3P_2	0.0050	–	–	–	–	–

Table 16 Digluon decay width of S and P-wave charmonia (in MeV)

State	Γ_{gg}	[70]	[121]	PDG [7]
1^1S_0	35.909	22.37	19.60	26.7 ± 3.0
2^1S_0	27.345	16.74	12.1	14.7 ± 0.7
3^1S_0	24.683	14.30	–	–
4^1S_0	23.281	–	–	–
5^1S_0	22.379	–	–	–
6^1S_0	23.736	–	–	–
1^3P_0	37.919	9.45	–	10.4 ± 0.7
1^3P_2	3.974	2.81	–	2.03 ± 0.12
2^3P_0	38.462	10.09	–	–
2^3P_2	4.034	7.34	–	–
3^3P_0	38.433	–	–	–
3^3P_2	4.028	–	–	–
4^3P_0	38.315	–	–	–
4^3P_2	4.016	–	–	–
5^3P_0	39.191	–	–	–
5^3P_2	4.003	–	–	–

Table 17 Digluon decay width of S and P-wave bottomonia (in MeV)

State	Γ_{gg}	[47]	[121]	[122]
1^1S_0	5.448	17.945	6.98	12.46
2^1S_0	3.710	–	3.47	–
3^1S_0	3.229	–	–	–
4^1S_0	2.985	–	–	–
5^1S_0	2.832	–	–	–
6^1S_0	2.274	–	–	–
1^3P_0	0.276	5.250	–	2.15
1^3P_2	0.073	0.822	–	0.22
2^3P_0	0.275	–	–	–
2^3P_2	0.073	–	–	–
3^3P_0	0.273	–	–	–
3^3P_2	0.072	–	–	–
4^3P_0	0.271	–	–	–
4^3P_2	0.072	–	–	–
5^3P_0	0.269	–	–	–
5^3P_2	0.071	–	–	–

need to introduce additional confinement strength parameter for computation of B_c spectra. Similar approach has been used earlier within QCD potential model [88]. Using model parameters and numerical wave function we compute the various decay properties of heavy quarkonia and B_c mesons namely leptonic decay constants, annihilation widths and electromagnetic transitions. In Tables 2 and 3, we present our result for charmonium mass spectra. We compare our results with PDG data [7], lattice QCD [17] data, relativistic quark model [27], nonrelativistic quark model [65,68], QCD relativistic functional approach [67], relativistic potential model [39] and nonrelativistic potential models [59,70,73,76]. Our results for S-wave are in excellent agreement with the experimental data [7]. We determine the mass difference for S-wave charmonia i.e. $M_{J/\psi} - M_{\eta_c} = 105$ MeV and $M_{\psi(2S)} - M_{\eta_c(2S)} = 79$ MeV while that from experimental data are 113 and 47 MeV respectively [7]. Our results for P-waves are also consistent with the PDG data [7] as well

Table 18 Dilepton decay width of charmonia (in keV)

State	$\Gamma_{\ell^+\ell^-}$	[73]	[52]	[39]	[31]	PDG [7]
$1S$	2.925	4.95	6.99	1.89	5.4	5.547 ± 0.14
$2S$	1.533	1.69	3.38	1.04	2.4	2.359 ± 0.04
$3S$	1.091	0.96	2.31	0.77	–	0.86 ± 0.07
$4S$	0.856	0.65	1.78	0.65	–	0.58 ± 0.07
$5S$	0.707	0.49	1.46	–	–	–
$6S$	0.602	0.39	1.24	–	–	–

Table 19 Dilepton decay width of bottomonia (in keV)

State	$\Gamma_{\ell^+\ell^-}$	[73]	[40]	[52]	[31]	[123]	PDG [7]
$1S$	1.098	1.20	1.33	1.61	1.3	0.98	1.340 ± 0.018
$2S$	0.670	0.52	0.62	0.87	0.5	0.41	0.612 ± 0.011
$3S$	0.541	0.33	0.48	0.66	–	0.27	0.443 ± 0.008
$4S$	0.470	0.24	0.40	0.53	–	0.20	0.272 ± 0.029
$5S$	0.422	0.19	–	0.44	–	0.16	–
$6S$	0.387	0.16	–	0.39	–	0.12	–

Table 20 $E1$ transition width of charmonia (in keV)

Transition	Present	[39]	[30]	[76]	[65]	PDG [7]
$2^3S_1 \to 1^3P_0$	21.863	45.0	51.7	74	22	29.8 ± 1.5
$2^3S_1 \to 1^3P_1$	43.292	40.9	44.9	62	42	27.9 ± 1.5
$2^3S_1 \to 1^3P_2$	62.312	26.5	30.9	43	38	26 ± 1.5
$2^1S_0 \to 1^1P_1$	36.197	8.3	8.6	146	49	–
$3^3S_1 \to 2^3P_0$	31.839	87.3	–	–	–	–
$3^3S_1 \to 2^3P_1$	64.234	65.7	–	–	–	–
$3^3S_1 \to 2^3P_2$	86.472	31.6	–	–	–	–
$3^1S_0 \to 2^1P_1$	51.917	–	–	–	–	–
$3^3S_1 \to 1^3P_0$	46.872	1.2	–	–	–	–
$3^3S_1 \to 1^3P_1$	107.088	2.5	–	–	–	–
$3^3S_1 \to 1^3P_2$	163.485	3.3	–	–	–	–
$3^1S_0 \to 1^1P_1$	178.312	–	–	–	–	–
$1^3P_0 \to 1^3S_1$	112.030	142.2	161	167	284	119.5 ± 8
$1^3P_1 \to 1^3S_1$	146.317	287.0	333	354	306	295 ± 13
$1^3P_2 \to 1^3S_1$	157.225	390.6	448	473	172	384.2 ± 16
$1^1P_1 \to 1^1S_0$	247.971	610.0	723	764	361	357 ± 280
$2^3P_0 \to 2^3S_1$	70.400	53.6	–	61	–	–
$2^3P_1 \to 2^3S_1$	102.672	208.3	–	103	–	–
$2^3P_2 \to 2^3S_1$	116.325	358.6	–	225	–	–
$2^1P_1 \to 2^1S_0$	163.646	–	–	309	–	–
$2^3P_0 \to 1^3S_1$	173.324	20.8	–	74	–	–
$2^3P_1 \to 1^3S_1$	210.958	28.4	–	83	–	–
$2^3P_2 \to 1^3S_1$	227.915	33.2	–	101	–	–
$2^1P_1 \to 1^1S_0$	329.384	–	–	134	–	–
$1^3D_1 \to 1^3P_0$	161.504	–	423	486	272	172 ± 30
$1^3D_1 \to 1^3P_1$	93.775	–	142	150	138	70 ± 17
$1^3D_1 \to 1^3P_2$	5.722	–	5.8	5.8	7.1	≤ 21
$1^3D_2 \to 1^3P_1$	165.176	317.3	297	342	285	–
$1^3D_2 \to 1^3P_2$	50.317	65.7	62	70	91	–
$1^3D_3 \to 1^3P_2$	175.212	62.7	252	284	350	–
$1^1D_2 \to 1^1P_1$	205.93	–	335	575	362	–

as LQCD [17] with less than 2% deviation. Since experimental/LQCD results are not available for P-wave charmonia beyond $n = 2$ states, we compare our results with the relativistic quark model [27] and it is also observed to have 1–2 % deviation throughout the spectra. For charmonia, only $1P$ states are available and for $2P$ only one state is available namely χ_{c2}. Our results for $1P$ and $2P$ states are also satisfactory. We also list the mass spectra of D and F wave and find it to be consistent with the theoretical predictions. Overall, computed charmonium spectra is consistent with PDG and other theoretical models.

In Tables 4 and 5, we compare our results of bottomonium spectra with PDG data [7], relativistic quark model [27,64], nonrelativistic quark model [66], QCD relativistic functional approach [67], relativistic potential model [40], nonrelativistic potential models [73,77] and covariant constituent quark model [69]. Similarly for S-wave bottomonia, up to $n = 3$ vector states are known experimentally and for pseudoscalar states, only $n = 1$ and 2 are available. Our results for $\Upsilon(1S)$ and $\Upsilon(3S)$ are in good agreement with the PDG data while for $\Upsilon(2S)$, $\Upsilon(4S)$ and $\Upsilon(5S)$, slight deviation (within 1%) is observed. Our results for $\eta_b(1S)$ and $\eta_b(3S)$ also match well with less than 0.5% deviation. We obtain $M_{\Upsilon(1S)} - M_{\eta_b} = 35$ MeV and for $M_{\Upsilon(2S)} - M_{\eta_b(2S)} = 24$ MeV against the PDG data of 62 and 24 MeV respectively. For P-wave, $1P$ and $2P$ states are reported and for $3P$, only χ_{b1} is reported. Our results for $1P$ bottomonia deviate by $\simeq 0.3\%$ from the experimental results but for $2P$, they are quite satisfactory and devi-

Table 21 $E1$ transition width of bottomonia (in keV)

Transition	Present	[39]	[30]	[77]	[66]	PDG [7]
$2^3S_1 \to 1^3P_0$	2.377	1.15	1.65	1.67	1.09	1.22 ± 0.11
$2^3S_1 \to 1^3P_1$	5.689	1.87	2.57	2.54	2.17	2.21 ± 0.19
$2^3S_1 \to 1^3P_2$	8.486	1.88	2.53	2.62	2.62	2.29 ± 0.20
$2^1S_0 \to 1^1P_1$	10.181	4.17	3.25	6.10	3.41	–
$3^3S_1 \to 2^3P_0$	3.330	1.67	1.65	1.83	1.21	1.20 ± 0.12
$3^3S_1 \to 2^3P_1$	7.936	2.74	2.65	2.96	2.61	2.56 ± 0.26
$3^3S_1 \to 2^3P_2$	11.447	2.80	2.89	3.23	3.16	2.66 ± 0.27
$3^3S_1 \to 1^3P_0$	0.594	0.03	0.124	0.07	0.097	0.055 ± 0.010
$3^3S_1 \to 1^3P_1$	1.518	0.09	0.307	0.17	0.0005	0.018 ± 0.010
$3^3S_1 \to 1^3P_2$	2.354	0.13	0.445	0.15	0.14	0.20 ± 0.03
$3^1S_0 \to 1^1P_1$	3.385	0.03	0.770	1.24	0.67	–
$3^1S_0 \to 2^1P_1$	13.981	–	3.07	11.0	4.25	–
$1^3P_2 \to 1^3S_1$	57.530	31.2	29.5	38.2	31.8	–
$1^3P_1 \to 1^3S_1$	54.927	27.3	37.1	33.6	31.9	–
$1^3P_0 \to 1^3S_1$	49.530	22.1	42.7	26.6	27.5	–
$1^1P_1 \to 1^1S_0$	72.094	37.9	54.4	55.8	35.8	–
$2^3P_2 \to 2^3S_1$	28.848	16.8	18.8	18.8	15.5	15.1 ± 5.6
$2^3P_1 \to 2^3S_1$	26.672	13.7	15.9	15.9	15.3	19.4 ± 5.0
$2^3P_0 \to 2^3S_1$	23.162	9.90	11.7	11.7	14.4	–
$2^1P_1 \to 2^1S_0$	35.578	–	23.6	24.7	16.2	–
$2^3P_2 \to 1^3S_1$	29.635	7.74	8.41	13.0	12.5	9.8 ± 2.3
$2^3P_1 \to 1^3S_1$	28.552	7.31	8.01	12.4	10.8	8.9 ± 2.2
$2^3P_0 \to 1^3S_1$	26.769	6.69	7.36	11.4	5.4	–
$2^1P_1 \to 1^1S_0$	34.815	–	9.9	15.9	16.1	–
$1^3D_1 \to 1^3P_0$	9.670	–	24.2	23.6	19.8	–
$1^3D_1 \to 1^3P_1$	6.313	–	12.9	12.3	13.3	–
$1^3D_1 \to 1^3P_2$	0.394	–	0.67	0.65	1.02	–
$1^3D_2 \to 1^3P_1$	11.489	19.3	24.8	23.8	21.8	–
$1^3D_2 \to 1^3P_2$	3.583	5.07	6.45	6.29	7.23	–
$1^3D_3 \to 1^3P_2$	14.013	21.7	26.7	26.4	32.1	–
$1^1D_2 \to 1^1P_1$	14.821	–	30.2	42.3	30.3	–

ating by 0.2% only from the PDG data. Our result for $\Upsilon(1D)$ also agrees well with the experimental data with 0.8% deviation. The F-wave mass spectra is also in good agreement with the theoretical predictions. Looking at the comparison with PDG data Ref. [7] and relativistic quark model Ref. [27], present quarkonium mass spectra deviate less than 2% for charmonia and less than 1% for bottomonia.

We now employ the quark masses and confinement strengths used for computing mass spectra of quarkonia to predict the spectroscopy of B_c mesons without introducing any additional parameter. Our results are tabulated in Tables 6 and 7. For B_c mesons, only 0^{-+} states are experimentally observed for $n = 1$ and 2 and our results are in very good agreement with the experimental results with less than 0.3 % error.

We note here that the masses of orbitally excited states (especially $n = 1$ states) of charmonia are systematically lower than the other models and experimental data. This tendency decreases as one moves to higher n states. Absence of similar trend in case of B_c and bottomonia systems suggests that relativistic treatment might improve the results in lower energy regime of charmonia.

Using the mass spectra of heavy quarkonia and B_c meson, we plot the Regge trajectories in (J, M^2) and (n_r, M^2) planes where $n_r = n - 1$. We use the following relations [27]

$$J = \alpha M^2 + \alpha_0 \tag{32}$$

$$n_r = \beta M^2 + \beta_0 \tag{33}$$

Table 22 $E1$ transition width of B_c meson (in keV)

Transition	Present	[30]	[63]	[46]
$2^3S_1 \to 1^3P_0$	4.782	5.53	2.9	0.94
$2^3S_1 \to 1^3P_1$	11.156	7.65	4.7	1.45
$2^3S_1 \to 1^3P_2$	16.823	7.59	5.7	2.28
$2^1S_0 \to 1^1P_1$	18.663	4.40	6.1	3.03
$3^3S_1 \to 2^3P_0$	7.406	–	–	–
$3^3S_1 \to 2^3P_1$	17.049	–	–	–
$3^3S_1 \to 2^3P_2$	25.112	–	–	–
$3^3S_1 \to 1^3P_0$	6.910	–	–	–
$3^3S_1 \to 1^3P_1$	17.563	–	–	–
$3^3S_1 \to 1^3P_2$	27.487	–	–	–
$3^1S_0 \to 1^1P_1$	38.755	–	–	–
$3^1S_0 \to 2^1P_1$	27.988	–	–	–
$1^3P_2 \to 1^3S_1$	55.761	122	83	64.24
$1^3P_1 \to 1^3S_1$	53.294	87.1	11	51.14
$1^3P_0 \to 1^3S_1$	46.862	75.5	55	58.55
$1^1P_1 \to 1^1S_0$	71.923	18.4	80	72.28
$2^3P_2 \to 2^3S_1$	41.259	75.3	55	64.92
$2^3P_1 \to 2^3S_1$	38.533	45.3	45	50.40
$2^3P_0 \to 2^3S_1$	38.308	34.0	42	55.05
$2^1P_1 \to 2^1S_0$	52.205	13.8	52	56.28
$2^3P_2 \to 1^3S_1$	60.195	–	14	–
$2^3P_1 \to 1^3S_1$	57.839	–	5.4	–
$2^3P_0 \to 1^3S_1$	52.508	–	1.0	–
$2^1P_1 \to 1^1S_0$	74.211	–	19	–
$1^3D_1 \to 1^3P_0$	44.783	133	55	–
$1^3D_1 \to 1^3P_1$	28.731	65.3	28	–
$1^3D_1 \to 1^3P_2$	1.786	3.82	1.8	–
$1^3D_2 \to 1^3P_1$	51.272	139	64	–
$1^3D_2 \to 1^3P_2$	16.073	23.6	15	–
$1^3D_3 \to 1^3P_2$	60.336	149	78	–
$1^1D_2 \to 1^1P_1$	66.020	143	63	–

Table 23 $M1$ transition width of charmonia (in keV)

Transition	Present	[39]	[30]	[65]	[75]	PDG [7]
$1^3S_1 \to 1^1S_0$	2.722	2.7	1.05	2.39	3.28	1.58 ± 0.37
$2^3S_1 \to 2^1S_0$	1.172	1.2	0.99	0.19	1.45	0.21 ± 0.15
$2^3S_1 \to 1^1S_0$	7.506	0.0	0.95	7.80	–	1.24 ± 0.29
$3^3S_1 \to 3^1S_0$	9.927	–	–	0.088	–	–

Table 24 $M1$ transition width of bottomonia (in eV)

Transition	Present	[39]	[30]	[66]	[75]	PDG [7]
$1^3S_1 \to 1^1S_0$	37.668	4.0	5.8	10	15.36	–
$2^3S_1 \to 2^1S_0$	5.619	0.05	1.40	0.59	1.82	–
$2^3S_1 \to 1^1S_0$	77.173	0.0	6.4	66	–	12.5 ± 4.9
$3^3S_1 \to 3^1S_0$	2.849	–	0.8	3.9	–	–
$3^3S_1 \to 2^1S_0$	36.177	–	1.5	11	–	≤ 14
$3^3S_1 \to 1^1S_0$	76.990	–	10.5	71	–	10 ± 2

Table 25 $M1$ transition width of B_c meson (in eV)

Transition	Present	[30]	[63]	[46]
$1^3S_1 \to 1^1S_0$	53.109	33	80	2.2
$2^3S_1 \to 2^1S_0$	21.119	17	10	0.014
$2^3S_1 \to 1^1S_0$	481.572	428	600	495
$2^1S_0 \to 1^3S_1$	568.346	488	300	1092

where α, β are slopes and α_0, β_0 are the intercepts that can be computed using the methods given in Ref. [27]. In Figs. 1, 2 and 3, we plot the Regge trajectories. Regge trajectories from present approach and relativistic quark model [27] show similar trend i.e. for charmonium spectra, the computed mass square fits very well to a linear trajectory and found to be almost parallel and equidistant in both the planes. Also, for bottomonia and B_c mesons, we observe the nonlinearity in the parent trajectories. The nonlinearity increases as we go from $c\bar{b}$ to $b\bar{b}$ mesons indicating increasing contribution from the inter-quark interaction over confinement.

According to the first principles of QCD, while the one-gluon-exchange interaction gives rise to employment of Coulomb potential with a strength proportional to the strong running coupling constant at very short distances, nonperturbative effect like confinement becomes prominent at larger distances. Charmonium belongs to neither purely nonrelativistic nor the relativistic regime where chiral symmetry breaking is more significant from physics point of view. Though Lattice QCD calculations in the quenched approximation have suggested a linearly increasing potential in the confinement range [8–18], a specific form of interaction potential in the full range is not yet known. At short distances relativistic effects are more important as they give rise to quark-antiquark pairs from the vacuum that in turn affect the nonrelativistic Coulomb interaction in the presence of sea quarks. The mass spectra of quarkonia is not sensitive to these relativistic effects at short distances. However, the decay properties show significant difference with inclusion of relativistic corrections. We have used the most accepted available correction terms for computation of decay properties [113,118–120] that improves the results significantly in most cases.

Using the potential parameters and numerical wave function, we compute the various decay properties of heavy quarkonia. We first compute the leptonic decay constants of pseudoscalar and vector mesons and our numerical results are tabulated in Tables 8, 9, 10, 11, 12 and 13. For the case

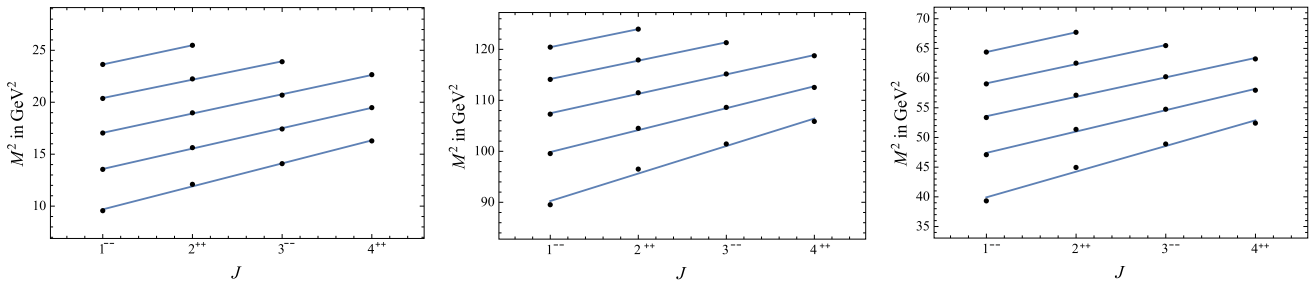

Fig. 1 Parent and daughter Regge trajectories (J, M^2) for charmonia (left), bottomonia (middle) and B_c (right) mesons with natural parity $(P = (-1)^J)$

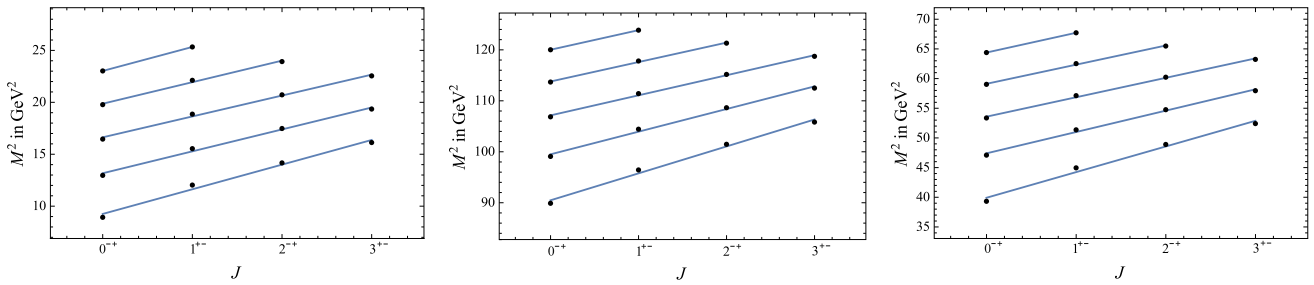

Fig. 2 Parent and daughter Regge trajectories (J, M^2) for charmonia (left), bottomonia (middle) and B_c (right) mesons with unnatural parity $(P = (-1)^{J+1})$

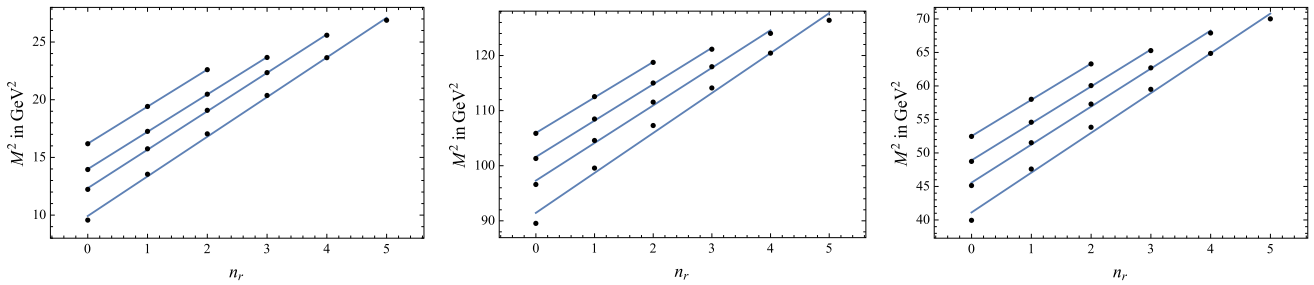

Fig. 3 Parent and daughter Regge trajectories $(n_r \rightarrow M^2)$ for charmonia (left), bottomonia (middle) and B_c (right) mesons

of charmonia, our results are higher than those using LQCD and QCDSR [100]. In order to overcome this discrepancy, we include the QCD correction factors given in Ref. [97] and the results are tabulated in Tables 8 and 9. After introducing the correction factors our results match with PDG, LQCD and QCDSR [100] along with other theoretical models. We also compute the decay constants for excited S-wave charmonia and we found that our results are consistent with the other theoretical predictions. We also compute the decay constants of bottomonia and B_c mesons. In this case, our results match with other theoretical predictions without incorporating the relativistic corrections. In the case of vector decay constants of bottomonia, our results are very close to experimental results as well as those obtained in LQCD Ref. [102]. For the decay constants of B_c mesons, we compare our results with nonrelativistic potential models [52,95].

Next we compute the digamma, digluon and dilepton decay widths using the relations Eqs. (13)–(16). Where the bracketed quantities are the first order radiative corrections to the decay widths. We compare our results with the available experimental results. We also compare our results with the theoretical models such as screened potential model [76,77], Martin-like potential model [73], relativistic quark model (RQM) [31,32], heavy quark spin symmetry [114], relativistic Salpeter model [121] and other theoretical data.

Tables 14 and 15 we present our results for digamma decay widths for charmonia and bottomonia. Our results for $\Gamma(\eta_c \rightarrow \gamma\gamma)$ and $\Gamma(\eta_c(2S) \rightarrow \gamma\gamma)$ are higher than the experimental results. Experimental observation of the two photon decays of pseudoscalar states are considered as an important probe for identification of flavour as well as internal structure of mesons. The first order radiative correction [bracketed terms in Eq. (13)] was utilized to incorporate the difference and it is observed that our results along with the correction match with the experimental results [7]. We also compute the digamma decay width of excited charmonia.

Our results for P-wave charmonia are higher than that of screened potential model [76] and relativistic quark model [32]. Our results for $\Gamma(\eta_b \rightarrow \gamma\gamma)$ match quite well with the experimental data while computed $\Gamma(\eta_b(2S) \rightarrow \gamma\gamma)$ value is overestimated when compared with the PDG data. For the excited state of S-wave bottomonia, our results fall in between those obtained in screened potential model [77] and relativistic quark model with linear confinement [64]. The scenario is similar with P-wave bottomonia and charmonia.

Di-gluon decay has substantial contribution to hadronic decay of quarkonia below $c\bar{c}$ and $b\bar{b}$ threshold. In Tables 16 and 17 we represent our results for digluon decay width of charmonia and bottomonia respectively. Our results for $\Gamma(\eta_c \rightarrow gg)$ match perfectly with the PDG data [7] but in the case of $\Gamma(\eta_c(2S) \rightarrow gg)$ our result is higher than the PDG data. We also compare the results obtained with that of the relativistic Salpeter method [121] and an approximate potential model [70]. It is seen from Table 16 that the relativistic corrections provide better results in case of P-wave charmonia where as that for bottomonia are underestimated in present calculations when compared to relativistic QCD potential model [122] and power potential model [47]. As the experimental data of digluon annihilation of bottomonia are not available, the validity of either of the approaches can be validated only after observations in forthcoming experiments.

We present the result of dilepton decay widths in the Tables 18 and 19 and it is observed that our results matches with the PDG data [7] upto $n = 3$ for both charmonia and bottomonia. The contribution of the correction factor is more significant in the excited states with compared to that in the ground states of the quarkonia, indicating different dynamics in the intermediate quark-antiquark distance. Our results are also in good accordance with the other theoretical models.

We present our results of $E1$ transitions in Tables 20, 21 and 22 in comparison with theoretical attempts such as relativistic potential model [39], quark model [30], nonrelativistic screened potential model [66,76,77]. We also compare our results of charmonia transitions with available experimental results. Our result for $\Gamma(\psi(2S) \rightarrow \chi_{cJ}(1P) + \gamma)$ is in good agreement with the experimental result for $J = 0$ but our results for $J = 1, 2$ are higher than the PDG data. Our results also agree well for the transition $\Gamma(\chi_{c2}(1P) \rightarrow J/\psi + \gamma)$. We also satisfy the experimental constraints for the transition $\Gamma(1^3D_1 \rightarrow \chi_{cJ} + \gamma)$ for $J = 0, 1, 2$. Our results share the same range with the results computed in other theoretical models. The $E1$ transitions of bottomonia agree fairly well except for the channel $\Gamma(\Upsilon(3S) \rightarrow \chi_{bJ}(3P))$, where our results are higher than the experimental results. The comparison of our results of $E1$ transitions in B_c mesons with relativistic quark model [30,63] and power potential model [46] are found to be in good agreement. In Tables 23, 24 and 25, we present our results of $M1$ transitions and also compared with relativistic potential model [39], quark model [30,64], nonrelativistic screened potential model [65,66], power potential [46] as well as with available experimental results. Our results of $\Gamma(\mathrm{n}\psi \rightarrow \mathrm{n}'\eta_c + \gamma)$ are in very good agreement with the PDG data as well with the other theoretical predictions. Computed $M1$ transitions in B_c mesons are also within the results obtained from theoretical predictions. The computed $M1$ transition of bottomonia are found to be higher than the PDG data and also theoretical predictions.

5 Conclusion

In this article, we have reported a comprehensive study of heavy quarkonia in the framework of nonrelativistic potential model considering linear confinement with least number of free model parameters such as confinement strength and quark mass. They are fine tuned to obtain the corresponding spin averaged ground state masses of charmonia and bottomonia determined from experimental data. The parameters are then used to predict the masses of excited states. In order to compute mass spectra of orbitally excited states, we incorporate contributions from the spin dependent part of confined one gluon exchange potential perturbatively.

Our results are found to be consistent with available PDG data, LQCD, relativistic quark model and other theoretical potential models. We also compute the digamma, digluon and dilepton decay widths of heavy quarkonia using nonrelativistic Van-Royen Weiskopf formula. The first order radiative corrections in calculation of these decays provide satisfactory results for the charmonia while no such correction is needed in case of bottomonia for being purely nonrelativistic system. We employ our parameters in computation of B_c spectroscopy employing the quark masses and mean value of confinement strength of charmonia and bottomonia and our results are also consistent with the PDG data. We also compute the weak decays of B_c mesons and the computed life time is also consistent with the PDG data. It is interesting to note here that despite having a c quark, the nonrelativistic calculation of B_c spectroscopy is in very good agreement with experimental and other theoretical models.

Acknowledgements J.N.P. acknowledges the support from the University Grants Commission of India under Major Research Project F.No. 42-775/2013(SR).

Funded by SCOAP[3].

References

1. E. Eichten, S. Godfrey, H. Mahlke, J.L. Rosner, Rev. Mod. Phys. **80**, 1161 (2008). https://doi.org/10.1103/RevModPhys.80.1161
2. S. Godfrey, S.L. Olsen, Ann. Rev. Nucl. Part. Sci. **58**, 51 (2008). https://doi.org/10.1146/annurev.nucl.58.110707.171145
3. T. Barnes, S.L. Olsen, Int. J. Mod. Phys. A **24S1**, 305 (2009). https://doi.org/10.1142/S0217751X09046576
4. N. Brambilla et al., Eur. Phys. J. C **71**, 1534 (2011). https://doi.org/10.1140/epjc/s10052-010-1534-9
5. N. Brambilla et al., Eur. Phys. J. C **74**(10), 2981 (2014). https://doi.org/10.1140/epjc/s10052-014-2981-5
6. A. Andronic et al., Eur. Phys. J. C **76**, 107 (2016). https://doi.org/10.1140/epjc/s10052-015-3819-59
7. C. Patrignani et al., Chin. Phys. C **40**(10), 100001 (2016). https://doi.org/10.1088/1674-1137/40/10/100001
8. J.J. Dudek, R.G. Edwards, N. Mathur, D.G. Richards, Phys. Rev. D **77**, 034501 (2008). https://doi.org/10.1103/PhysRevD.77.034501
9. S. Meinel, Phys. Rev. D **79**, 094501 (2009). https://doi.org/10.1103/PhysRevD.79.094501
10. T. Burch, C. DeTar, M. Di Pierro, A.X. El-Khadra, E.D. Freeland, S. Gottlieb, A.S. Kronfeld, L. Levkova, P.B. Mackenzie, J.N. Simone, Phys. Rev. D **81**, 034508 (2010). https://doi.org/10.1103/PhysRevD.81.034508
11. L. Liu, G. Moir, M. Peardon, S.M. Ryan, C.E. Thomas, P. Vilaseca, J.J. Dudek, R.G. Edwards, B. Joo, D.G. Richards, JHEP **07**, 126 (2012). https://doi.org/10.1007/JHEP07(2012)126
12. C. McNeile, C.T.H. Davies, E. Follana, K. Hornbostel, G.P. Lepage, Phys. Rev. D **86**, 074503 (2012). https://doi.org/10.1103/PhysRevD.86.074503
13. J.O. Daldrop, C.T.H. Davies, R.J. Dowdall, Phys. Rev. Lett. **108**, 102003 (2012). https://doi.org/10.1103/PhysRevLett.108.102003
14. T. Kawanai, S. Sasaki, Phys. Rev. D **89**(5), 054507 (2014). https://doi.org/10.1103/PhysRevD.89.054507
15. T. Kawanai, S. Sasaki, Phys. Rev. Lett. **107**, 091601 (2011). https://doi.org/10.1103/PhysRevLett.107.091601
16. Y. Burnier, O. Kaczmarek, A. Rothkopf, JHEP **12**, 101 (2015). https://doi.org/10.1007/JHEP12(2015)101
17. M. Kalinowski, M. Wagner, Phys. Rev. D **92**(9), 094508 (2015). https://doi.org/10.1103/PhysRevD.92.094508
18. Y. Burnier, O. Kaczmarek, A. Rothkopf, JHEP **10**, 032 (2016). https://doi.org/10.1007/JHEP10(2016)032
19. T. Hilger, C. Popovici, M. Gomez-Rocha, A. Krassnigg, Phys. Rev. D **91**(3), 034013 (2015). https://doi.org/10.1103/PhysRevD.91.034013
20. M.B. Voloshin, Prog. Part. Nucl. Phys. **61**, 455 (2008). https://doi.org/10.1016/j.ppnp.2008.02.001
21. S. Cho, K. Hattori, S.H. Lee, K. Morita, S. Ozaki, Phys. Rev. D **91**(4), 045025 (2015). https://doi.org/10.1103/PhysRevD.91.045025
22. S.S. Gershtein, V.V. Kiselev, A.K. Likhoded, A.V. Tkabladze, Phys. Rev. D **51**, 3613 (1995). https://doi.org/10.1103/PhysRevD.51.3613
23. Y. Kiyo, Y. Sumino, Phys. Lett. B **730**, 76 (2014). https://doi.org/10.1016/j.physletb.2014.01.030
24. T. Liu, A.A. Penin, A. Rayyan, JHEP **02**, 084 (2017). https://doi.org/10.1007/JHEP02(2017)084
25. R.J. Dowdall, C.T.H. Davies, T. Hammant, R.R. Horgan, Phys. Rev. D **89**(3), 031502 (2014). https://doi.org/10.1103/PhysRevD.92.039904, https://doi.org/10.1103/PhysRevD.89.031502. [Erratum: Phys. Rev. D **92**, 039904 (2015)]
26. M. Neubert, Phys. Rep. **245**, 259 (1994). https://doi.org/10.1016/0370-1573(94)90091-4
27. D. Ebert, R.N. Faustov, V.O. Galkin, Eur. Phys. J. C **71**, 1825 (2011). https://doi.org/10.1140/epjc/s10052-011-1825-9
28. D. Ebert, R.N. Faustov, V.O. Galkin, Phys. Rev. D **79**, 114029 (2009). https://doi.org/10.1103/PhysRevD.79.114029
29. D. Ebert, R.N. Faustov, V.O. Galkin, Eur. Phys. J. C **47**, 745 (2006). https://doi.org/10.1140/epjc/s2006-02601-0
30. D. Ebert, R.N. Faustov, V.O. Galkin, Phys. Rev. D **67**, 014027 (2003). https://doi.org/10.1103/PhysRevD.67.014027
31. D. Ebert, R.N. Faustov, V.O. Galkin, Mod. Phys. Lett. A **18**, 1597 (2003). https://doi.org/10.1142/S0217732303011307
32. D. Ebert, R.N. Faustov, V.O. Galkin, Mod. Phys. Lett. A **18**, 601 (2003). https://doi.org/10.1142/S021773230300971X
33. D. Ebert, R.N. Faustov, V.O. Galkin, Phys. Rev. D **62**, 034014 (2000). https://doi.org/10.1103/PhysRevD.62.034014
34. S.N. Gupta, S.F. Radford, Phys. Rev. D **24**, 2309 (1981). https://doi.org/10.1103/PhysRevD.24.2309
35. S.N. Gupta, S.F. Radford, W.W. Repko, Phys. Rev. D **26**, 3305 (1982). https://doi.org/10.1103/PhysRevD.26.3305
36. S.N. Gupta, S.F. Radford, Phys. Rev. D **25**, 3430 (1982). https://doi.org/10.1103/PhysRevD.25.3430
37. J.T. Pantaleone, S.H.H. Tye, Y.J. Ng, Phys. Rev. D **33**, 777 (1986). https://doi.org/10.1103/PhysRevD.33.777
38. K.M. Maung, D.E. Kahana, J.W. Norbury, Phys. Rev. D **47**, 1182 (1993). https://doi.org/10.1103/PhysRevD.47.1182
39. S.F. Radford, W.W. Repko, Phys. Rev. D **75**, 074031 (2007). https://doi.org/10.1103/PhysRevD.75.074031
40. S.F. Radford, W.W. Repko, Nucl. Phys. A **865**, 69 (2011). https://doi.org/10.1016/j.nuclphysa.2011.06.032
41. S.N. Gupta, S.F. Radford, W.W. Repko, Phys. Rev. D **34**, 201 (1986). https://doi.org/10.1103/PhysRevD.34.201
42. P.C. Vinodkumar, J.N. Pandya, V.M. Bannur, S.B. Khadkikar, Eur. Phys. J. A **4**, 83 (1999). https://doi.org/10.1007/s100500050206
43. J.N. Pandya, P.C. Vinodkumar, Pramana **57**, 821 (2001). https://doi.org/10.1007/s12043-001-0031-y
44. A.K. Rai, J.N. Pandya, P.C. Vinodkumar, Eur. Phys. J. A **38**, 77 (2008). https://doi.org/10.1140/epja/i2008-10639-9
45. J.N. Pandya, N.R. Soni, N. Devlani, A.K. Rai, Chin. Phys. C **39**(12), 123101 (2015). https://doi.org/10.1088/1674-1137/39/12/123101
46. N. Devlani, V. Kher, A.K. Rai, Eur. Phys. J. A **50**(10), 154 (2014). https://doi.org/10.1140/epja/i2014-14154-2
47. A. Parmar, B. Patel, P.C. Vinodkumar, Nucl. Phys. A **848**, 299 (2010). https://doi.org/10.1016/j.nuclphysa.2010.08.016
48. A.K. Rai, R.H. Parmar, P.C. Vinodkumar, J. Phys. G **28**, 2275 (2002). https://doi.org/10.1088/0954-3899/28/8/313
49. A. Kumar Rai, P.C. Vinodkumar, J.N. Pandya, J. Phys. G **31**, 1453 (2005). https://doi.org/10.1088/0954-3899/31/12/007
50. A.K. Rai, P.C. Vinodkumar, Pramana **66**, 953 (2006). https://doi.org/10.1007/BF02704795
51. A.K. Rai, B. Patel, P.C. Vinodkumar, Phys. Rev. C **78**, 055202 (2008). https://doi.org/10.1103/PhysRevC.78.055202
52. B. Patel, P.C. Vinodkumar, J. Phys. G **36**, 035003 (2009). https://doi.org/10.1088/0954-3899/36/3/035003
53. M. Fabre De La Ripelle, Phys. Lett. B **205**, 97 (1988). https://doi.org/10.1016/0370-2693(88)90406-6
54. E. Eichten, K. Gottfried, T. Kinoshita, J.B. Kogut, K.D. Lane, T.M. Yan, Phys. Rev. Lett. **34**, 369 (1975). https://doi.org/10.1103/PhysRevLett.34.369. [Erratum: Phys. Rev. Lett. **36**, 1276 (1976)]
55. E. Eichten, K. Gottfried, T. Kinoshita, K.D. Lane, T.M. Yan, Phys. Rev. D **17**, 3090 (1978). https://doi.org/10.1103/PhysRevD.17.3090, https://doi.org/10.1103/PhysRevD.21.313. [Erratum: Phys. Rev. D **21**, 313 (1980)]
56. E. Eichten, K. Gottfried, T. Kinoshita, K.D. Lane, T.M. Yan, Phys. Rev. D **21**, 203 (1980). https://doi.org/10.1103/PhysRevD.21.203

57. C. Quigg, J.L. Rosner, Phys. Rep. **56**, 167 (1979). https://doi.org/10.1016/0370-1573(79)90095-4
58. E. Eichten, F. Feinberg, Phys. Rev. D **23**, 2724 (1981). https://doi.org/10.1103/PhysRevD.23.2724
59. T. Barnes, S. Godfrey, E.S. Swanson, Phys. Rev. D **72**, 054026 (2005). https://doi.org/10.1103/PhysRevD.72.054026
60. V. Sauli, Phys. Rev. D **86**, 096004 (2012). https://doi.org/10.1103/PhysRevD.86.096004
61. S. Leitão, A. Stadler, M.T. Peña, E.P. Biernat, Phys. Rev. D **90**(9), 096003 (2014). https://doi.org/10.1103/PhysRevD.90.096003
62. S. Godfrey, N. Isgur, Phys. Rev. D **32**, 189 (1985). https://doi.org/10.1103/PhysRevD.32.189
63. S. Godfrey, Phys. Rev. D **70**, 054017 (2004). https://doi.org/10.1103/PhysRevD.70.054017
64. S. Godfrey, K. Moats, Phys. Rev. D **92**(5), 054034 (2015). https://doi.org/10.1103/PhysRevD.92.054034
65. W.J. Deng, H. Liu, L.C. Gui, X.H. Zhong, Phys. Rev. D **95**(3), 034026 (2017). https://doi.org/10.1103/PhysRevD.95.034026
66. W.J. Deng, H. Liu, L.C. Gui, X.H. Zhong, Phys. Rev. D **95**(7), 074002 (2017). https://doi.org/10.1103/PhysRevD.95.074002
67. C.S. Fischer, S. Kubrak, R. Williams, Eur. Phys. J. A **51**, 10 (2015). https://doi.org/10.1140/epja/i2015-15010-7
68. O. Lakhina, E.S. Swanson, Phys. Rev. D **74**, 014012 (2006). https://doi.org/10.1103/PhysRevD.74.014012
69. J. Segovia, P.G. Ortega, D.R. Entem, F. Fernández, Phys. Rev. D **93**(7), 074027 (2016). https://doi.org/10.1103/PhysRevD.93.074027
70. S. Patel, P.C. Vinodkumar, S. Bhatnagar, Chin. Phys. C **40**(5), 053102 (2016). https://doi.org/10.1088/1674-1137/40/5/053102
71. C. Bonati, M. D'Elia, A. Rucci, Phys. Rev. D **92**(5), 054014 (2015). https://doi.org/10.1103/PhysRevD.92.054014
72. T. Gutsche, V.E. Lyubovitskij, I. Schmidt, A. Vega, Phys. Rev. D **90**(9), 096007 (2014). https://doi.org/10.1103/PhysRevD.90.096007
73. M. Shah, A. Parmar, P.C. Vinodkumar, Phys. Rev. D **86**, 034015 (2012). https://doi.org/10.1103/PhysRevD.86.034015
74. H. Negash, S. Bhatnagar, Int. J. Mod. Phys. E **25**(08), 1650059 (2016). https://doi.org/10.1142/S0218301316500592
75. K.B.Vijaya Bhaghyesh, A.P.Monteiro Kumar, Phys. G **38**, 085001 (2011). https://doi.org/10.1088/0954-3899/38/8/085001
76. B.Q. Li, K.T. Chao, Phys. Rev. D **79**, 094004 (2009). https://doi.org/10.1103/PhysRevD.79.094004
77. B.Q. Li, K.T. Chao, Commun. Theor. Phys. **52**, 653 (2009). https://doi.org/10.1088/0253-6102/52/4/20
78. C. Quigg, J.L. Rosner, Phys. Lett. B **71**, 153 (1977). https://doi.org/10.1016/0370-2693(77)90765-1
79. A. Martin, Phys. Lett. B **93**(3), 338 (1980). https://doi.org/10.1016/0370-2693(80)90527-4
80. W. Buchmuller, S.H.H. Tye, Phys. Rev. D **24**, 132 (1981). https://doi.org/10.1103/PhysRevD.24.132
81. Wk Kwong, J.L. Rosner, Phys. Rev. D **44**, 212 (1991). https://doi.org/10.1103/PhysRevD.44.212
82. E.J. Eichten, C. Quigg, Phys. Rev. D **49**, 5845 (1994). https://doi.org/10.1103/PhysRevD.49.5845
83. F. Abe et al., Phys. Rev. Lett. **81**, 2432 (1998). https://doi.org/10.1103/PhysRevLett.81.2432
84. V.M. Abazov et al., Phys. Rev. Lett. **101**, 012001 (2008). https://doi.org/10.1103/PhysRevLett.101.012001
85. R. Aaij et al., Phys. Rev. Lett. **109**, 232001 (2012). https://doi.org/10.1103/PhysRevLett.109.232001
86. R. Aaij et al., Eur. Phys. J. C **74**(5), 2839 (2014). https://doi.org/10.1140/epjc/s10052-014-2839-x
87. G. Aad et al., Phys. Rev. Lett. **113**(21), 212004 (2014). https://doi.org/10.1103/PhysRevLett.113.212004
88. S.N. Gupta, J.M. Johnson, Phys. Rev. D **53**, 312 (1996). https://doi.org/10.1103/PhysRevD.53.312
89. G.S. Bali, B. Bolder, N. Eicker, T. Lippert, B. Orth, P. Ueberholz, K. Schilling, T. Struckmann, Phys. Rev. D **62**, 054503 (2000). https://doi.org/10.1103/PhysRevD.62.054503
90. G.S. Bali, Phys. Rep. **343**, 1 (2001). https://doi.org/10.1016/S0370-1573(00)00079-X
91. C. Alexandrou, P. de Forcrand, O. Jahn, Nucl. Phys. Proc. Suppl. **119**, 667 (2003)
92. N. Isgur, G. Karl, Phys. Rev. D **18**, 4187 (1978). https://doi.org/10.1103/PhysRevD.18.4187
93. K.B. Vijaya Kumar, A.K. Rath, S.B. Khadkikar, Pramana **48**, 997 (1997). https://doi.org/10.1007/BF02847459
94. W. Lucha, F.F. Schoberl, Int. J. Mod. Phys. C **10**, 607 (1999). https://doi.org/10.1142/S0129183199000450
95. A.P. Monteiro, M. Bhat, K.B. Vijaya Kumar, Phys. Rev. D **95**(5), 054016 (2017). https://doi.org/10.1103/PhysRevD.95.054016
96. R. Van Royen, V.F. Weisskopf, Nuovo Cim. A **50**, 617 (1967). https://doi.org/10.1007/BF02823542. [Erratum: Nuovo Cim. A **51**, 583 (1967)]
97. E. Braaten, S. Fleming, Phys. Rev. D **52**, 181 (1995). https://doi.org/10.1103/PhysRevD.52.181
98. A.V. Berezhnoy, V.V. Kiselev, A.K. Likhoded, Z. Phys. A **356**, 89 (1996). https://doi.org/10.1007/s002180050152
99. A. Krassnigg, M. Gomez-Rocha, T. Hilger, J. Phys. Conf. Ser. **742**(1), 012032 (2016). https://doi.org/10.1088/1742-6596/742/1/012032
100. D. Bečirević, G. Duplančić, B. Klajn, B. Melić, F. Sanfilippo, Nucl. Phys. B **883**, 306 (2014). https://doi.org/10.1016/j.nuclphysb.2014.03.024
101. G.L. Wang, Phys. Lett. B **633**, 492 (2006). https://doi.org/10.1016/j.physletb.2005.12.005
102. B. Colquhoun, R.J. Dowdall, C.T.H. Davies, K. Hornbostel, G.P. Lepage, Phys. Rev. D **91**(7), 074514 (2015). https://doi.org/10.1103/PhysRevD.91.074514
103. K.M. Ecklund et al., Phys. Rev. D **78**, 091501 (2008). https://doi.org/10.1103/PhysRevD.78.091501
104. J.P. Lees et al., Phys. Rev. D **81**, 052010 (2010). https://doi.org/10.1103/PhysRevD.81.052010
105. M. Ablikim et al., Phys. Rev. D **85**, 112008 (2012). https://doi.org/10.1103/PhysRevD.85.112008
106. J.J. Dudek, R.G. Edwards, Phys. Rev. Lett. **97**, 172001 (2006). https://doi.org/10.1103/PhysRevLett.97.172001
107. T. Chen et al., Eur. Phys. J. C **76**(7), 358 (2016). https://doi.org/10.1140/epjc/s10052-016-4212-8
108. G.T. Bodwin, E. Braaten, G.P. Lepage, Phys. Rev. D **51**, 1125 (1995). https://doi.org/10.1103/PhysRevD.55.5853, https://doi.org/10.1103/PhysRevD.51.1125. [Erratum: Phys. Rev. D **55**, 5853 (1997)]
109. H. Khan, P. Hoodbhoy, Phys. Rev. D **53**, 2534 (1996). https://doi.org/10.1103/PhysRevD.53.2534
110. G.A. Schuler, F.A. Berends, R. van Gulik, Nucl. Phys. B **523**, 423 (1998). https://doi.org/10.1016/S0550-3213(98)00128-X
111. G.T. Bodwin, D. Kang, J. Lee, Phys. Rev. D **74**, 014014 (2006). https://doi.org/10.1103/PhysRevD.74.014014
112. G.T. Bodwin, H.S. Chung, D. Kang, J. Lee, C. Yu, Phys. Rev. D **77**, 094017 (2008). https://doi.org/10.1103/PhysRevD.77.094017
113. J.P. Lansberg, T.N. Pham, Phys. Rev. D **79**, 094016 (2009). https://doi.org/10.1103/PhysRevD.79.094016
114. J.P. Lansberg, T.N. Pham, Phys. Rev. D **74**, 034001 (2006). https://doi.org/10.1103/PhysRevD.74.034001
115. W.L. Sang, F. Feng, Y. Jia, S.R. Liang, Phys. Rev. D **94**(11), 111501 (2016). https://doi.org/10.1103/PhysRevD.94.111501
116. L.D. Landau, Dokl. Akad. Nauk Ser. Fiz. **60**(2), 207 (1948). https://doi.org/10.1016/B978-0-08-010586-4.50070-5
117. C.N. Yang, Phys. Rev. **77**, 242 (1950). https://doi.org/10.1103/PhysRev.77.242

118. W. Kwong, P.B. Mackenzie, R. Rosenfeld, J.L. Rosner, Phys. Rev. D **37**, 3210 (1988). https://doi.org/10.1103/PhysRevD.37.3210
119. R. Barbieri, M. Caffo, R. Gatto, E. Remiddi, Nucl. Phys. B **192**, 61 (1981). https://doi.org/10.1016/0550-3213(81)90192-9
120. M.L. Mangano, A. Petrelli, Phys. Lett. B **352**, 445 (1995). https://doi.org/10.1016/0370-2693(95)00516-N
121. C.S. Kim, T. Lee, G.L. Wang, Phys. Lett. B **606**, 323 (2005). https://doi.org/10.1016/j.physletb.2004.11.084
122. S.N. Gupta, J.M. Johnson, W.W. Repko, Phys. Rev. D **54**, 2075 (1996). https://doi.org/10.1103/PhysRevD.54.2075
123. P. Gonzalez, A. Valcarce, H. Garcilazo, J. Vijande, Phys. Rev. D **68**, 034007 (2003). https://doi.org/10.1103/PhysRevD.68.034007
124. N. Brambilla, Y. Jia, A. Vairo, Phys. Rev. D **D73**, 054005 (2006). https://doi.org/10.1103/PhysRevD.73.054005
125. D.M. Li, P.F. Ji, B. Ma, Eur. Phys. J. C **71**, 1582 (2011). https://doi.org/10.1140/epjc/s10052-011-1582-9
126. A. Abd El-Hady, M.A.K. Lodhi, J.P. Vary, Phys. Rev. D **59**, 094001 (1999). https://doi.org/10.1103/PhysRevD.59.094001

Semileptonic $D_{(s)}$-meson decays in the light of recent data

N. R. Soni,[1,*] M. A. Ivanov,[2,†] J. G. Körner,[3,‡] J. N. Pandya,[1,§] P. Santorelli,[4,5,‖] and C. T. Tran[6,4,¶]

[1]*Applied Physics Department, Faculty of Technology and Engineering, The Maharaja Sayajirao University of Baroda, Vadodara 390001, Gujarat, India*

[2]*Bogoliubov Laboratory of Theoretical Physics, Joint Institute for Nuclear Research, 141980 Dubna, Russia*

[3]*PRISMA Cluster of Excellence, Institut für Physik, Johannes Gutenberg-Universität, D-55099 Mainz, Germany*

[4]*Dipartimento di Fisica "E. Pancini," Università di Napoli Federico II, Complesso Universitario di Monte S. Angelo, Via Cintia, Edificio 6, 80126 Napoli, Italy*

[5]*Istituto Nazionale di Fisica Nucleare, Sezione di Napoli, 80126 Napoli, Italy*

[6]*Institute of Research and Development, Duy Tan University, 550000 Da Nang, Vietnam*

(Received 1 November 2018; published 26 December 2018)

Inspired by recent improved measurements of charm semileptonic decays at BESIII, we study a large set of $D(D_s)$-meson semileptonic decays where the hadron in the final state is one of D^0, ρ, ω, $\eta^{(\prime)}$ in the case of D^+ decays, and D^0, ϕ, K^0, $K^*(892)^0$, $\eta^{(\prime)}$ in the case of D_s^+ decays. The required hadronic form factors are computed in the full kinematical range of momentum transfer by employing the covariant confined quark model developed by us. A detailed comparison of the form factors with those from other approaches is provided. We calculate the decay branching fractions and their ratios, which show good agreement with available experimental data. We also give predictions for the forward-backward asymmetry and the longitudinal and transverse polarizations of the charged lepton in the final state.

DOI: 10.1103/PhysRevD.98.114031

I. INTRODUCTION

Semileptonic $D(D_s)$-meson decays provide a good platform to study both the weak and strong interactions in the charm sector (for a review, see e.g., Ref. [1]). Measurements of their decay rates allow a direct determination of the Cabibbo-Kobayashi-Maskawa (CKM) matrix elements $|V_{cs}|$ and $|V_{cd}|$. In particular, the average of the measurements of *BABAR* [2,3], Belle [4], BESIII [5], and CLEO [6] of the decays $D \to \pi(K)\ell\nu$ was used to extract the elements $|V_{cd(s)}|$, as recently reported by the Particle Data Group (PDG) [7]. Such extraction of the CKM matrix elements from experiments requires theoretical knowledge of the hadronic form factors which take into account the nonperturbative quantum chromodynamics (QCD) effects.

The elements $|V_{cs}|$ and $|V_{cd}|$ can also be determined indirectly by using the unitarity constraint on the CKM matrix. This method was very useful in the past when the direct measurements still suffered from large uncertainties, both experimental and theoretical. Once these matrix elements are determined, whether directly or indirectly, one can in reverse study the strong interaction effects in various charm semileptonic channels to reveal the decay dynamics. One can also test the predictions of different theoretical approaches, such as the form factors and the branching fractions. In this manner, the study of semileptonic charm decays can indirectly contribute to a more precise determination of other CKM matrix elements such as $|V_{ub}|$, in the sense that constraints provided by charm decays can improve the theoretical inputs needed for extracting $|V_{ub}|$ from exclusive charmless B semileptonic decays.

Recent progresses in experimental facilities and theoretical studies have made more and more stringent tests of the standard model (SM) available in the charm sector and have opened a new window through which to look for possible new physics effects beyond the SM. These tests include the CKM matrix unitarity, charge-conjugation-parity violation, isospin symmetry, and lepton flavor universality (LFU). Notably, the BESIII collaboration has reported recently measurements of many semimuonic

*nrsoni-apphy@msubaroda.ac.in
†ivanovm@theor.jinr.ru
‡jukoerne@uni-mainz.de
§jnpandya-apphy@msubaroda.ac.in
‖Pietro.Santorelli@na.infn.it
¶corresponding author.
tranchienthang1347@gmail.com

charm decays [8–10], some for the first time and some with much improved precision. This paves the way to the search for signals of LFU violations in these channels. In addition, the study of the decays $D_s \to \eta^{(\prime)}\ell^+\nu_\ell$ provides information about the $\eta-\eta'$ mixing angle and helps probe the interesting $\eta-\eta'$-glueball mixing [11,12].

From the theoretical point of view, the calculation of hadronic form factors plays a crucial role in the study of charm semileptonic decays. This calculation is carried out by nonperturbative methods including lattice QCD (LQCD) [13–15], QCD sum rules [16–18], light-cone sum rules (LCSR) [19–25], and phenomenological quark models. Regarding the quark models used in studies of semileptonic D decays, one can mention the Isgur-Scora-Grinstein-Wise (ISGW) model [26] and its updated version ISGW2 [27], the constituent quark model (CQM) [28], the relativistic quark model based on the quasipotential approach [29], the chiral quark model [30], the light-front quark model (LFQM) [31–33], and the model based on the combination of heavy meson and chiral symmetries (HMχT) [34,35]. Several semileptonic decay channels of the $D_{(s)}$ mesons were also studied in the large energy effective theory [36], chiral perturbation theory [37], the so-called chiral unitary approach (χUA) [38], and a new approach assuming pure heavy quark symmetry [39]. Recently, a simple expression for $D \to K$ semileptonic form factors was studied in Ref. [40]. We also mention here early attempts to account for flavor symmetry breaking in pseudoscalar meson decay constants by the authors of Ref. [41]. It is worth noting that each method has only a limited range of applicability, and their combination will give a better picture of the underlined physics [28].

In this paper, we compute the form factors of the semileptonic $D(D_s)$ decays in the framework of the covariant confined quark model (CCQM) [42–45]. To be more specific, we study the decays $D^+ \to (D^0,\rho^0,\omega,\eta,\eta')\ell^+\nu_\ell$, $D_s^+ \to (D^0,\phi,K^0,K^*(892)^0,\eta,\eta')\ell^+\nu_\ell$, and $D^0 \to \rho^-\ell^+\nu_\ell$. This paper follows our previous study [46] in which some of us have considered the decays $D \to K^{(*)}\ell^+\nu_\ell$ and $D \to \pi\ell^+\nu_\ell$ in great detail. Our aim is to provide a systematic and independent study of $D_{(s)}$ semileptonic channels in the same theoretical framework. This will shed more light on the theoretical study of the charm decays, especially on the shape of the corresponding form factors, since the CCQM predicts the form factors in the whole physical range of momentum transfer without using any extrapolations. Besides, many of the studies mentioned in the previous paragraph were done about a decade ago, with the main focus on the branching fraction. In light of recent data, more up-to-date predictions are necessary, not only for the branching fraction but also for other physical observables such as the forward-backward asymmetry and the lepton polarization. Finally, such a systematic study is necessary to test our model's predictions and to better estimate its theoretical error.

The rest of the paper is organized as follows. In Sec. II, we briefly provide the definitions of the semileptonic matrix element and hadronic form factors. Then we give the decay distribution in terms of the helicity amplitudes. In Sec. III, we introduce the essential ingredients of the covariant confined quark model and describe in some detail the calculation of the form factors in our approach. Numerical results for the form factors, the decay branching fractions, and other physical observables are presented in Sec. IV. We compare our findings with other theoretical approaches as well as experimental data including recent LQCD calculations and BESIII data. Finally, the conclusion is given in Sec. V.

II. MATRIX ELEMENT AND DECAY DISTRIBUTION

Within the SM, the matrix element for semileptonic decays of the $D_{(s)}$ meson to a pseudoscalar (P) or a vector (V) meson in the final state is written as

$$\mathcal{M}(D_{(s)} \to (P,V)\ell^+\nu_\ell) = \frac{G_F}{\sqrt{2}} V_{cq} \langle (P,V)|\bar{q}O^\mu c|D_{(s)}\rangle [\ell^+ O_\mu \nu_\ell], \tag{1}$$

where $O^\mu = \gamma^\mu(1-\gamma_5)$, and $q = d, s$. The hadronic part in the matrix element is parametrized by the invariant form factors which depend on the momentum transfer squared q^2 between the two mesons as follows:

$$\begin{aligned}
\langle P(p_2)|\bar{q}O^\mu c|D_{(s)}(p_1)\rangle &= F_+(q^2)P^\mu + F_-(q^2)q^\mu,\\
\langle V(p_2,\epsilon_2)|\bar{q}O^\mu c|D_{(s)}(p_1)\rangle &= \frac{\epsilon_{2\alpha}^\dagger}{M_1+M_2}[-g^{\mu\alpha}PqA_0(q^2)\\
&\quad + P^\mu P^\alpha A_+(q^2) + q^\mu P^\alpha A_-(q^2)\\
&\quad + i\varepsilon^{\mu\alpha Pq}V(q^2)],
\end{aligned} \tag{2}$$

where $P = p_1 + p_2$, $q = p_1 - p_2$, and ϵ_2 is the polarization vector of the vector meson V, so that $\epsilon_2^\dagger \cdot p_2 = 0$. The mesons are on shell: $p_1^2 = m_{D_{(s)}}^2 = M_1^2$, $p_2^2 = m_{P,V}^2 = M_2^2$.

For later comparison of the form factors with other studies, we relate our form factors defined in Eq. (2) to the well-known Bauer-Stech-Wirbel (BSW) form factors [47], namely, $F_{+,0}$ for $D_{(s)} \to P$ and $A_{0,1,2}$ and V for $D_{(s)} \to V$. Note that in Ref. [47] the notation F_1 was used instead of F_+. The relations read

$$\begin{aligned}
&\tilde{A}_2 = A_+, \qquad \tilde{V} = V, \qquad \tilde{F}_+ = F_+,\\
&\tilde{A}_1 = \frac{M_1-M_2}{M_1+M_2}A_0, \qquad \tilde{F}_0 = F_+ + \frac{q^2}{M_1^2-M_2^2}F_-,\\
&\tilde{A}_0 = \frac{M_1-M_2}{2M_2}\left(A_0 - A_+ - \frac{q^2}{M_1^2-M_2^2}A_-\right).
\end{aligned} \tag{3}$$

Here, the BSW form factors are denoted with a tilde to distinguish from our form factors. However, for simplicity, we will omit the tilde in what follows. In all comparisons of the form factors to appear below, we use the BSW ones.

Once the form factors are known, one can easily calculate the semileptonic decay rates. However, it is more convenient to write down the differential decay width in terms of the so-called helicity amplitudes which are combinations of the form factors. This is known as the helicity technique, first described in Ref. [48] and further discussed in our recent papers [49,50]. One has

$$\frac{d\Gamma(D_{(s)}\to(P,V)\ell^+\nu_\ell)}{dq^2} = \frac{G_F^2|V_{cq}|^2|\mathbf{p_2}|q^2}{96\pi^3 M_1^2}\left(1-\frac{m_\ell^2}{q^2}\right)^2 \times\left[\left(1+\frac{m_\ell^2}{2q^2}\right)(|H_+|^2+|H_-|^2+|H_0|^2)+\frac{3m_\ell^2}{2q^2}|H_t|^2\right], \quad (4)$$

where $|\mathbf{p_2}|=\lambda^{1/2}(M_1^2,M_2^2,q^2)/2M_1$ is the momentum of the daughter meson in the rest frame of the parent meson. Here, the helicity amplitudes for the decays $D_{(s)}\to V\ell^+\nu_\ell$ are defined as

$$\begin{aligned} H_\pm &= \frac{1}{M_1+M_2}(-PqA_0 \pm 2M_1|\mathbf{p_2}|V), \\ H_0 &= \frac{1}{M_1+M_2}\frac{1}{2M_2\sqrt{q^2}}[-Pq(M_1^2-M_2^2-q^2)A_0 \\ &\quad + 4M_1^2|\mathbf{p_2}|^2A_+], \\ H_t &= \frac{1}{M_1+M_2}\frac{M_1|\mathbf{p_2}|}{M_2\sqrt{q^2}}[Pq(-A_0+A_+)+q^2A_-]. \end{aligned} \quad (5)$$

In the case of the decays $D_{(s)}\to P\ell^+\nu_\ell$ one has

$$\begin{aligned} H_\pm &= 0, \qquad H_0 = \frac{2M_1|\mathbf{p_2}|}{\sqrt{q^2}}F_+, \\ H_t &= \frac{1}{\sqrt{q^2}}(PqF_+ + q^2F_-). \end{aligned} \quad (6)$$

In order to study the lepton-mass effects, one can define several physical observables such as the forward-backward asymmetry $\mathcal{A}_{\rm FB}^\ell(q^2)$ and the longitudinal $P_L^\ell(q^2)$ and transverse $P_T^\ell(q^2)$ polarization of the charged lepton in the final state. This requires the angular decay distribution, which was described elsewhere [50]. In short, one can write down these observables in terms of the helicity amplitudes as follows:

$$\mathcal{A}_{\rm FB}^\ell(q^2) = -\frac{3}{4}\frac{|H_+|^2-|H_-|^2+4\delta_\ell H_0H_t}{(1+\delta_\ell)\sum|H_n|^2+3\delta_\ell|H_t|^2}, \quad (7)$$

$$P_L^\ell(q^2) = -\frac{(1-\delta_\ell)\sum|H_n|^2-3\delta_\ell|H_t|^2}{(1+\delta_\ell)\sum|H_n|^2+3\delta_\ell|H_t|^2}, \quad (8)$$

$$P_T^\ell(q^2) = -\frac{3\pi}{4\sqrt{2}}\frac{\sqrt{\delta_\ell}(|H_+|^2-|H_-|^2-2H_0H_t)}{(1+\delta_\ell)\sum|H_n|^2+3\delta_\ell|H_t|^2}, \quad (9)$$

where $\delta_\ell=m_\ell^2/2q^2$ is the helicity-flip factor, and the index n runs through $(+,-,0)$. The average of these observables over the q^2 range is better suited for experimental measurements with low statistics. To calculate the average one has to multiply the numerator and denominator of e.g., Eq. (7) by the phase-space factor $C(q^2)=|\mathbf{p_2}|(q^2-m_\ell^2)^2/q^2$ and integrate them separately. These observables are sensitive to contributions of physics beyond the SM and can be used to test LFU violations [51–57].

III. FORM FACTORS IN THE COVARIANT CONFINED QUARK MODEL

In this study, the semileptonic form factors are calculated in the framework of the CCQM [42,43]. The CCQM is an effective quantum field approach to the calculation of hadronic transitions. The model is built on the assumption that hadrons interact via constituent quark exchange only. This is realized by adopting a relativistic invariant Lagrangian that describes the coupling of a hadron to its constituent quarks. This approach can be used to treat not only mesons [58–62], but also baryons [63–65], tetraquarks [66–68], and other multiquark states [69] in a consistent way. For a detailed description of the model and the calculation techniques we refer the reader to the references mentioned above. We list below only several key features of the CCQM for completeness.

For the simplest hadronic system, i.e., a meson M, the interaction Lagrangian is given by

$$\mathcal{L}_{\rm int} = g_M M(x)\int dx_1dx_2F_M(x;x_1,x_2) \times\bar{q}_2(x_2)\Gamma_M q_1(x_1)+{\rm H.c.}, \quad (10)$$

where g_M is the quark-meson coupling and Γ_M is the Dirac matrix. For a pseudoscalar (vector) meson $\Gamma_M=\gamma_5$ ($\Gamma_M=\gamma_\mu$). The vertex function $F_M(x,x_1,x_2)$ effectively describes the quark distribution in the meson and is given by

$$F_M(x,x_1,x_2)=\delta\left(x-\sum_{i=1}^2 w_ix_i\right)\cdot\Phi_M((x_1-x_2)^2), \quad (11)$$

where $w_{q_i}=m_{q_i}/(m_{q_1}+m_{q_2})$ such that $w_1+w_2=1$. The function Φ_M depends on the effective size of the meson. In order to avoid ultraviolet divergences in the quark loop integrals, it is required that the Fourier transform of Φ_M has an appropriate falloff behavior in the Euclidean region. Since the final results are not sensitive to the specific form of Φ_M, for simplicity, we choose a Gaussian form as follows:

$$\tilde{\Phi}_M(-p^2) = \int dx e^{ipx} \Phi_M(x^2) = e^{p^2/\Lambda_M^2}, \quad (12)$$

where the parameter Λ_M characterizes the finite size of the meson.

The coupling strength g_M is determined by the compositeness condition $Z_M = 0$ [70], where Z_M is the wave function renormalization constant of the meson. This condition ensures the absence of any bare quark state in the physical mesonic state and, therefore, helps avoid double counting and provides an effective description of a bound state.

In order to calculate the form factors, one first writes down the matrix element of the hadronic transition. In the CCQM, the hadronic matrix element is described by the one-loop Feynman diagram depicted in Fig. 1 and is constructed from the convolution of quark propagators and vertex functions as follows:

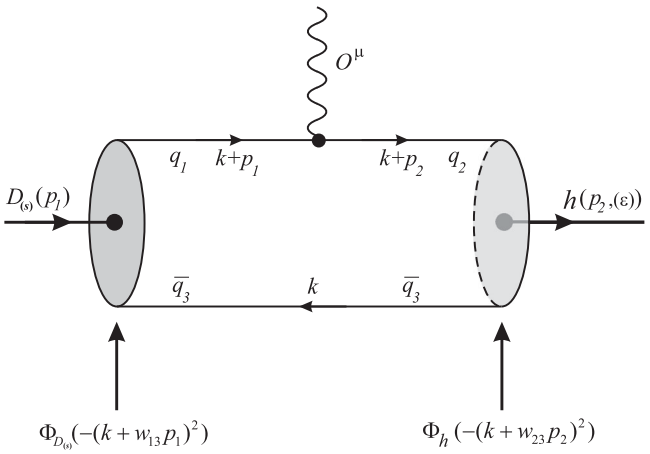

FIG. 1. Quark model diagram for the $D_{(s)}$-meson semileptonic decay.

$$\langle P(p_2)|\bar{q}O^\mu c|D_{(s)}(p_1)\rangle = N_c g_{D_{(s)}} g_P \int \frac{d^4k}{(2\pi)^4 i} \tilde{\Phi}_{D_{(s)}}(-(k+w_{13}p_1)^2)\tilde{\Phi}_P(-(k+w_{23}p_2)^2) \times \mathrm{tr}[O^\mu S_1(k+p_1)\gamma^5 S_3(k)\gamma^5 S_2(k+p_2)], \quad (13)$$

$$\langle V(p_2,\epsilon_2)|\bar{q}O^\mu c|D_{(s)}(p_1)\rangle = N_c g_{D_{(s)}} g_V \int \frac{d^4k}{(2\pi)^4 i} \tilde{\Phi}_{D_{(s)}}(-(k+w_{13}p_1)^2)\tilde{\Phi}_V(-(k+w_{23}p_2)^2) \times \mathrm{tr}[O^\mu S_1(k+p_1)\gamma^5 S_3(k)\not{\epsilon}_2^\dagger S_2(k+p_2)], \quad (14)$$

where $N_c = 3$ is the number of colors, $w_{ij} = m_{q_j}/(m_{q_i} + m_{q_j})$, and $S_{1,2}$ are quark propagators, for which we use the Fock-Schwinger representation

$$S_i(k) = (m_{q_i} + \not{k}) \int_0^\infty d\alpha_i \exp[-\alpha_i(m_{q_i}^2 - k^2)]. \quad (15)$$

It should be noted that all loop integrations are carried out in Euclidean space.

Using various techniques described in our previous papers, a form factor F can be finally written in the form of a threefold integral

$$F = N_c g_{D_{(s)}} g_{(P,V)} \int_0^{1/\lambda^2} dt t \int_0^1 d\alpha_1 \times \int_0^1 d\alpha_2 \delta(1-\alpha_1-\alpha_2) f(t\alpha_1, t\alpha_2), \quad (16)$$

where $f(t\alpha_1, t\alpha_2)$ is the resulting integrand corresponding to the form factor F, and λ is the so-called infrared cutoff parameter, which is introduced to avoid the appearance of the branching point corresponding to the creation of free quarks and taken to be universal for all physical processes.

The model parameters, namely, the meson size parameters, the constituent quark masses, and the infrared cutoff parameter are determined by fitting the radiative and leptonic decay constants to experimental data or LQCD calculations. The model parameters required for the calculation in this paper are listed in Tables I and II. Other parameters such as the mass and lifetime of mesons and leptons, the CKM matrix elements, and physical constants are taken from the recent report of the PDG [7]. In particular, we adopt the following values for the CKM matrix elements: $|V_{cd}| = 0.218$ and $|V_{cs}| = 0.997$.

Once the model parameters are fixed, the form factors are obtained by calculating the threefold integral in Eq. (16).

TABLE I. Meson size parameters in GeV.

Λ_D	Λ_{D_s}	Λ_K	Λ_{K^*}	Λ_ϕ	Λ_ρ	Λ_ω	$\Lambda_\eta^{q\bar{q}}$	$\Lambda_\eta^{s\bar{s}}$	$\Lambda_{\eta'}^{q\bar{q}}$	$\Lambda_{\eta'}^{s\bar{s}}$
1.600	1.750	1.014	0.805	0.880	0.610	0.488	0.881	1.973	0.257	2.797

TABLE II. Quark masses and infrared cutoff parameter in GeV.

$m_{u/d}$	m_s	m_c	m_b	λ
0.241	0.428	1.672	5.05	0.181

This is done by using MATHEMATICA as well as FORTRAN code. In the CCQM, the form factors are calculable in the entire range of momentum transfer. The calculated form factors are very well represented by the double-pole parametrization

$$F(q^2) = \frac{F(0)}{1 - a\hat{s} + b\hat{s}^2}, \qquad \hat{s} = \frac{q^2}{m^2_{D_{(s)}}}. \tag{17}$$

Our results for the parameters $F(0)$, a, and b appearing in the parametrization Eq. (17) are given in Table III.

It is worth noting here that in the calculation of the $D_{(s)} \to \eta^{(\prime)}$ form factors one has to take into account the mixing of the light and the s-quark components. By assuming $m_u = m_d \equiv m_q$, the quark content can be written as

$$\begin{pmatrix} \eta \\ \eta' \end{pmatrix} = -\begin{pmatrix} \sin\delta & \cos\delta \\ -\cos\delta & \sin\delta \end{pmatrix} \begin{pmatrix} q\bar{q} \\ s\bar{s} \end{pmatrix},$$
$$q\bar{q} \equiv \frac{u\bar{u} + d\bar{d}}{\sqrt{2}}. \tag{18}$$

The angle δ is defined by $\delta = \theta_P - \theta_I$, where $\theta_I = \arctan(1/\sqrt{2})$ is the ideal mixing angle. We adopt the value $\theta_P = -15.4°$ from Ref. [71].

TABLE III. Parameters of the double-pole parametrization Eq. (17) for the form factors.

F	$F(0)$	a	b	F	$F(0)$	a	b
$A_+^{D\to\rho}$	0.57	0.96	0.15	$A_-^{D\to\rho}$	−0.74	1.11	0.22
$A_0^{D\to\rho}$	1.47	0.47	−0.10	$V^{D\to\rho}$	0.76	1.13	0.23
$A_+^{D\to\omega}$	0.55	1.01	0.17	$A_-^{D\to\omega}$	−0.69	1.17	0.26
$A_0^{D\to\omega}$	1.41	0.53	−0.10	$V^{D\to\omega}$	0.72	1.19	0.27
$A_+^{D_s\to\phi}$	0.67	1.06	0.17	$A_-^{D_s\to\phi}$	−0.95	1.20	0.26
$A_0^{D_s\to\phi}$	2.13	0.59	−0.12	$V^{D_s\to\phi}$	0.91	1.20	0.25
$A_+^{D_s\to K^*}$	0.57	1.13	0.21	$A_-^{D_s\to K^*}$	−0.82	1.32	0.34
$A_0^{D_s\to K^*}$	1.53	0.61	−0.11	$V^{D_s\to K^*}$	0.80	1.32	0.33
$F_+^{D\to\eta}$	0.67	0.93	0.12	$F_-^{D\to\eta}$	−0.37	1.02	0.18
$F_+^{D\to\eta'}$	0.76	1.23	0.23	$F_-^{D\to\eta'}$	−0.064	2.29	1.71
$F_+^{D\to D^0}$	0.91	5.88	4.40	$F_-^{D\to D^0}$	−0.026	6.32	8.37
$F_+^{D_s\to\eta}$	0.78	0.69	0.002	$F_-^{D_s\to\eta}$	−0.42	0.74	0.008
$F_+^{D_s\to\eta'}$	0.73	0.88	0.018	$F_-^{D_s\to\eta'}$	−0.28	0.92	0.009
$F_+^{D_s\to K}$	0.60	1.05	0.18	$F_-^{D_s\to K}$	−0.38	1.14	0.24
$F_+^{D_s\to D^0}$	0.92	5.08	2.25	$F_-^{D_s\to D^0}$	−0.34	6.79	8.91

IV. RESULTS AND DISCUSSION

A. Form factors

In this subsection, we compare our form factors with those from other theoretical approaches and from experimental measurements. For convenience, we relate all form factors from different studies to the BSW form factors, as mentioned in Sec. II. In the SM, the hadronic matrix element between two mesons is parametrized by two form factors (F_+ and F_0) for the $P \to P'$ transition and four form factors ($A_{0,1,2}$ and V) for the $P \to V$ one. However, in semileptonic decays of D and D_s mesons, the form factors F_0 and A_0 are less interesting because their contributions to the decay rate vanish in the zero lepton-mass limit (the tau mode is kinematically forbidden). Therefore, we focus more on the form factors F_+, A_1, A_2, and V. We note that the uncertainties of our form factors mainly come from the errors of the model parameters. These parameters are determined from a least-squares fit to available experimental data and some lattice calculations. We have observed that the errors of the fitted parameters are within 10%. We then calculated the propagation of these errors on the form factors and found the uncertainties on the form factors to be of order 20% at small q^2 and 30% at high q^2. At maximum recoil $q^2 = 0$, the form factor uncertainties are of order 15%.

We start with the $D_{(s)} \to P$ transition form factor $F_+(q^2)$. In Table IV, we compare the maximum-recoil values $F_+(q^2 = 0)$ with other theoretical approaches. It is observed that our results are in good agreement with other quark models, especially with the CQM [28] and the LFQM [32]. Besides, quark model predictions for $F_+(0)$ of the $D_{(s)} \to \eta^{(\prime)}$ channels are in general higher than those obtained by LCSR [22,24] and LQCD [14]. This suggests that more studies of these form factors are needed. For example, a better LQCD calculation of $F_+(0)$ is expected. Note that the authors of Ref. [14] considered their LQCD calculation as a pilot study rather than a conclusive one.

Regarding the $D_{(s)} \to V$ transition form factors A_1, A_2, and V, it is more interesting to compare their ratios at maximum recoil. The ratios are defined as follows:

$$r_2 = \frac{A_2(q^2 = 0)}{A_1(q^2 = 0)}, \qquad r_V = \frac{V(q^2 = 0)}{A_1(q^2 = 0)}. \tag{19}$$

In Table V, we compare these ratios with the world average given by the PDG [7] and with other theoretical results obtained in CQM [28], LFQM [32], HMχT [35], and LQCD [13]. Our results for the form factor ratios r_2 and r_V agree well with the PDG data within uncertainty except for the ratio $r_V(D_s^+ \to \phi)$, for which our prediction is much lower than that from PDG. Note that our prediction $r_V(D_s^+ \to \phi) = 1.34$ is close to the value 1.42 from the LFQM [32]. It is also seen that for most cases, the HMχT predictions [35] for the ratios at $q^2 = 0$ are largely different

TABLE IV. Comparison of $F_+(0)$ for $D_{(s)} \to P$ transitions.

	$D \to \eta$	$D \to \eta'$	$D_s \to \eta$	$D_s \to \eta'$	$D_s \to K^0$
Present	0.67 ± 0.10	0.76 ± 0.11	0.78 ± 0.12	0.73 ± 0.11	0.60 ± 0.09
CQM [28]	⋯	⋯	0.78	0.78	0.72
LFQM [32]	0.71	⋯	0.76	⋯	0.66
LQCD$_{M_\pi=470\ \mathrm{MeV}}$[14]	⋯	⋯	0.564(11)	0.437(18)	⋯
LQCD$_{M_\pi=370\ \mathrm{MeV}}$[14]	⋯	⋯	0.542(13)	0.404(25)	⋯
LCSR [22]	0.552 ± 0.051	0.458 ± 0.105	0.432 ± 0.033	0.520 ± 0.080	⋯
LCSR [24]	$0.429^{+0.165}_{-0.141}$	$0.292^{+0.113}_{-0.104}$	$0.495^{+0.030}_{-0.029}$	$0.558^{+0.047}_{-0.045}$	⋯

TABLE V. Ratios of the $D_{(s)} \to V$ transition form factors at maximum recoil.

Channel	Ratio	Present	PDG [7]	LQCD [13]	CQM [28]	LFQM [32]	HMχT [35]
$D \to \rho$	r_2	0.93 ± 0.19	0.83 ± 0.12	⋯	0.83	0.78	0.51
	r_V	1.26 ± 0.25	1.48 ± 0.16	⋯	1.53	1.47	1.72
$D^+ \to \omega$	r_2	0.95 ± 0.19	1.06 ± 0.16	⋯	⋯	0.84	0.51
	r_V	1.24 ± 0.25	1.24 ± 0.11	⋯	⋯	1.47	1.72
$D_s^+ \to \phi$	r_2	0.99 ± 0.20	0.84 ± 0.11	0.74(12)	0.73	0.86	0.52
	r_V	1.34 ± 0.27	1.80 ± 0.08	1.72(21)	1.72	1.42	1.80
$D_s^+ \to K^{*0}$	r_2	0.99 ± 0.20	⋯	⋯	0.74	0.82	0.55
	r_V	1.40 ± 0.28	⋯	⋯	1.82	1.55	1.93

from the PDG values, demonstrating the fact that this model is more suitable for the high q^2 region.

In order to have a better picture of the form factors in the whole q^2 range $0 \le q^2 \le q^2_{\mathrm{max}} = (m_{D_{(s)}} - m_{P/V})^2$ we plot in Figs. 2–5 their q^2 dependence from various studies. It is very interesting to note that, in all cases, our form factors are close to those obtained in the covariant LFQM [32], and this is not for the first time such a good agreement is observed. In a previous study of the semileptonic decays $B_c \to J/\psi(\eta_c)\ell\nu$ [72] it was seen that the corresponding form factors agree very well between our model and the covariant LFQM [73]. This suggests that a comparison of the two models in more detail may be fruitful. It is also worth noting that the HMχT [35] prediction for the form factor $A_0(q^2)$ is systematically much higher than that from other theoretical calculations.

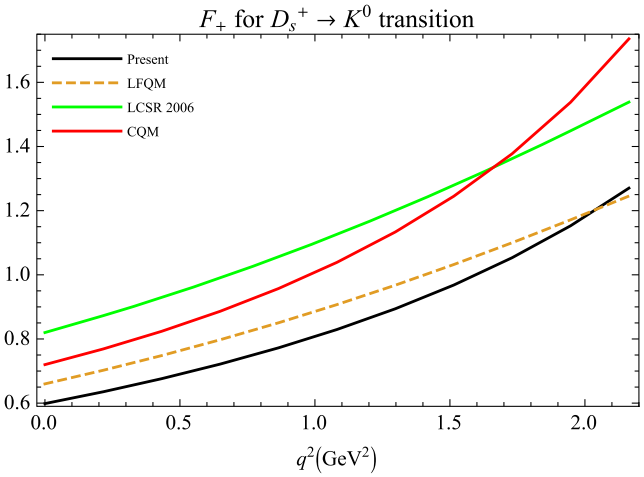

FIG. 2. Form factor $F_+(q^2)$ for $D_s^+ \to K^0$ in our model, LFQM [32], LCSR [20], and CQM [28].

Very recently, the ETM collaboration has provided the lattice determination [75] for the full set of the form factors characterizing the semileptonic $D \to \pi(K)\ell\nu$ and rare $D \to \pi(K)\ell\ell$ decays within and beyond the SM, when an additional tensor coupling is considered. As mentioned before, the decays $D \to \pi(K)\ell\nu$ have been studied in our model already [46]. However, we compute the $D \to \pi(K)\ell\nu$ form factors including the tensor one in this paper, in order to compare with the recent ETM results. This demonstrates the fidelity of the CCQM predictions for the hadronic form factors and helps us better estimate the theoretical uncertainties of our model. Moreover, the tensor and scalar form factors are essential for the study of possible new physics in these decays [for more detail we refer to a similar calculation of the full set of $B \to D^{(*)}$ and $B \to \pi(\rho)$ form factors in our model [76,77]].

The new tensor form factor is defined by

$$\langle P(p_2)|\bar{q}\sigma^{\mu\nu}(1-\gamma^5)c|D(p_1)\rangle = \frac{iF^T(q^2)}{M_1+M_2}(P^\mu q^\nu - P^\nu q^\mu + i\epsilon^{\mu\nu Pq}). \quad (20)$$

Note that we obtained $F_0(q^2)$ by using the form factors $F_+(q^2)$ and $F_-(q^2)$ defined in Eq. (2), with the help of the relation

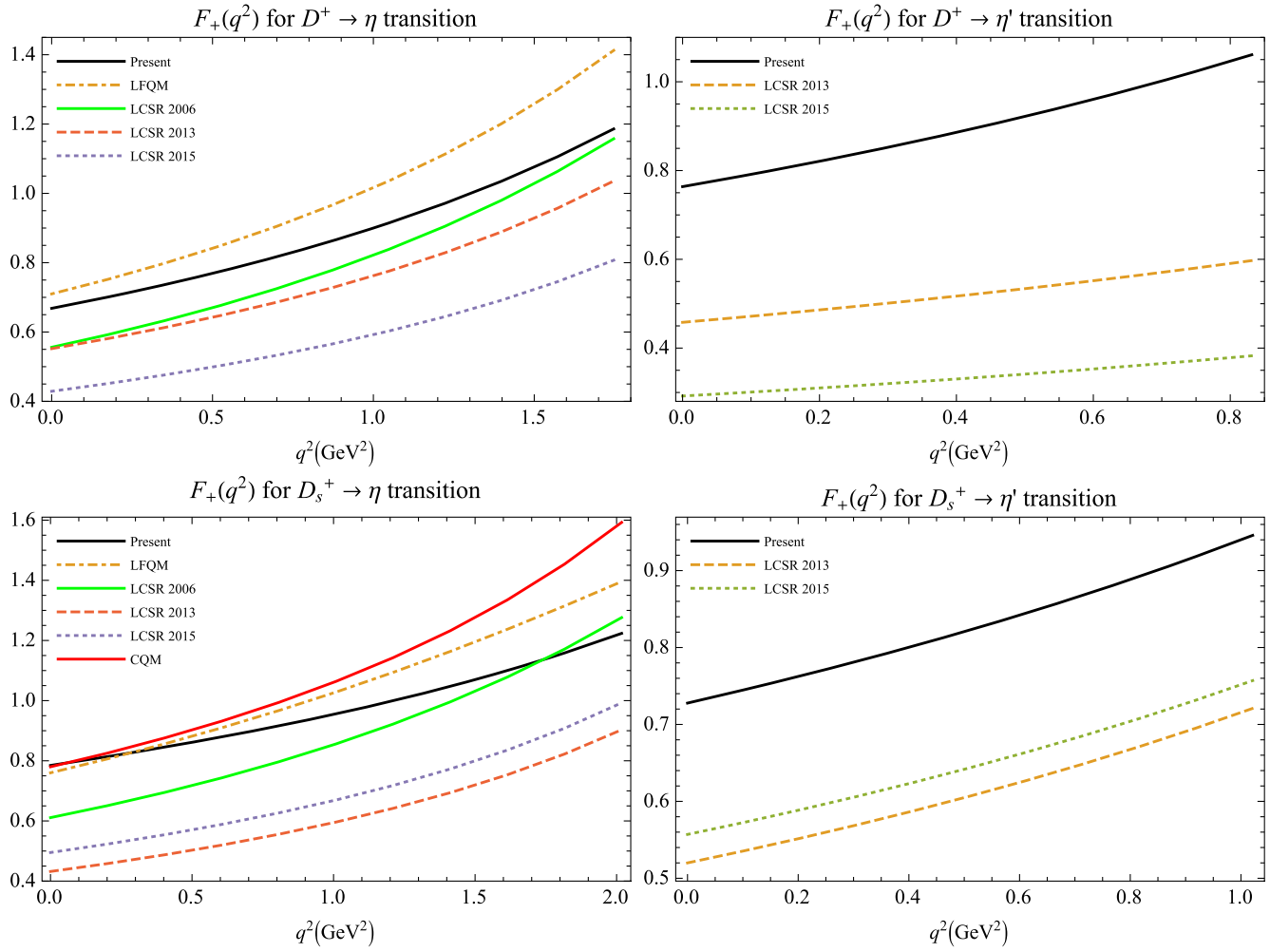

FIG. 3. Form factor $F_+(q^2)$ for $D^+_{(s)} \to \eta^{(\prime)}$ in our model, LCSR [20,22,24], and CQM [28].

$$F_0(q^2) = F_+(q^2) + \frac{q^2}{M_1^2 - M_2^2} F_-(q^2). \tag{21}$$

Meanwhile, the ETM collaboration directly calculated the scalar matrix element $\langle P(p_2)|\bar{q}c|D(p_1)\rangle$ and then determined $F_0(q^2)$ using the equation of motion. In this way, the final result becomes sensitive to the quark mass difference.

In Fig. 6 we compare the form factors $F_0(q^2)$, $F_+(q^2)$, and $F_T(q^2)$ of the $D \to \pi(K)\ell\nu$ transitions with those obtained by the ETM collaboration. It is seen that our $F_0(q^2)$ agrees well with the ETM only in the low q^2 region. However, our results for $F_+(q^2)$ are very close to those of the ETM. Note that the determination of $F_+(q^2)$ by the ETM is dependent on $F_0(q^2)$. It is interesting that the tensor form factors between the two studies are in perfect agreement. Even though this form factor does not appear within the SM, this agreement has an important meaning because, in both approaches, the tensor form factor is determined directly from the corresponding matrix element without any additional assumptions. In Table VI, we present the values of the form factors and their ratios at maximum recoil. One sees that our results agree with the ETM calculation within uncertainty.

B. Branching fractions and other observables

In Tables VII and VIII, we summarize our predictions for the semileptonic branching fractions of the D and D_s mesons, respectively. For comparison, we also list results of other theoretical calculations and the most recent experimental data given by the CLEO and BESIII collaborations. Note that the uncertainties of our predictions for the branching fractions and other polarization observables are of order 50%, taking into account only the main source of uncertainties related to the form factors.

In general, our results for the branching fractions are consistent with experimental data as well as with other theoretical calculations. It is worth mentioning that, for such a large set of decays considered in this study, our branching fractions agree very well with all available experimental data except for one channel, the $D_s^+ \to K^0\ell^+\nu_\ell$. In this case, our prediction is nearly twice

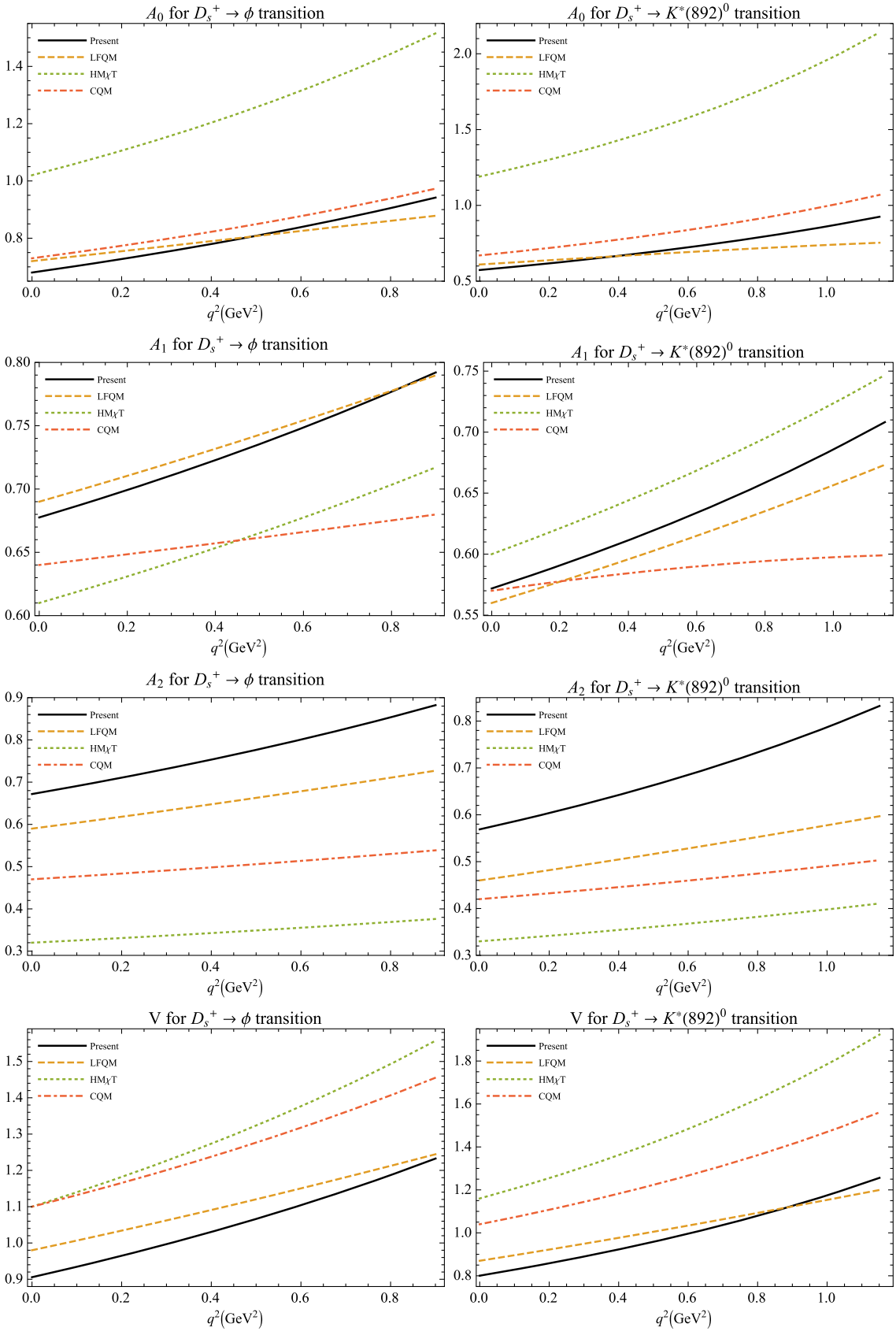

FIG. 4. Form factors for $D_s^+ \to \phi$ (left) and $D_s^+ \to K^*(892)^0$ (right) in our model, LFQM [32], HMχT [35], and CQM [28].

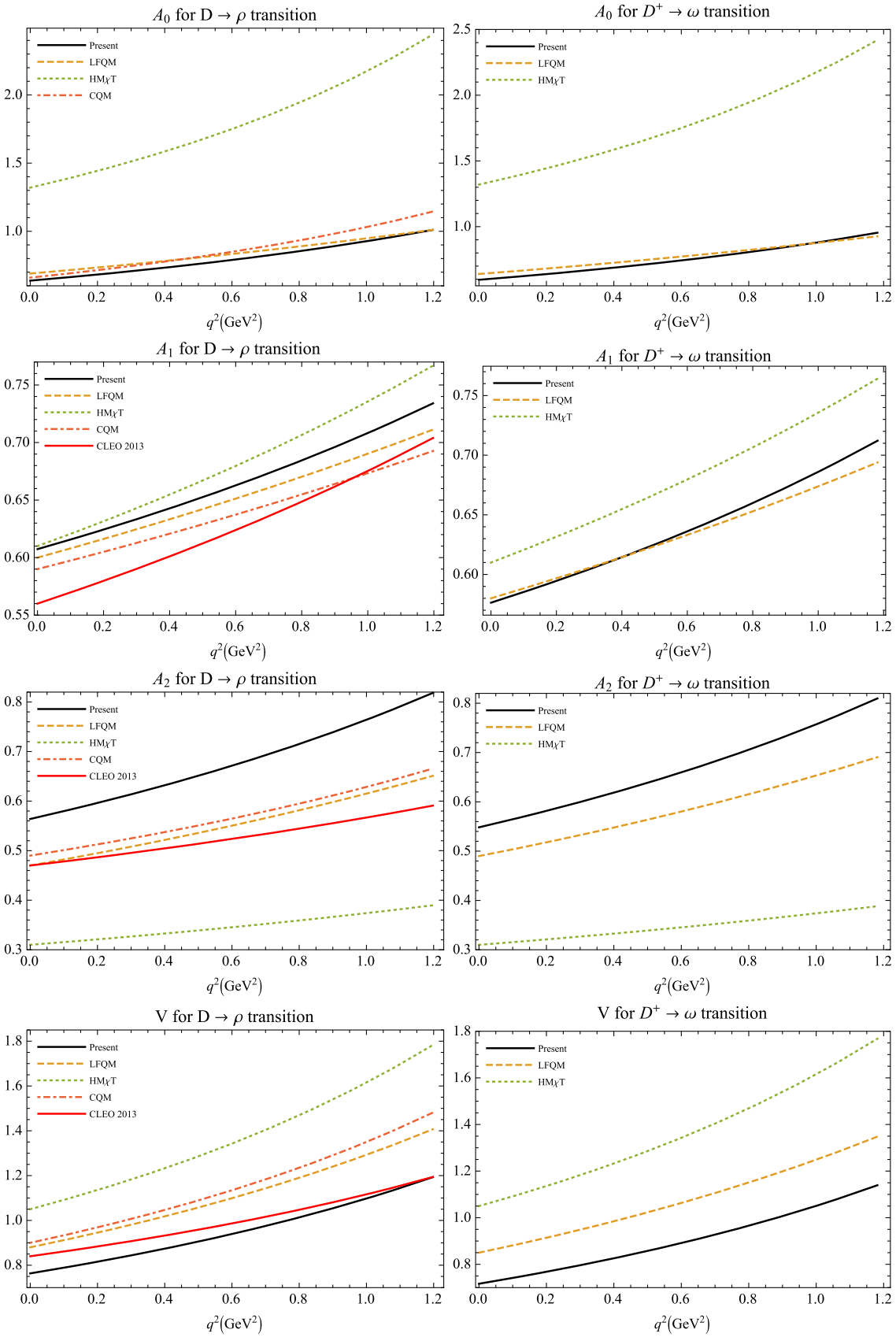

FIG. 5. Form factors for $D \to \rho$ (left) and $D^+ \to \omega$ (right) in our model, LFQM [32], HMχT [35], CQM [28], and CLEO data [74].

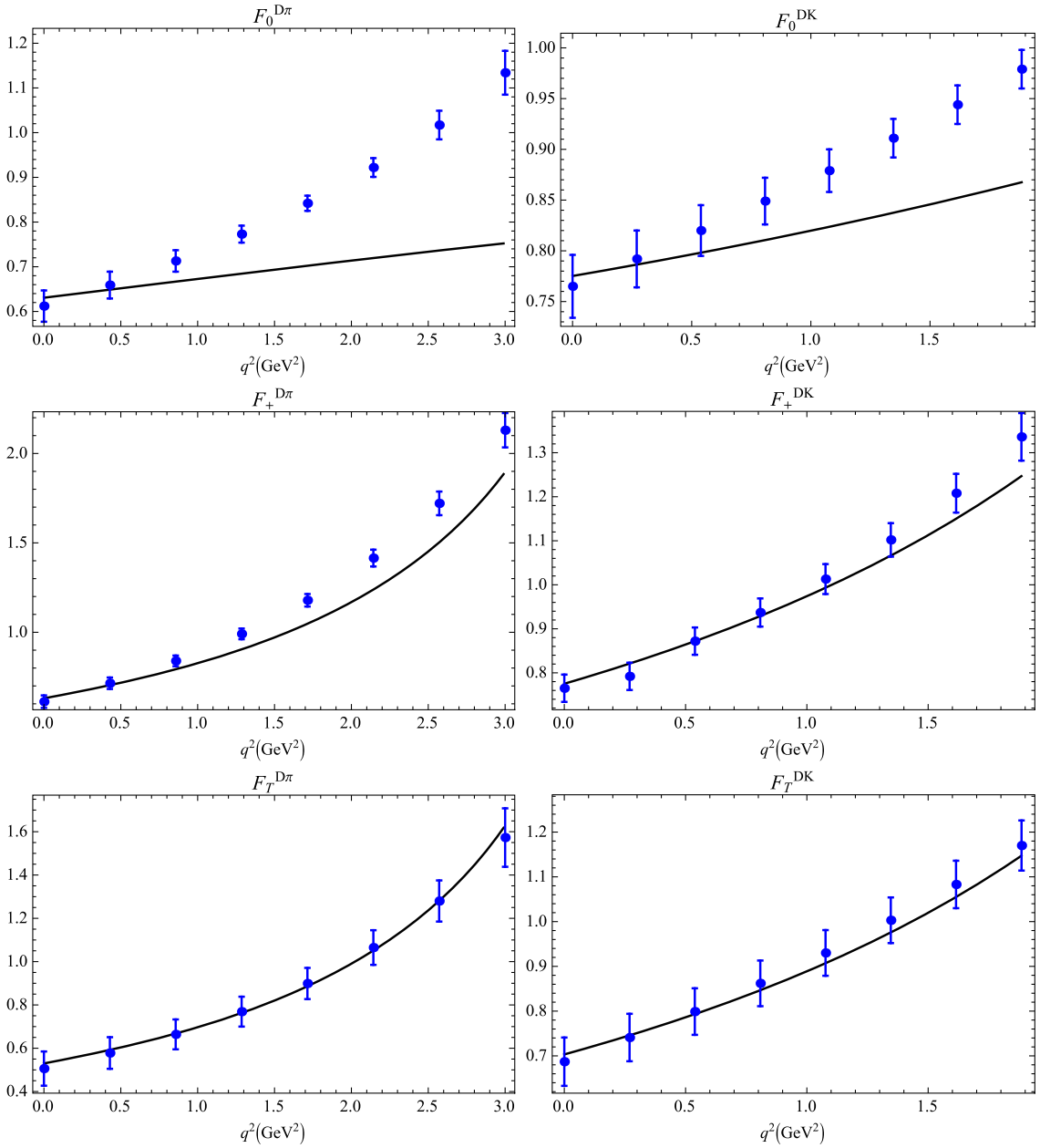

FIG. 6. $D \to \pi(K)\ell\nu$ form factors obtained in our model (solid lines) and in lattice calculation (dots with error bars) by the ETM collaboration [75].

as small as the CLEO central value [83] and about 30% smaller than the LFQM prediction [33].

We also give prediction for the ratio $\Gamma(D^0 \to \rho^- e^+ \nu_e)/2\Gamma(D^+ \to \rho^0 e^+ \nu_e)$ which should be equal to unity in the SM, assuming isospin invariance. Our calculation yields 0.98, in agreement with CLEO's result of $1.03 \pm 0.09^{+0.08}_{-0.02}$ [74]. Besides, our ratio of branching fractions $\mathcal{B}(D_s^+ \to \eta' e^+ \nu_e)/\mathcal{B}(D_s^+ \to \eta e^+ \nu_e) = 0.37$ coincides with the result 0.36 ± 0.14 obtained by CLEO [85] and the more recent value 0.40 ± 0.14 by BESIII [84].

TABLE VI. $D \to \pi(K)\ell\nu$ form factors and their ratios at $q^2 = 0$.

	$f_+^{D\pi}(0)$	$f_+^{DK}(0)$	$f_T^{D\pi}(0)$	$f_T^{DK}(0)$	$f_T^{D\pi}(0)/f_+^{D\pi}(0)$	$f_T^{DK}(0)/f_+^{DK}(0)$
Present	0.63	0.78	0.53	0.70	0.84	0.90
ETM [75]	0.612(35)	0.765(31)	0.506(79)	0.687(54)	0.827(114)	0.898(50)

TABLE VII. Branching fractions of $D^+(D^0)$-meson semileptonic decays.

Channel	Unit	Present	Other	Reference	Data	Reference
$D^0 \to \rho^- e^+ \nu_e$	10^{-3}	1.62	1.97	χUA [38]	$1.445 \pm 0.058 \pm 0.039$	BESIII [78]
			$1.749^{+0.421}_{-0.297} \pm 0.006$	LCSR [25]	$1.77 \pm 0.12 \pm 0.10$	CLEO [74]
			2.0	HMχT [35]		
$D^0 \to \rho^- \mu^+ \nu_\mu$	10^{-3}	1.55	1.84	χUA [38]		
$D^+ \to \rho^0 e^+ \nu_e$	10^{-3}	2.09	2.54	χUA [38]	$1.860 \pm 0.070 \pm 0.061$	BESIII [78]
			$2.217^{+0.534}_{-0.376} \pm 0.015$	LCSR [25]	$2.17 \pm 0.12^{+0.12}_{-0.22}$	CLEO [74]
			2.5	HMχT [35]		
$D^+ \to \rho^0 \mu^+ \nu_\mu$	10^{-3}	2.01	2.37	χUA [38]	2.4 ± 0.4	PDG [7]
$D^+ \to \omega e^+ \nu_e$	10^{-3}	1.85	2.46	χUA [38]	$1.63 \pm 0.11 \pm 0.08$	BESIII [79]
			2.5	HMχT [35]	$1.82 \pm 0.18 \pm 0.07$	CLEO [74]
			2.1 ± 0.2	LFQM [33]		
$D^+ \to \omega \mu^+ \nu_\mu$	10^{-3}	1.78	2.29	χUA [38]		
			2.0 ± 0.2	LFQM [33]		
$D^+ \to \eta e^+ \nu_e$	10^{-4}	9.37	12 ± 1	LFQM [33]	$10.74 \pm 0.81 \pm 0.51$	BESIII [80]
			24.5 ± 5.26	LCSR [22]	$11.4 \pm 0.9 \pm 0.4$	CLEO [81]
			14.24 ± 10.98	LCSR [24]		
$D^+ \to \eta \mu^+ \nu_\mu$	10^{-4}	9.12	12 ± 1	LFQM [33]		
$D^+ \to \eta' e^+ \nu_e$	10^{-4}	2.00	1.8 ± 0.2	LFQM [33]	$1.91 \pm 0.51 \pm 0.13$	BESIII [80]
			3.86 ± 1.77	LCSR [22]	$2.16 \pm 0.53 \pm 0.07$	CLEO [81]
			1.52 ± 1.17	LCSR [24]		
$D^+ \to \eta' \mu^+ \nu_\mu$	10^{-4}	1.90	1.7 ± 0.2	LFQM [33]		

TABLE VIII. Branching fractions of D_s-meson semileptonic decays (in %).

Channel	Present	Other	Reference	Data	Reference
$D_s^+ \to \phi e^+ \nu_e$	3.01	2.12	χUA [38]	$2.26 \pm 0.45 \pm 0.09$	BESIII [9]
		3.1 ± 0.3	LFQM [33]	$2.61 \pm 0.03 \pm 0.08 \pm 0.15$	*BABAR* [82]
		2.4	HMχT [35]	$2.14 \pm 0.17 \pm 0.08$	CLEO [83]
$D_s^+ \to \phi \mu^+ \nu_\mu$	2.85	1.94	χUA [38]		
		2.9 ± 0.3	LFQM [33]	$1.94 \pm 0.53 \pm 0.09$	BESIII [9]
$D_s^+ \to K^0 e^+ \nu_e$	0.20	0.27 ± 0.02	LFQM [33]	$0.39 \pm 0.08 \pm 0.03$	CLEO [83]
$D_s^+ \to K^0 \mu^+ \nu_\mu$	0.20	0.26 ± 0.02	LFQM [33]		
$D_s^+ \to K^{*0} e^+ \nu_e$	0.18	0.202	χUA [38]	$0.18 \pm 0.04 \pm 0.01$	CLEO [83]
		0.19 ± 0.02	LFQM [33]		
		0.22	HMχT [35]		
$D_s^+ \to K^{*0} \mu^+ \nu_\mu$	0.17	0.189	χUA [38]		
		0.19 ± 0.02	LFQM [33]		
$D_s^+ \to \eta e^+ \nu_e$	2.24	2.26 ± 0.21	LFQM [33]	$2.30 \pm 0.31 \pm 0.08$	BESIII [84]
		2.00 ± 0.32	LCSR [22]	$2.28 \pm 0.14 \pm 0.19$	CLEO [83]
		2.40 ± 0.28	LCSR [24]		
$D_s^+ \to \eta \mu^+ \nu_\mu$	2.18	2.22 ± 0.20	LFQM [33]	$2.42 \pm 0.46 \pm 0.11$	BESIII [9]
$D_s^+ \to \eta' e^+ \nu_e$	0.83	0.89 ± 0.09	LFQM [33]	$0.93 \pm 0.30 \pm 0.05$	BESIII [84]
		0.75 ± 0.23	LCSR [22]	$0.68 \pm 0.15 \pm 0.06$	CLEO [83]
		0.79 ± 0.14	LCSR [24]		
$D_s^+ \to \eta' \mu^+ \nu_\mu$	0.79	0.85 ± 0.08	LFQM [33]	$1.06 \pm 0.54 \pm 0.07$	BESIII [9]

TABLE IX. Semileptonic branching fractions for $D^+_{(s)} \to D^0 \ell^+ \nu_\ell$.

Channel	Present	Other	Reference	Data	Reference
$D^+ \to D^0 e^+ \nu_e$	2.23×10^{-13}	2.78×10^{-13}	[88]	$< 1.0 \times 10^{-4}$	BESIII [87]
		2.71×10^{-13}	[89]		
$D_s^+ \to D^0 e^+ \nu_e$	2.52×10^{-8}	$(2.97 \pm 0.03) \times 10^{-8}$	[88]	...	...
		3.34×10^{-8}	[89]		

TABLE X. Forward-backward asymmetry and lepton polarization components.

	$\langle \mathcal{A}^e_{\rm FB} \rangle$	$\langle \mathcal{A}^\mu_{\rm FB} \rangle$	$\langle P^e_L \rangle$	$\langle P^\mu_L \rangle$	$\langle P^e_T \rangle$	$\langle P^\mu_T \rangle$
$D^0 \to \rho^- \ell^+ \nu_\ell$	0.21	0.19	−1.00	−0.92	1.4×10^{-3}	0.22
$D^+ \to \rho^0 \ell^+ \nu_\ell$	0.22	0.19	−1.00	−0.92	1.4×10^{-3}	0.22
$D^+ \to \omega \ell^+ \nu_\ell$	0.21	0.19	−1.00	−0.92	1.4×10^{-3}	0.22
$D^+ \to \eta \ell^+ \nu_\ell$	-6.4×10^{-6}	−0.06	−1.00	−0.83	2.8×10^{-3}	0.44
$D^+ \to \eta' \ell^+ \nu_\ell$	-13.0×10^{-6}	−0.10	−1.00	−0.70	4.2×10^{-3}	0.59
$D^+ \to D^0 \ell^+ \nu_\ell$	−0.10	...	−0.72	...	0.56	...
$D_s^+ \to \phi \ell^+ \nu_\ell$	0.18	0.15	−1.00	−0.91	1.5×10^{-3}	0.23
$D_s^+ \to K^{*0} \ell^+ \nu_\ell$	0.22	0.20	−1.00	−0.92	1.4×10^{-3}	0.22
$D_s^+ \to K^0 \ell^+ \nu_\ell$	-5.0×10^{-6}	−0.05	−1.00	−0.86	2.4×10^{-3}	0.39
$D_s^+ \to \eta \ell^+ \nu_\ell$	-6.0×10^{-6}	−0.06	−1.00	−0.84	2.7×10^{-3}	0.42
$D_s^+ \to \eta' \ell^+ \nu_\ell$	-11.2×10^{-6}	−0.09	−1.00	−0.75	3.8×10^{-3}	0.54
$D_s^+ \to D^0 \ell^+ \nu_\ell$	-7.37×10^{-4}	...	−1.00	...	0.038	...

Finally, we predict $\mathcal{B}(D^+ \to \eta' e^+ \nu_e)/\mathcal{B}(D^+ \to \eta e^+ \nu_e) = 0.21$, which agrees very well with the values 0.19 ± 0.05 and 0.18 ± 0.05 we got from experimental data by CLEO [81] and BESIII [80], respectively. It is worth mentioning here that very recently, the BESIII collaboration has reported their measurement of $\mathcal{B}(D^0 \to K^- \mu^+ \nu_\mu)$ [86] with significantly improved precision. In their paper, they also approved the prediction of our model for the ratio $\mathcal{B}(D^0 \to K^- \mu^+ \nu_\mu)/\mathcal{B}(D^0 \to K^- e^+ \nu_e)$ provided in Ref. [46].

In Table IX, we present our results for the semileptonic decays $D^+_{(s)} \to D^0 e^+ \nu_e$, which are rare in the SM due to phase-space suppression. These decays are of particular interest since they are induced by the light quark decay, while the heavy quark acts as the spectator. Besides, the small phase space helps reduce the theoretical errors. The first experimental constraint on the branching fraction $\mathcal{B}(D^+ \to D^0 e^+ \nu_e)$ was recently obtained by the BESIII collaboration [87]. However, the experimental upper limit is still far above the SM predictions. The branching fractions obtained in our model are comparable with other theoretical calculations using the flavor SU(3) symmetry in the light quark sector [88,89].

Finally, in Table X we list our predictions for the forward-backward asymmetry $\langle \mathcal{A}^\ell_{\rm FB} \rangle$, the longitudinal polarization $\langle P^\ell_L \rangle$, and the transverse polarization $\langle P^\ell_T \rangle$ of the charged lepton in the final state. It is seen that, for the $P \to V$ transitions, the lepton-mass effect in $\langle \mathcal{A}^\ell_{\rm FB} \rangle$ is small, resulting in a difference of only 10%–15% between the corresponding electron and muon modes. For the $P \to P'$ transitions, $\langle \mathcal{A}^\mu_{\rm FB} \rangle$ are about 10^4 times larger than $\langle \mathcal{A}^e_{\rm FB} \rangle$. This is readily seen from Eq. (7): for $P \to P'$ transitions the two helicity amplitudes $H_\pm$ vanish and the forward-backward asymmetry is proportional to the lepton mass squared. Regarding the longitudinal polarization, the difference between $\langle P^\mu_L \rangle$ and $\langle P^e_L \rangle$ is 10%–30%. One sees that the lepton-mass effect in the transverse polarization is much more significant than that in the longitudinal one. This is true for both $P \to P'$ and $P \to V$ transitions. Note that the values of $\langle \mathcal{A}^e_{\rm FB} \rangle$ and $\langle P^e_{L(T)} \rangle$ for the rare decays $D^+_{(s)} \to D^0 e^+ \nu_e$ are quite different in comparison with other $P \to P'$ transitions due to their extremely small kinematical regions.

V. SUMMARY AND CONCLUSION

We have presented a systematic study of the D and D_s semileptonic decays within the framework of the CCQM. All the relevant form factors are calculated in the entire range of momentum transfer squared. We have also provided a detailed comparison of the form factors with other theoretical predictions and, in some cases, with available experimental data. In particular, we have observed a good agreement with the form factors obtained in the covariant LFQM, for all decays. It is worth noting that our tensor form factors for the $D \to \pi(K) \ell \nu$ decays are in perfect agreement with the recent LQCD calculation by the ETM collaboration [75].

We have given our predictions for the semileptonic branching fractions and their ratios. In general, our results are in good agreement with other theoretical approaches and with recent experimental data obtained by *BABAR*, CLEO, and BESIII. In all cases, our predictions for the

branching fractions agree with experimental data within 10%, except for the $D_s^+ \to K^0 \ell^+ \nu_\ell$ channel. Our predictions for the ratios of branching fractions are in full agreement with experimental data. To conclude, we have provided the first ever theoretical predictions for the forward-backward asymmetries and lepton longitudinal and transverse polarizations, which are important for future experiments.

ACKNOWLEDGMENTS

J. N. P. acknowledges financial support from University Grants Commission of India under Major Research Project F.No. 42-775/2013(SR). P. S. acknowledges support from Istituto Nazionale di Fisica Nucleare, I. S. QFT_HEP. M. A. I., J. G. K., and C. T. T. thank Heisenberg-Landau Grant for providing support for their collaboration. M. A. I. acknowledges financial support of PRISMA Cluster of Excellence at University of Mainz. N. R. S. thanks Bogoliubov Laboratory of Theoretical Physics, Joint Institute for Nuclear Research for warm hospitality during Helmholtz-DIAS International Summer School "Quantum Field Theory at the Limits: from Strong Field to Heavy Quarks" where this work was initiated. C. T. T. acknowledges support from Duy Tan University during the beginning stage of this work. M. A. I. and C. T. T. appreciate warm hospitality of Mainz Institute for Theoretical Physics at University of Mainz, where part of this work was done.

Note added.—Recently, we became aware of the paper [90] where the BESIII collaboration reported their new measurements of the branching fractions for the decays $D_s^+ \to K^0 e^+ \nu_e$ and $D_s^+ \to K^{*0} e^+ \nu_e$ with improved precision. They also obtained for the first time the values of the form factors at maximum recoil. Our predictions for the branching fraction $\mathcal{B}(D_s^+ \to K^{*0} e^+ \nu_e)$ as well as the form factor parameters $f_+^{D_s K}(0)$, $r_V^{D_s K^*}(0)$, and $r_2^{D_s K^*}(0)$ agree with the new BESIII results. Regarding their result $\mathcal{B}(D_s^+ \to K^0 e^+ \nu_e) = (3.25 \pm 0.41) \times 10^{-3}$, the central value is closer to our prediction, in comparison with the CLEO result [83]. However, the BESIII result is still at 1σ larger than ours.

[1] J. D. Richman and P. R. Burchat, Rev. Mod. Phys. **67**, 893 (1995).
[2] J. P. Lees *et al.* (*BABAR* Collaboration), Phys. Rev. D **91**, 052022 (2015).
[3] B. Aubert *et al.* (*BABAR* Collaboration), Phys. Rev. D **76**, 052005 (2007).
[4] L. Widhalm *et al.* (Belle Collaboration), Phys. Rev. Lett. **97**, 061804 (2006).
[5] M. Ablikim *et al.* (BESIII Collaboration), Phys. Rev. D **92**, 072012 (2015).
[6] D. Besson *et al.* (CLEO Collaboration), Phys. Rev. D **80**, 032005 (2009).
[7] M. Tanabashi *et al.* (Particle Data Group), Phys. Rev. D **98**, 030001 (2018).
[8] M. Ablikim *et al.* (BESIII Collaboration), Eur. Phys. J. C **76**, 369 (2016).
[9] M. Ablikim *et al.* (BESIII Collaboration), Phys. Rev. D **97**, 012006 (2018).
[10] M. Ablikim *et al.* (BESIII Collaboration), Phys. Rev. Lett. **121**, 171803 (2018).
[11] V. V. Anisovich, D. V. Bugg, D. I. Melikhov, and V. A. Nikonov, Phys. Lett. B **404**, 166 (1997).
[12] C. Di Donato, G. Ricciardi, and I. Bigi, Phys. Rev. D **85**, 013016 (2012).
[13] G. C. Donald, C. T. H. Davies, J. Koponen, and G. P. Lepage (HPQCD Collaboration), Phys. Rev. D **90**, 074506 (2014).
[14] G. S. Bali, S. Collins, S. Dürr, and I. Kanamori, Phys. Rev. D **91**, 014503 (2015).
[15] S. Aoki *et al.*, Eur. Phys. J. C **77**, 112 (2017).
[16] P. Ball, Phys. Rev. D **48**, 3190 (1993).
[17] P. Colangelo and F. De Fazio, Phys. Lett. B **520**, 78 (2001).
[18] D. S. Du, J. W. Li, and M. Z. Yang, Eur. Phys. J. C **37**, 173 (2004).
[19] A. Khodjamirian, R. Ruckl, S. Weinzierl, C. W. Winhart, and O. I. Yakovlev, Phys. Rev. D **62**, 114002 (2000).
[20] Y. L. Wu, M. Zhong, and Y. B. Zuo, Int. J. Mod. Phys. A **21**, 6125 (2006).
[21] K. Azizi, R. Khosravi, and F. Falahati, J. Phys. G **38**, 095001 (2011).
[22] N. Offen, F. A. Porkert, and A. Schäfer, Phys. Rev. D **88**, 034023 (2013).
[23] U. G. Meißner and W. Wang, Phys. Lett. B **730**, 336 (2014).
[24] G. Duplancic and B. Melic, J. High Energy Phys. 11 (2015) 138.
[25] H. B. Fu, X. Yang, R. Lü, L. Zeng, W. Cheng, and X. G. Wu, arXiv:1808.06412.
[26] N. Isgur, D. Scora, B. Grinstein, and M. B. Wise, Phys. Rev. D **39**, 799 (1989).
[27] D. Scora and N. Isgur, Phys. Rev. D **52**, 2783 (1995).
[28] D. Melikhov and B. Stech, Phys. Rev. D **62**, 014006 (2000).
[29] R. N. Faustov, V. O. Galkin, and A. Y. Mishurov, Phys. Rev. D **53**, 1391 (1996).
[30] T. Palmer and J. O. Eeg, Phys. Rev. D **89**, 034013 (2014).
[31] Z. T. Wei, H. W. Ke, and X. F. Yang, Phys. Rev. D **80**, 015022 (2009).
[32] R. C. Verma, J. Phys. G **39**, 025005 (2012).
[33] H. Y. Cheng and X. W. Kang, Eur. Phys. J. C **77**, 587 (2017); **77**, 863(E) (2017).
[34] S. Fajfer and J. F. Kamenik, Phys. Rev. D **71**, 014020 (2005).

[35] S. Fajfer and J. F. Kamenik, Phys. Rev. D **72**, 034029 (2005).
[36] J. Charles, A. Le Yaouanc, L. Oliver, O. Pene, and J. C. Raynal, Phys. Rev. D **60**, 014001 (1999).
[37] J. Bijnens and I. Jemos, Nucl. Phys. **B846**, 145 (2011).
[38] T. Sekihara and E. Oset, Phys. Rev. D **92**, 054038 (2015).
[39] L. R. Dai, X. Zhang, and E. Oset, Phys. Rev. D **98**, 036004 (2018).
[40] T. N. Pham, Int. J. Mod. Phys. A **33**, 1850160 (2018).
[41] S. S. Gershtein and M. Y. Khlopov, Pis'ma Zh. Eksp. Teor. Fiz. **23**, 374 (1976); M. Y. Khlopov, Yad. Fiz. **28**, 1134 (1978) [Sov. J. Nucl. Phys. **28**, 583 (1978)].
[42] G. V. Efimov and M. A. Ivanov, Int. J. Mod. Phys. A **04**, 2031 (1989); *The Quark Confinement Model of Hadrons* (CRC Press, Boca Raton, 1993).
[43] T. Branz, A. Faessler, T. Gutsche, M. A. Ivanov, J. G. Körner, and V. E. Lyubovitskij, Phys. Rev. D **81**, 034010 (2010).
[44] M. A. Ivanov, J. G. Körner, S. G. Kovalenko, P. Santorelli, and G. G. Saidullaeva, Phys. Rev. D **85**, 034004 (2012).
[45] T. Gutsche, M. A. Ivanov, J. G. Körner, V. E. Lyubovitskij, and P. Santorelli, Phys. Rev. D **86**, 074013 (2012).
[46] N. R. Soni and J. N. Pandya, Phys. Rev. D **96**, 016017 (2017).
[47] M. Wirbel, B. Stech, and M. Bauer, Z. Phys. C **29**, 637 (1985).
[48] J. G. Körner and G. A. Schuler, Z. Phys. C **38**, 511 (1988); **41**, 690(E) (1989); Phys. Lett. B **231**, 306 (1989); Z. Phys. C **46**, 93 (1990).
[49] T. Gutsche, M. A. Ivanov, J. G. Körner, V. E. Lyubovitskij, P. Santorelli, and N. Habyl, Phys. Rev. D **91**, 074001 (2015); **91**, 119907(E) (2015).
[50] M. A. Ivanov, J. G. Körner, and C. T. Tran, Phys. Rev. D **92**, 114022 (2015).
[51] S. Bifani, S. Descotes-Genon, A. Romero Vidal, and M. H. Schune, arXiv:1809.06229.
[52] M. A. Ivanov, J. G. Körner, and C. T. Tran, Phys. Rev. D **95**, 036021 (2017).
[53] Q. Y. Hu, X. Q. Li, and Y. D. Yang, arXiv:1810.04939.
[54] P. Asadi, M. R. Buckley, and D. Shih, arXiv:1810.06597.
[55] N. Rajeev and R. Dutta, Phys. Rev. D **98**, 055024 (2018).
[56] F. Feruglio, P. Paradisi, and O. Sumensari, arXiv:1806.10155.
[57] R. Alonso, J. Martin Camalich, and S. Westhoff, arXiv:1811.05664.
[58] M. A. Ivanov and P. Santorelli, Phys. Lett. B **456**, 248 (1999).
[59] A. Faessler, T. Gutsche, M. A. Ivanov, J. G. Körner, and V. E. Lyubovitskij, Eur. Phys. J. Direct **4**, 1 (2002).
[60] M. A. Ivanov, J. G. Körner, and P. Santorelli, Phys. Rev. D **73**, 054024 (2006).
[61] M. A. Ivanov and C. T. Tran, Phys. Rev. D **92**, 074030 (2015).
[62] S. Dubnička, A. Z. Dubničková, M. A. Ivanov, A. Liptaj, P. Santorelli, and C. T. Tran, arXiv:1808.06261.
[63] T. Gutsche, M. A. Ivanov, J. G. Körner, V. E. Lyubovitskij, and P. Santorelli, Phys. Rev. D **87**, 074031 (2013).
[64] T. Gutsche, M. A. Ivanov, J. G. Körner, and V. E. Lyubovitskij, Phys. Rev. D **96**, 054013 (2017).
[65] T. Gutsche, M. A. Ivanov, J. G. Körner, V. E. Lyubovitskij, P. Santorelli, and C. T. Tran, Phys. Rev. D **98**, 053003 (2018).
[66] S. Dubnicka, A. Z. Dubnickova, M. A. Ivanov, J. G. Körner, P. Santorelli, and G. G. Saidullaeva, Phys. Rev. D **84**, 014006 (2011).
[67] F. Goerke, T. Gutsche, M. A. Ivanov, J. G. Körner, V. E. Lyubovitskij, and P. Santorelli, Phys. Rev. D **94**, 094017 (2016).
[68] F. Goerke, T. Gutsche, M. A. Ivanov, J. G. Körner, and V. E. Lyubovitskij, Phys. Rev. D **96**, 054028 (2017).
[69] T. Gutsche, M. A. Ivanov, J. G. Körner, V. E. Lyubovitskij, and K. Xu, Phys. Rev. D **96**, 114004 (2017).
[70] A. Salam, Nuovo Cimento **25**, 224 (1962); S. Weinberg, Phys. Rev. **130**, 776 (1963).
[71] T. Feldmann, P. Kroll, and B. Stech, Phys. Rev. D **58**, 114006 (1998).
[72] C. T. Tran, M. A. Ivanov, J. G. Körner, and P. Santorelli, Phys. Rev. D **97**, 054014 (2018).
[73] W. Wang, Y. L. Shen, and C. D. Lu, Phys. Rev. D **79**, 054012 (2009).
[74] S. Dobbs *et al.* (CLEO Collaboration), Phys. Rev. Lett. **110**, 131802 (2013).
[75] V. Lubicz, L. Riggio, G. Salerno, S. Simula, and C. Tarantino (ETM Collaboration), Phys. Rev. D **96**, 054514 (2017); **98**, 014516 (2018).
[76] M. A. Ivanov, J. G. Körner, and C. T. Tran, Phys. Rev. D **94**, 094028 (2016).
[77] M. A. Ivanov, J. G. Körner, and C. T. Tran, Phys. Part. Nucl. Lett. **14**, 669 (2017).
[78] M. Ablikim *et al.* (BESIII Collaboration), arXiv:1809.06496.
[79] M. Ablikim *et al.* (BESIII Collaboration), Phys. Rev. D **92**, 071101 (2015).
[80] M. Ablikim *et al.* (BESIII Collaboration), Phys. Rev. D **97**, 092009 (2018).
[81] J. Yelton *et al.* (CLEO Collaboration), Phys. Rev. D **84**, 032001 (2011).
[82] B. Aubert *et al.* (*BABAR* Collaboration), Phys. Rev. D **78**, 051101 (2008).
[83] J. Hietala, D. Cronin-Hennessy, T. Pedlar, and I. Shipsey, Phys. Rev. D **92**, 012009 (2015).
[84] M. Ablikim *et al.* (BESIII Collaboration), Phys. Rev. D **94**, 112003 (2016).
[85] J. Yelton *et al.* (CLEO Collaboration), Phys. Rev. D **80**, 052007 (2009).
[86] M. Ablikim *et al.* (BESIII Collaboration), arXiv:1810.03127.
[87] M. Ablikim *et al.* (BESIII Collaboration), Phys. Rev. D **96**, 092002 (2017).
[88] H. B. Li and M. Z. Yang, Eur. Phys. J. C **59**, 841 (2009).
[89] S. Faller and T. Mannel, Phys. Lett. B **750**, 653 (2015).
[90] M. Ablikim *et al.* (BESIII Collaboration), arXiv:1811.02911.